ADVANCING THERMAL FIELD-FLOW FRACTIONATION FOR INDUSTRIAL POLYMER CHARACTERIZATION

by

Michael David Toney

A thesis submitted to the Faculty and the Board of Trustees of the Colorado School of Mines in partial fulfillment of the requirements for the degree of Doctor of Philosophy (Applied Chemistry).

Golden, Colorado

Date _____

Signed: _____

Michael David Toney

Signed: _____

Dr. Kim R. Williams
Thesis Advisor

Golden, Colorado

Date _____

Signed: _____

Dr. Thomas Gennett
Professor and Department Head
Department of Chemistry

ABSTRACT

Field-flow fractionation (FFF) is a family of techniques known for its open channel design and ability to separate polymers and colloids. The applied field in an FFF technique determines the physiochemical properties by which the separation occurs. A well-established theory relates retention time to a retention parameter that is defined by the interaction between the analyte and the applied field as well as the analyte's diffusion coefficient (D). This imparts the ability for FFF techniques to be used as both a separation and characterization tool. In the case of flow FFF, the retention parameter is dependent solely on D which subsequently relates to hydrodynamic size. For thermal FFF (ThFFF), the retention parameter is dependent on the Soret coefficient (S_T), a ratio of the thermal diffusion coefficient (D_T) and D. Existing studies of the thermophoresis of polymers in dilute solutions have revealed trends that may be utilized to solve challenges in polymer analysis. Specifically, D_T has been observed to be molar mass independent (above 10^3 to 10^4 Da), polymer-solvent dependent, and recently – dependent on architecture. The polymer-solvent dependence of D_T has been leveraged to characterize the composition of di- and tri-block polymer systems. This polymer-solvent dependence, while useful in driving separations, has proven to be challenging when analyzing new polymer chemistries because of incomplete understanding of thermophoresis and the resulting trial-and-error approach to selecting a carrier liquid that imparts sufficient polymer retention.

This thesis aims to increase the adoption of ThFFF by expanding the scope of polymer chemistries and architectures studied. The work presented here leveraged a leading polymer thermophoresis model to identify a suitable carrier liquid for characterizing the architecture of bottlebrush polymers. The S_T values were calculated from measured ThFFF retention times and their relationships to the degree of polymerization of the brush backbone and sidechains were established. Information about bottlebrush architecture was then obtained using the recently introduced Soret contraction factor (g''), defined as the ratio of the Soret coefficient of a branched polymer ($S_{T,br}$) to that of linear polymer ($S_{T,lin}$) with the same molar mass. Linear analogs were not available for these polyacrylates-containing bottlebrush polymers and thus $S_{T,lin}$ values were approximated using models for thermal and translational diffusion. A plot of log g'' versus the number of chain-ends of a bottlebrush showed the expected decrease in log g'' when the number of chain ends increased from 120 to 400. Differences in log g'' were also noticeable between 30% and 100% grafting densities. This work demonstrated the feasibility of estimating

$S_{T,lin}$ and opens the door for architecture characterization in the absence of a linear polymer analog.

The *g''* approach described above has been successfully utilized for model polymer systems derived from well controlled synthesis and orthogonal characterization. Ultimately, the question is whether *g''* can be used to characterize polymers in complex formulations of industrial importance. A polydimethylsiloxane (PDMS) containing formulation was targeted because of its relative 'greenness' when compared to petrochemical derived polymers. This PDMS system proved to be challenging on multiple fronts. First, D_T calculations did not yield trends useful to solvent selection due to the observed double Hansen Solubility sphere. This yielded two distinct values for D_T for each solvent system, both of which were inaccurate (>100% difference). Second, the industrial formulation contained a low (< 10%) amount of crosslinked PDMS amidst a large amount (> 90%) of PDMS diluent as well as gels and microgels. This low level of crosslinked PDMS and the broad size polydispersity required development of a sample preparation procedure. Different sample preparation methods were evaluated using ThFFF-MALS and the molar mass profiles indicated that centrifugation followed by filtration was the most suitable. Next, PDMS samples with different levels of crosslinking were analyzed and the log *g''* distribution for the more crosslinked sample was observed to extend to lower values (more contraction). This is as expected and showed that the *g''* approach can be used for a new polymer chemistry, PDMS, and a complex sample mixture. To date, there has been no additional verification of the Soret contraction approach. PDMS offered a unique opportunity to address this gap because this polymer can be depolymerized and GC-MS used to determine products indicative of branching. GC-MS results confirmed the degree of branching trend indicated by *g''* values and is an important step forward.

The final project presented in this thesis explores the link between D_T and the glass transition temperature (T_g). This work presents a comprehensive compilation of polymer thermal diffusion data and the first comparison of experimental D_T and T_g. Across multiple solvent systems, a strong positive correlation was observed. To understand if there is a physical connection between these two properties, the results of a first principles T_g model were compared to experimental D_T values. This work suggests that entropic forces may contribute to D_T, a factor which was explicitly ignored in the derivation of the current leading predictive model. In addition, T_g may be an alternative metric for carrier liquid selection for ThFFF analyses.

In summary, ThFFF has become an increasingly powerful tool for the characterization of complex polymer systems. This thesis presents the first reported estimation of S_T for a linear polymer utilizing leading models of translational and thermal diffusion, which has expanded the accessibility of *g''* analysis beyond systems with available linear analogs. The scope of architecture studied by *g''* now includes bottlebrushes and crosslinked networks along with the previously reported branched systems. Analyses of crosslinked PDMS also presents the first application of *g''* to an industrial polymer system. These results were also the first to be verified by alternative means. In addition, a potential link between D_T and T_g was observed that could lead to improvements in predictive models. This relationship may also serve as a simple metric for approximating the relative magnitude of D_T for polymers.

TABLE OF CONTENTS

ABSTRACT iii
LIST OF FIGURES x
LIST OF TABLES xiv
ACKNOWLEDGEMENT xv
DEDICATION xvi
CHAPTER 1 INTRODUCTION 1
1.1 Analytical Challenges and Motivation 1
1.2 Methods for Separation and Characterization of Polymers 2
1.3 Outline of Chapters 3
1.4 References 4
CHAPTER 2 BACKGROUND AND LITERATURE REVIEW 8
2.1 Separation Mechanism and Retention Theory (Normal Mode) 10
2.1.1 Sample Relaxation and Overloading in FFF 13
2.2 Flow FFF 16
2.2.1 Retention Theory 17
2.2.2 Instrumentation 18
2.2.3 Methodology 22
2.2.4 Solvent Selection 22
2.2.5 Advances in Flow FFF Instrumentation 26
2.2.6 Applications 30
2.3 Thermal Field-Flow Fractionation (ThFFF) 33
2.3.1 Analyte Retention 34
2.3.2 Methodology 36
2.3.3 Instrumentation 40
2.3.4 Advances in ThFFF Instrumentation 41
2.3.5 Applications 43
2.4 Summary 50
2.5 Acknowledgements 50
2.6 Bibliography 50

CHAPTER 3 CHARACTERIZATION OF THE ARCHITECTURAL TRAITS OF MOLECULAR BRUSHES BY SORET COEFFICIENTS FROM THERMAL FIELD-FLOW FRACTIONATION 68
3.1 Abstract 68
3.2 Introduction 69
3.3 Materials and Methods 72
3.3.1 Materials 72
3.3.2 Instrumentation 73
3.4 Theory and Calculations 73
3.4.1 Thermal Diffusion Model 73
3.4.2 Estimating D of a Linear Polymer 74
3.4.3 Measuring D for Branched Polymers 74
3.4.4 Calculating S_T for Branched and Linear Polymers 74
3.5 Results and Discussion 75
3.5.1 Comparison of Molar Masses Determined by SEC, NMR, and ThFFF-MALS-dRI 75
3.5.2 Impact of Backbone and Sidechain DP on Thermal and Translational Diffusion Coefficients 77
3.5.3 Impact of Backbone and Sidechain DP on S_T 79
3.5.4 Estimation of Linear S_T 81
3.5.5 Architectural Analysis of Bottlebrushes Via the Soret Contraction Factor 81
3.6 Conclusions 84
3.7 Acknowledgments 85
3.8 Supporting Information 85
3.9 References 87
CHAPTER 4 SAMPLE PREPARATION AND ARCHITECTURAL ANALYSIS OF AN INDUSTRIAL POLYMER FORMULATION VIA THERMAL FIELD-FLOW FRACTIONATION 93
4.1 Abstract 93
4.2 Introduction 94
4.2.1 Crosslinked Polysiloxanes 94
4.2.2 Current Sample Preparation and Characterization Methods 94
4.2.3 Objective of This Work 96
4.3 Materials and Methods 97
4.3.1 Synthesis of Crosslinked Polysiloxane 97

4.3.2 Removal of the Diluent Via Precipitation 97
4.3.3 Removal of Insoluble Gels and Soluble Microgels (> 1 μm) 97
4.3.4 Summary of Sample Preparation Steps 98
4.3.5 Thermal Field-Flow Fractionation (ThFFF) with Online Detection 98
4.3.6 Solvent Selection 99
4.3.7 Calculation of g" 99
4.3.8 Depolymerization and GC-MS of Crosslinked Polysiloxanes 100
4.3.9 GC-MS of Depolymerization Products 100
4.4 Results 101
4.4.1 Gravimetric Determination of Insoluble Gel Content 101
4.4.2 ThFFF-MALS-dRI Fractograms of Ultracentrifugation Layer Fractions 101
4.4.3 Light Scattering Results from Filtered Samples 102
4.4.4 Summary of ThFFF-MALS-dRI Results for Each Sample Preparation Method 103
4.4.5 Thermal Diffusion Coefficient of Linear and Crosslinked PDMS 104
4.4.6 Soret Contraction Factor (g") 105
4.4.7 Semi-Quantitative Gas Chromatography (GC-MS) 106
4.5 Discussion 107
4.5.1 Removal of Insoluble Gel Content 107
4.5.2 Comparison of Molar Mass Results for PDMSx1 and PDMSx2 108
4.5.3 Linear Calibration of S_T 109
4.5.4 Soret Contraction Factor Analysis 109
4.5.5 Validation of g" by GC-MS 110
4.6 Conclusion 110
4.7 Supplemental Information 111
4.8 References 112
CHAPTER 5 THE ROLE OF CHAIN DYNAMICS IN THERMAL DIFFUSION 116
5.1 Abstract 116
5.2 Introduction 116
5.2.1 Polymer Thermal Diffusion 117
5.2.2 Impact of Composition and Architecture 117
5.2.3 Predictive Models of Thermal Diffusion 118
5.2.4 The Locally Correlated Lattice Model 119

5.3 Results and Discussion 119
5.4 Conclusions 122
5.5 Experimental 123
5.6 References 123
CHAPTER 6 SUMMARY AND OUTLOOK 126
6.1 Summary 126
6.2 Outlook 127
6.3 References 128
APPENDIX A COPYRIGHT PERMISSIONS 129

LIST OF FIGURES

Figure 1.1. Representative schematic of the diversity in polymer architecture 2

Figure 2.1. General schematic of a field-flow fractionation channel operating in normal mode. A field is applied orthogonally to the flow and drives analytes towards the accumulation wall. This field-induced flux is countered by diffusion and at equilibrium analytes reach some mean layer thickness, ℓ, which may be related to the retention ratio, R, through Equations 2.2 and 2.4. In a channel of thickness, *w*, separation of retained analytes occurs near the accumulation wall. 10

Figure 2.2. Comparison of linear, quadratic, and cubic approximations of the exact retention expression relating both dimensionless retention ratio (R) and retention parameter (λ). 13

Figure 2.3. (A) Overloading behavior of 200 kDa polystyrene in THF with increasing concentration from 0.5 mg/mL to 4 mg/mL and 20 µL sample volume. (B) Black trace is an ultra-high molecular weight bottlebrush polymer which has been in solution for 24 hours and is not fully solubilized; the dotted trace is the same polymer which has been in solution for 1 week. 16

Figure 2.4. Different variants of flow FFF. (A) symmetrical flow FFF has a rectangular channel geometry with two permeable walls and was the original configuration, (B) asymmetrical flow FFF (AF4) also uses in a rectangular channel geometry but has only one permeable wall, and (C) hollow fiber flow FFF uses a hollow fiber membrane or ceramic tube. (Reprinted with permission from [39].) 19

Figure 2.5. AF4 fractograms. (A) mixture of 5 µg each of polystyrene sulfonate (PSS) polymer standards in Tris buffer. (B) protein mixture: 1- carbonic anhydrase (29 kDa), 2- bovine serum albumin (66 kDa), 3- alcohol dehydrogenase (150 kDa), 4- apoferritin (444 kDa), and 5- thyroglobulin (669 kDa). (Reprinted with permission from [41] and [42]) 20

Figure 2.6. Schematic representation of an AF4 channel during the fractionation steps. (A) focusing/relaxation: Sample is introduced through the injection port, while two opposing carrier flows are pumped in from both the channel inlet and outlet. Fluid exits through the semipermeable membrane and porous frit wall while providing the essential crossflow that drives analytes to the accumulation wall. Upon relaxation, two different *D* (or size) species have two different mean layer thicknesses. (B) elution: A single flow of carrier fluid from the channel inlet serves as the source of both the crossflow and the channel flow. The latter carries analytes down the length of the channel towards the detector. 26

Figure 2.7. (A) Schematic representation of AF4 separation with flat microstructured membranes. (B) Electron microscopy image of microstructured membrane. (Reprinted with permission from [85].) 27

Figure 2.8. Fractograms of polystyrene latex beads (46 and 100 nm in diameter) obtained with channel of different dimensions. The respective values of b_L= minimum channel breadth and b_0 = maximum channel breadth are reported in the graph. (Reprinted with permission from [86].) 29

Figure 2.9. Comparison of fractograms of mixtures of polystyrene nanoparticles in a conventional (black) and a miniaturized (red) AF4 channel. Insert shows the crossflow profile utilized. (Reprinted with permission from [95].) 30

Figure 2.10. Variation of the *v*-parameter with respect to the Andrade scaling parameter (*B*) for various solvents. Note that curves were calculated for several cold wall temperatures (T_c) assuming a constant ΔT of 80 K and that variation of ΔT yields a new set of curves. A value for *v* (open star) was determined based on typical ThFFF conditions: T_c = 27°C, ΔT = 80 K, and *B* = 1627.7 K. Figure 2.10b depicts the temperature variation in viscosity for ethanol, an exponential decay in the form displayed allows for the determination of *B* used in Figure 2.10a. 36

Figure 2.11. Programmed temperature field decay separation of PS standards (23.8, 104, 254, 575, 1290, and 3150 kDa) using Equation 2.13 where t_1 = 10, t_a = -20, p = 2. Carrier fluid is methyl ethyl ketone, t^0 = 10 min. 39

Figure 2.12. FTIR data collected from online fractionation of PS-PMMA copolymer blends by ThFFF. ΔT = 60 K, T_c = 25°C, and flow rate = 0.3 mL/min. (Reprinted with permission from [189]) 43

Figure 2.13. Mole fraction component analysis of terpolymer comprised of PS, PMMA, and poly(tert-butyl acrylate) (PtBA). (Reprinted with permission from [190]) 45

Figure 2.14. Distribution of g" within each sample where SY-# indicates the degree of branching as determined by NMR. The dashed lines represent error for the linear region. (Reprinted with permission from [196]) 47

Figure 2.15. ThFFF-MALS analysis of unfiltered and filtered PVAc10 (poly (vinyl acetate)). The filter was 0.5 μm pore-size. (A) Intensity at 90° angle (I_{90}) fractograms and molar masses and (B) dRI fractograms and r_{rms}. Solid and dashed lines represent the fractograms of unfiltered and filtered PVAc10, respectively. The black and gray lines correspond to MW or r_{rms} of the unfiltered and filtered PVAc10, respectively. (Reprinted with permission from [146]). 49

Figure 3.1. Effect of polymer architecture on retention level R_L (normalized to account for varied flowrates and MALS detector intensity). A) fractograms of 100g22 (black), 100g60 (red), and 100g120 (blue) and B) fractograms of 400g49 (black) and 100g60 (red). The channel flow rate was 0.2 mL min^{-1} except for 100g22 which was 0.1 mL min^{-1}. 79

Figure 3.2 Change in Soret coefficient with respect to A) backbone length (DP) and B) sidechain length (DP). Labels indicate the DP of the sidechain (A) and backbone (B). 80

Figure 3.3. Plot of $S_{T,br}$ vs. $S_{T,lin}$ for bottlebrushes with 100% (▲) and 30% (●) grafting density, where $S_{T,lin}$ is approximated at an equivalent molar mass to $S_{T,br}$. Branched polymers are expected to fall below the solid line (y = x), as their physiochemical properties are contracted relative to that of a linear analog. 82

Figure 3.4. Plot of log (*g''*) versus molar mass for bottlebrushes with 100% (▲) and 30% (●) grafting density. 83

Figure 3.5. Plot of log (*g''*) with respect to the number of chain ends for branched polyesters (●), bottlebrushes of 30% (●), and 100% (▲) grafting density. Data for hyperbranched polyesters is from literature [21]. 84

Figure 3.6. R_g is unavailable for some polymers in the series (where R_g < 10 nm), a plot of g_{Rh} (or the contraction in R_h) is used in comparison to *g''* results seen in Figures 3.5 and 3.7. 86

Figure 3.7 A plot of log (*g''*) with respect to the number of chain-ends for branched polyesters (●), bottlebrushes of 30% (●), and 100% (▲) grafting density. Poly(methyl methacrylate) (PMMA), like PnBA but with readily available linear standards, was chosen as an alternative linear analog. $S_{T,lin}$ in **(A)** was estimated as outlined in *Theory and Calculations*. $S_{T,lin}$ in **(B)** was estimated via an experimentally determined calibration curve of S_T with respect to the molar mass (from 100-300 kDa). The degree of contraction for higher molar mass brushes was considerably increased using PMMA instead of PnBA in the theoretical approach. The experimentally determined calibration curve yielded results more similar to Figure 3.5. 86

Figure 4.1. Sample preparation schemes for gel containing polymer formulation. 98

Figure 4.2. MALS (upper) and dRI (lower) fractograms of PDMSx1 fractionated by ultracentrifugation into three volumetric layers. Layer one is in black, layer two in red, and layer three in blue. 102

Figure 4.3. Fractograms with molar mass and root mean square radii results for filtered PDMSx1 (A), filtered PDMSx2 (C), ultracentrifuged and filtered PDMSx1 (B), and ultracentrifuged and filtered PDMSx2 (D). 103

Figure 4.4. Plots of triplicate chromatograms with the MALS intensity at 90° and log g" for PDMSx1 (top) and PDMSx2 (bottom) with their corresponding histograms on the right. 106

Figure 4.5. Overloading behavior of PMDSx2 as a function of concentration before removal of the diluent. 111

Figure 4.6. A fractogram, where the Y-axis is the MALS intensity at 90°, of replicate injections of PDMSx2 at a concentration of 2 mgmL^{-1}. These samples were injected after the diluent was removed and with no further preparation. 111

Figure 4.7. The bottom plot is a fractogram of triplicate injections of the linear analog, vinyl terminated PDMS, with molar mass (MM) plotted in a log scale. Using Equation 4.1, this data was processed into a log-log plot (top) relating molar mass to S_T. 112

Figure 4.8. Triplicate fractograms of PDMSx2 layer one fractions from ultracentrifugation carried out for different times: (A) 3 hours, (B) 6 hours, and (C) 12 hours. Results displaying RMS (A1-C1) are accompanied by the MALS trace and results displaying molar mass (A2-C2) are accompanied by the dRI trace. 112

Figure 5.1. Experimental D_T of polymers dissolved in organic solvents where the x-axis is arranged in order of increasing relative polarity. 120

Figure 5.2. Observed relationship between D_T and T_g for polymers dissolved in tetrahydrofuran, toluene, cyclohexane, and methyl ethyl ketone. 121

Figure 5.3. Observed relationship between D_T and entropy per segment, as calculated by the locally correlated lattice model [31], for polymers in tetrahydrofuran, toluene, cyclohexane, and methyl ethyl ketone. 122

LIST OF TABLES

Table 2.1. Selected examples of membrane chemistry and MWCO recently used in AF4 characterization of different samples. 21

Table 2.2. Selected examples of carriers recently used in flow FFF characterization of different samples. 23

Table 2.3. List of common polymer-solvent combinations for ThFFF. 37

Table 3.1. Summary of bottlebrush characterization results by NMR, SEC, and ThFFF-MALS-dRI..... 76

Table 3.2. Measured S_T, D_T, and D values for bottlebrush library..... 78

Table 3.3. Bottlebrush root-mean-square (R_{rms}) and hydrodynamic radii (R_h) determined by online MALS and QELS. 85

Table 4.1. Calculated D_T values for linear PDMS in various organic solvents as determined by methods outline in literature[18], [26]. 99

Table 4.2. Molar mass and gel content results for PDMSx1 and PDMSx2..... 104

Table 4.3. Thermal diffusion coefficients for linear PDMS and PDMSx2. 105

Table 4.4. Peak area of relevant GC-MS peaks and the normalized area of the ethylene linkage. 107

ACKNOWLEDGEMENT

Life offers many transformative experiences which can reshape our view of the world – love, death, achievement, and tragedy. The years that are compressed into this thesis have borne witness to each of these. I would like to give a special thank you to the people who carried me through the difficult times and filled my life in moments of joy. Christine, Glory, Daniel, Daniel, Vu, Asa, Nick, Kara, Chiqui, Nicholas, Scott, Nolan, Margaret, Gun, An, Alison – our time together was truly a treasure.

My deepest gratitude to Dr. Billy Smith for his patience and guidance in passing the torch. Dr. Kim Williams, your abundant patience with your argumentative pupil has not gone unnoticed. The Williams Group, past and present, thank you for your invaluable contributions and countless hours in group meetings. Charlie and Carmen, while we did not overlap, your advice and friendship have made the research group truly feel like an extended family. Our work would not be possible without the Colorado School of Mines Chemistry Department, the wonderful people who built it up, and those who have kept it running – thank you for making Mines a special place. I will miss cruising by the front office to bug Samuel, Megan, and Tom but I am sure they will not miss me as much as my officemate. I would also like to thank Ed Dempsey for his tireless efforts to repair everything that we break. If I manage to work half as hard as you, I will consider myself successful.

Ron White, thank you for the enjoyable technical discussions and encouragement to explore the world of polymer physical chemistry. The entire Dow team for their continued support through the GOALI project, which provided the resources and direction for much of my time at Mines.

Completing this thesis has been one of the most challenging and rewarding experiences of my life. Thank you for riding the rollercoaster with me Faith.

To my grandmothers who gave me
the most important education.

Amar es encontrar en la felicidad
de otro la propia felicidad

CHAPTER 1
INTRODUCTION

1.1 Analytical Challenges and Motivation

Advanced polymer materials are at the forefront of technological advancement in areas ranging from medicine to agriculture and other industrial applications [1]–[4]. The broad versatility of these materials can be attributed to the high degree of tunability in polymer chemistry. Simply increasing the length of a chain (molar mass) can result in different solution and bulk properties. Alternatively, altering chemical composition can greatly change its physiochemical properties. For example, control of π-conjugation in a polymer chain can be used to tune the band gap, a useful electronic property for device manufacturing [2]. Conversely, a polymer without π-conjugation may be an insulator with good mechanical properties and serve a different function in a device stack [2]. A polymer chain may also be composed of multiple compositions, where the components are either arranged in blocks or randomly distributed throughout the chain. This leads to greater diversity in physiochemical properties as well as additional characterization challenges. In addition to composition, a polymer chain may be modified by the addition of branching. A schematic representation of the architectural diversity in polymers is shown in Figure 1.1. Different branching structures can impart distinct functions to the polymer chain or modify existing ones [3], [5], [6]. It is well established that crosslinking increases mechanical and thermal stability. In the case of lithium ion conducting polymers, it was shown that star-shapes are one to two times more conductive than their linear counterparts [7]. However, in polymer synthesis there can be heterogeneities in all the aforementioned properties: molar mass (size), composition, and architecture [8], [9]. To probe the relationship between structure and function, each of these properties and their heterogeneities need to be well characterized. Common ensemble techniques like Fourier transform infrared (FTIR) spectroscopy [10], nuclear magnetic resonance (NMR) spectroscopy [11], light scattering [12], [13], and mass spectrometry [14] are limited to reporting only average values. For polymers, it is generally accepted that separation of the analyte prior to analysis by an ensemble method is essential to obtaining information about distributions in measured properties.

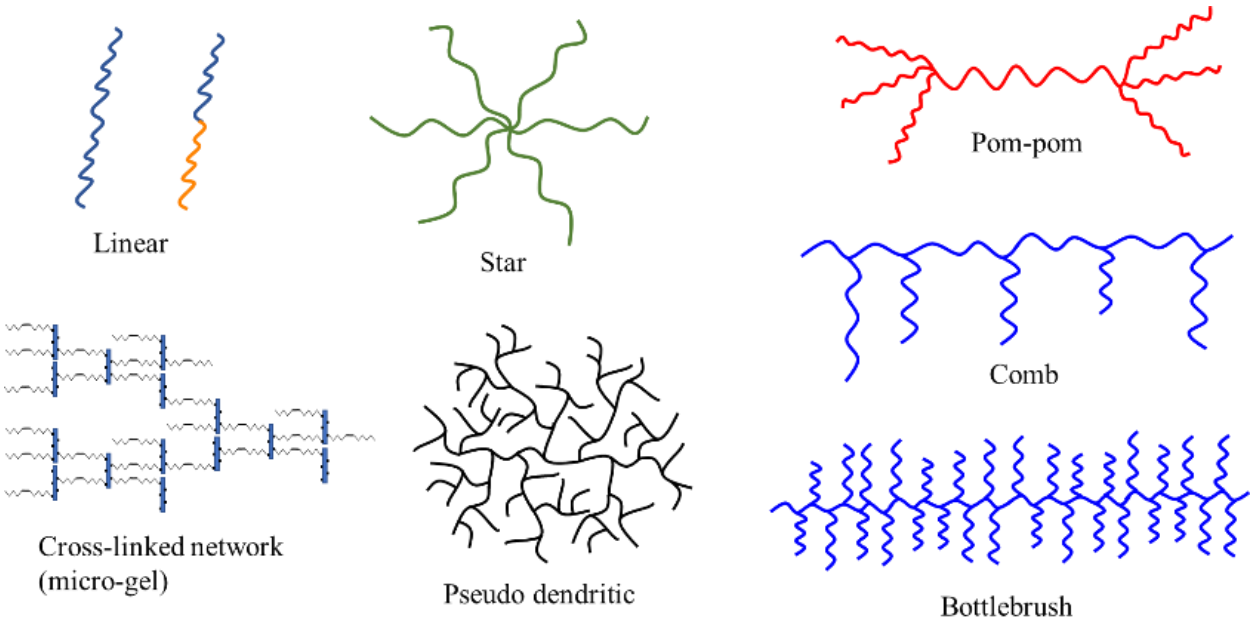

Figure 1.1. Representative schematic of the diversity in polymer architecture

1.2 Methods for Separation and Characterization of Polymers

Chromatography has long been the standard for polymer separations [15]. Of the chromatographic methods, size exclusion chromatography (SEC) is most used for its simplicity as it separates only by hydrodynamic diameter under ideal elution conditions. Ideally, this is an entropic based separation with no enthalpic interactions between the stationary phase and the analyte [15]. The quality of the separation may then be modulated by changing the pore size of the packing material or altering the size of the solvated polymer by changing the thermodynamic quality of the solvent. Separations may also be designed around a polymer's enthalpic interactions with the packing material. In this case, elution may be controlled by altering the eluent composition to drive differential elution based upon the strength of the interaction [15]. Alternatively, since enthalpic interactions are temperature dependent, the ambient temperature of the column compartment may be adjusted to drive retention or elution of the species [16]. This technique is known as temperature gradient interaction chromatography and may result in separations based on composition, architecture, or both. The last major category of chromatography is under the critical condition where entropy and enthalpy are balanced, resulting in a separation driven solely by composition. No theoretical description has been developed which can predict the retention time of an analyte under a set of chromatographic conditions or determine a physiochemical property based upon the retention time, unless a

calibration using known standards is first employed [17]. For this reason, online detection schemes that measure properties such as size, molar mass, composition, and branching [18] of eluting components are essential. The most ubiquitous online detector for characterizing molar mass, size, and branching is multi-angle light scattering (MALS). To calculate the molar mass of the analyte, the concentration must be known. This is typically achieved through a differential refractometer which relates the change in refractive index (dRI) to concentration. Alternatively, species which absorb ultraviolet (UV) light can be quantified by online UV-vis detectors. If the polymer is comprised of two different monomers, it is sometimes possible to use MALS in combination with UV-vis and dRI to determine the mass, and thus molar mass, of each component [19]. Other typical detectors include viscometers for determination of intrinsic viscosity and dynamic light scattering (DLS) for determination of the hydrodynamic radius. These online detection schemes are typically used in two ways to assess branching, i.) comparison of the mass scaling relationship between either intrinsic viscosity or radius to a linear analog and ii.) the ratio of a physical property of a branched polymer to that of a linear analog of the same molar mass [8], [20], [21]. In either case, these analyses may be frustrated by the non-ideal elution of a polymer [8], [21].

Chromatographic methods are generally hindered by the non-ideal elution of polymers with high molar mass and branching ($>10^6$ Da) [8]. It is hypothesized that the non-ideal elution profiles are the result of chain anchoring on the packing beads of a chromatographic column. This can lead to irreversible adsorption or even chain scissions. Field-flow fractionation (FFF) is a family of techniques in which the separation occurs in an open channel instead of a packed column [22], [23]. This allows for the analysis of materials which would typically elute non-ideally or require additional sample preparation [24]. An in-depth discussion on the separation and characterization of polymers via FFF and the use of online detectors can be found in Chapter 2.

1.3 Outline of Chapters

The purpose of this research is to study the thermophoretic behavior of complex polymers and leverage this knowledge to advance the capabilities of Thermal FFF for the characterization of industrially relevant materials. A summary of the specific research objectives of this work are as follows. Chapter 2 is a comprehensive practical guide to the theory and

modern applications of ThFFF with multiple detectors for the separation and characterization of polymers [22]. Chapter 3 is an investigation of the relationship between the Soret coefficient (S_T) and the architectural characteristics of a model bottlebrush polymer library. This work demonstrated a linear relationship between S_T and the degree of polymerization of the backbone and sidechain, which could be exploited in the routine analysis of this bottlebrush material via ThFFF. In addition, it was shown that the S_T of a linear polymer could be estimated using a predictive model of thermal diffusion which is a factor in the calculation of the Soret contraction factor (*g''*), a novel method of branching analysis. This yielded insights into the thermophoretic behavior of branched polymers and expanded the scope of *g''* literature to include novel architectures and polymer chemistries. With the addition of my work on bottlebrushes, *g''* literature now spans a more diverse set of polymer chemistries and architecture. However, to become industrially relevant it must be expanded further to the analysis of polymer-based formulations. Chapter 4 describes both the unique sample preparation required for an industrial formulation containing crosslinked polysiloxanes and its architectural analysis through *g''*. This work was validated by GC-MS experiments, a possibility afforded by the ability to depolymerize polysiloxanes. In addition, this work demonstrated the same thermophoretic trend observed in Chapter 3 – the thermal diffusion coefficient (D_T) of a branched polymer was significantly lower than that of the linear analog. This is an important finding in the development of *g''* analysis as it may impact the analysis. The decrease in D_T for a branched polymer is not readily predicted by current models and to-date there is no theoretical description for thermophoresis of polymers in solution [25], [26]. This led to Chapter 5, an investigation into the relationship between D_T and the glass transition temperature (T_g), a property also impacted by branching. Although thermal diffusion is strongly solvent dependent, polymers with a high T_g have a corresponding large D_T, relative to other polymers in that solvent system. A first principles model of T_g indicates that the segmental entropy of a polymer chain is the primary factor controlling this property [27], [28]. By relation, this indicates that entropic forces may also be a factor in thermophoresis. Current predictive models ignore entropic contributions to D_T.

1.4 References

[1] R. Hsissou, R. Seghiri, Z. Benzekri, M. Hilali, M. Rafik, and A. Elharfi, "Polymer composite materials: A comprehensive review," *Compos Struct*, vol. 262, no. November 2020, p. 113640, Apr. 2021, doi: 10.1016/j.compstruct.2021.113640.

[2] D. Gao, J. Lv, and P. S. Lee, “Natural Polymer in Soft Electronics: Opportunities, Challenges, and Future Prospects,” *Advanced Materials*, vol. 34, no. 25, p. 2105020, Jun. 2022, doi: 10.1002/adma.202105020.

[3] L. Y. Qiu and Y. H. Bae, “Polymer architecture and drug delivery,” *Pharm Res*, vol. 23, no. 1, pp. 1–30, 2006, doi: 10.1007/s11095-005-9046-2.

[4] F. Puoci, F. Iemma, U. G. Spizzirri, G. Cirillo, M. Curcio, and N. Picci, “Polymer in agriculture: A review,” *American Journal of Agricultural and Biological Science*, vol. 3, no. 1, pp. 299–314, 2008, doi: 10.3844/ajabssp.2008.299.314.

[5] B. Voit and D. Appelhans, “Glycopolymers of various architectures-more than mimicking nature,” *Macromol Chem Phys*, vol. 211, no. 7, pp. 727–735, 2010, doi: 10.1002/macp.201000007.

[6] X. Zhu, Y. Zhou, and D. Yan, “Influence of branching architecture on polymer properties,” *J Polym Sci B Polym Phys*, vol. 49, no. 18, pp. 1277–1286, 2011, doi: 10.1002/polb.22320.

[7] S. M. Hao *et al.*, “Lithium-Conducting Branched Polymers: New Paradigm of Solid-State Electrolytes for Batteries,” *Nano Lett*, vol. 21, no. 18, pp. 7435–7447, 2021, doi: 10.1021/acs.nanolett.1c02558.

[8] S. Podzimek, T. Vlcek, and C. Johann, “Characterization of branched polymers by size exclusion chromatography coupled with multiangle light scattering detector. I. Size exclusion chromatography elution behavior of branched polymers,” *J Appl Polym Sci*, vol. 81, no. 7, pp. 1588–1594, Aug. 2001, doi: 10.1002/app.1589.

[9] S. Podzimek, “Molar mass distribution by size exclusion chromatography: Comparison of multi-angle light scattering and universal calibration,” *J Appl Polym Sci*, vol. 136, no. 21, p. 47561, Jun. 2019, doi: 10.1002/app.47561.

[10] S. L. Hsu, J. Patel, and W. Zhao, “Vibrational spectroscopy of polymers,” in *Molecular Characterization of Polymers*, M. I. Malik, J. Mays, and M. R. B. T.-M. C. of P. Shah, Eds. Elsevier, 2021, pp. 369–407. doi: 10.1016/B978-0-12-819768-4.00010-5.

[11] T. Miyoshi, “Characterization of polymers by NMR,” in *Molecular Characterization of Polymers*, M. I. Malik, J. Mays, and M. R. B. T.-M. C. of P. Shah, Eds. Elsevier, 2021, pp. 409–440. doi: 10.1016/B978-0-12-819768-4.00013-0.

[12] P. S. Russo, K. A. Streletzky, W. Huberty, X. Zhang, and N. Edwin, “Characterization of polymers by static light scattering,” in *Molecular Characterization of Polymers*, M. I. Malik, J. Mays, and M. R. B. T.-M. C. of P. Shah, Eds. Elsevier, 2021, pp. 499–532. doi: 10.1016/B978-0-12-819768-4.00015-4.

[13] P. S. Russo, K. A. Streletzky, A. Gorman, W. Huberty, and X. Zhang, “Characterization of polymers by dynamic light scattering,” in *Molecular Characterization of Polymers*, M. I. Malik, J. Mays, and M. R. B. T.-M. C. of P. Shah, Eds. Elsevier, 2021, pp. 441–498. doi: 10.1016/B978-0-12-819768-4.00014-2.

[14] A. P. Gies, “Mass spectrometry of polymers,” in *Molecular Characterization of Polymers*, M. I. Malik, J. Mays, and M. R. B. T.-M. C. of P. Shah, Eds. Elsevier, 2021, pp. 305–368. doi: 10.1016/B978-0-12-819768-4.00006-3.

[15] M. I. Malik and H. Pasch, “Basic principles of size exclusion and liquid interaction chromatography of polymers,” in *Molecular Characterization of Polymers*, M. I. Malik, J. Mays, and M. R. B. T.-M. C. of P. Shah, Eds. Elsevier, 2021, pp. 1–59. doi: 10.1016/B978-0-12-819768-4.00007-5.

[16] T. Chang, H. C. Lee, W. Lee, S. Park, and C. Ko, “Polymer characterization by temperature gradient interaction chromatography,” *Macromol Chem Phys*, vol. 200, no. 10, pp. 2188–2204, 1999, doi: 10.1002/(sici)1521-3935(19991001)200:10<2188::aid-macp2188>3.3.co;2-6.

[17] S. Podzimek, “Truths and myths about the determination of molar mass distribution of synthetic and natural polymers by size exclusion chromatography,” *J Appl Polym Sci*, vol. 131, no. 7, pp. 1–9, 2014, doi: 10.1002/app.40111.

[18] A. Lederer and J. Brandt, “Multidetector size exclusion chromatography of polymers,” in *Molecular Characterization of Polymers*, M. I. Malik, J. Mays, and M. R. B. T.-M. C. of P. Shah, Eds. Elsevier, 2021, pp. 61–96. doi: 10.1016/B978-0-12-819768-4.00012-9.

[19] C. A. Ponyik, D. T. Wu, and S. K. R. Williams, “Separation and composition distribution determination of triblock copolymers by thermal field-flow fractionation,” *Anal Bioanal Chem*, vol. 405, no. 28, pp. 9033–9040, Nov. 2013, doi: 10.1007/s00216-013-7282-6.

[20] K. Haydukivska, V. Blavatska, and J. Paturej, “Universal size ratios of Gaussian polymers with complex architecture: radius of gyration vs hydrodynamic radius,” *Sci Rep*, vol. 10, no. 1, pp. 1–11, 2020, doi: 10.1038/s41598-020-70649-z.

[21] S. Podzimek and T. Vlcek, “Characterization of branched polymers by SEC coupled with a multiangle light scattering detector. II. Data processing and interpretation,” *J Appl Polym Sci*, vol. 82, no. 2, pp. 454–460, Oct. 2001, doi: 10.1002/app.1871.

[22] M. Toney, L. Baiamonte, W. C. Smith, S. Kim Ratanathanwongs Williams, S. Kim Ratanathanawongs Williams, and S. K. R. Williams, “Field-flow fractionation techniques for polymer characterization,” in *Molecular Characterization of Polymers*, Elsevier, 2021, pp. 129–171. doi: 10.1016/B978-0-12-819768-4.00004-X.

[23] C. L. Plavchak, W. C. Smith, C. R. M. Bria, and S. K. R. Williams, “New Advances and Applications in Field-Flow Fractionation,” *Annual Review of Analytical Chemistry*, vol. 14, no. 1, pp. 257–279, 2021, doi: 10.1146/annurev-anchem-091520-052742.

[24] D. Lee and S. K. R. Williams, “Thermal field-flow fractionation and multiangle light scattering of polyvinyl acetate with broad polydispersity and ultrahigh molecular weight microgel components,” *J Chromatogr A*, vol. 1217, no. 10, pp. 1667–1673, 2010, doi: 10.1016/j.chroma.2010.01.035.

[25] J. R. Runyon and S. K. R. Williams, “A theory-based approach to thermal field-flow fractionation of polyacrylates,” *J Chromatogr A*, vol. 1218, no. 39, pp. 7016–7022, Aug. 2011, doi: 10.1016/j.chroma.2011.08.007.

[26] M. Geisler, L. Plüschke, J. Merna, and A. Lederer, “The Role of Solubility in Thermal Field-Flow Fractionation: A Revisited Theoretical Approach for Tuning the Separation of Chain Walking Polymerized Polyethylene,” *Anal Chem*, vol. 92, no. 21, pp. 14822–14829, Nov. 2020, doi: 10.1021/acs.analchem.0c03686.

[27] R. P. White and J. E. G. Lipson, “A Simple New Way to Account for Free Volume in Glassy Dynamics: Model-Free Estimation of the Close-Packed Volume from PVT Data,” *Journal of Physical Chemistry B*, vol. 125, no. 16, pp. 4221–4231, 2021, doi: 10.1021/acs.jpcb.1c01620.

[28] R. P. White and J. E. G. Lipson, “How Free Volume Does Influence the Dynamics of Glass Forming Liquids,” *ACS Macro Lett*, vol. 6, no. 5, pp. 529–534, 2017, doi: 10.1021/acsmacrolett.7b00179.

CHAPTER 2
BACKGROUND AND LITERATURE REVIEW

Originally published in *Molecular Characterization of Polymers*.[1]
Michael Toney[2], Luca Baiamonte[2], William C. Smith[2], S. Kim Ratanathanwongs Williams[2]

Field-flow fractionation (FFF) was introduced in a seminal paper by the late J. Calvin Giddings in 1966 [1]. Herein he laid the foundational principles by which FFF operates; analytes introduced into a separation chamber with laminar flow may be differentially separated by an applied field which is orthogonal to the flow stream. The many variants of channel design and field types make FFF uniquely adaptable for the characterization and separation of macromolecules, colloids, and micrometer-sized particles [2]–[9]. The FFF separation bears resemblances to chromatography and the latter serves as a useful point of comparison. Like chromatography, FFF operation entails the injection of a narrow sample band into an elongated flow chamber, differential elution of analyte species in a laminar flow, and on-line detection. Unlike chromatography, whose retention mechanism is governed by analytes partitioning in a two-phase system, FFF relies on an externally applied field that interacts with and transports analytes to different velocity streams across an open channel. Various 'fields' (electric, thermal, gravitational, crossflow, magnetic, dielectrophoretic, etc.) are applied to drive separations based on different physiochemical properties and give rise to different FFF techniques. In 1967, the first FFF experiment employed a temperature gradient to separate 3 and 400 kDa polystyrene. In the following years, new techniques were added to the family which leverages other fields: sedimentation [10], flow [11], electrical [12], magnetic [13], dielectric [14], electric [12], and light [15]. A general schematic of an FFF channel operating in normal mode separation is illustrated in Figure 2.1.

FFF techniques in general possess several advantages due to their open channel design. Shear stress and degradation are greatly reduced which allows for the analysis of fragile

[1]M. I. Malik, J. W. Mays, and M. R. Shah, *Molecular characterization of polymers: A fundamental guide*. Elsevier, 2021.
[2]*Laboratory for Advanced Separations Technologies, Department of Chemistry, Colorado School of Mines, Golden, USA.*

materials such as loosely bound complexes and ultrahigh molecular weight macromolecules [16]. Sample recovery is often superior to chromatography due to reduced channel surface area and a different separation mechanism. FFF can also separate analytes which are highly disperse and range in size from a few nanometers to approximately one micron in normal mode. This represents a significantly larger range and higher exclusion limit than size exclusion chromatography (SEC) [17]. Another advantage to the open channel design is that sample preparation is minimal. Microgels, which would normally be removed by filtration prior to SEC, may be injected directly into a channel and information obtained about the soluble polymer and microgel components [18]. In polymer analysis, flow FFF (FlFFF) and thermal FFF (ThFFF) stand out for their complementary and unique features. The FFF separation mechanism takes two forms depending on the size of the analyte species. In the normal mode, analytes from a few nanometers to approximately one micrometer in size are separated with the high diffusing (or small size) species eluting first contrary to the elution order for SEC. Furthermore, the retention time-size relationship can be predicted by FFF theory for normal mode (< 1 μm), particularly for FlFFF. When analytes are micrometers in size, the separation mechanism changes to steric or hyperlayer mode with large species eluting first and sizes are determined from calibration plots established using size standards [19], [20]. Only normal mode flow and thermal FFF will be covered in this chapter.

The remainder of Section 2.1 addresses FFF theory and practices from a general perspective that encompasses all FFF techniques. Section 2.2 focusses on flow FFF and Section 2.3 emphasizes thermal FFF with discussions on FFF theory, instrumentation, practices, applications, and advances.

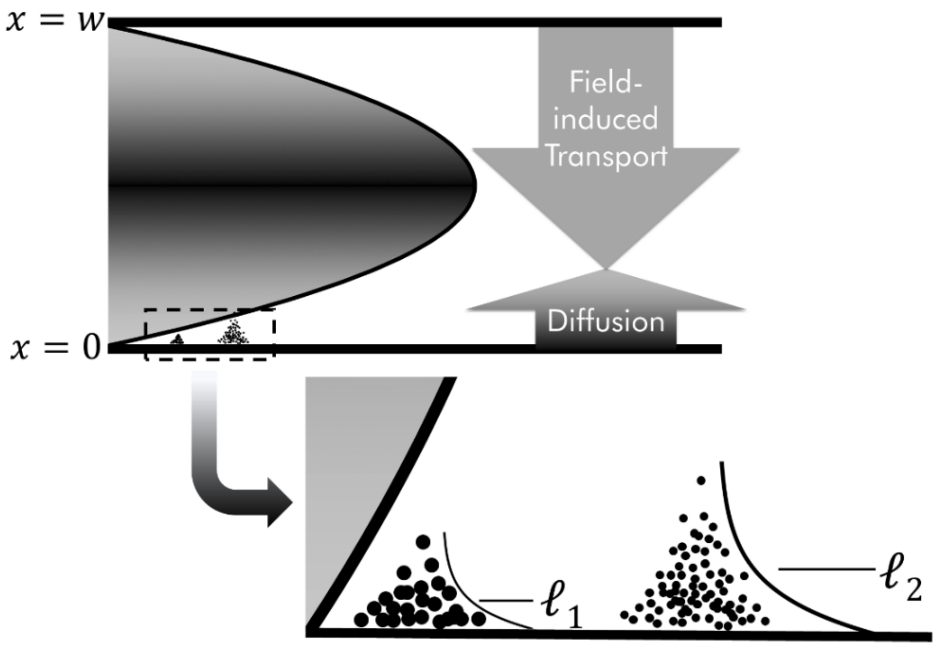

Figure 2.1. General schematic of a field-flow fractionation channel operating in normal mode. A field is applied orthogonally to the flow and drives analytes towards the accumulation wall. This field-induced flux is countered by diffusion and at equilibrium analytes reach some mean layer thickness, ℓ, which may be related to the retention ratio, R, through Equations 2.2 and 2.4. In a channel of thickness, *w*, separation of retained analytes occurs near the accumulation wall.

2.1 Separation Mechanism and Retention Theory (Normal Mode)

The mathematical basis of the FFF retention mechanism is founded on the assumption that particles behave ideally at infinite dilution where analyte species are of negligible size with respect to the channel thickness [21]. Due to the high aspect ratio of the channel breadth (*b*) to thickness (*w*), liquid flowing through the channel can be treated as flowing between two infinitely parallel plates. At low flow rates, and accordingly low Reynolds numbers, the velocity profile of the carrier fluid is parabolic with the maximum velocity in the center of the channel and the minima at the walls, where due to frictional drag, velocity approaches zero. With no external field applied, an analyte will sample every flow streamline in the velocity profile. The analyte will then travel at the average speed of the eluent and elute from the channel at void time (t^0), which is dictated by the volumetric flow rate and channel dimensions. With an external field, analyte retention is governed by the specific interaction between the physiochemical properties of the analyte. Retention typically increases with the magnitude of the applied field. The type of field used gives rise to different FFF techniques such as electrical FFF (for charged

analytes), crossflow FFF (for different hydrodynamic size), thermal FFF (for size and composition), sedimentation FFF (for different mass), and so on [22].

Existing equations relating field strength and analyte physicochemical properties combined with the known equation for parabolic flow enables prediction of retention times. Alternately, analyte properties can be calculated from measured retention times, imparting both separation and characterization capabilities to FFF. In an FFF experiment, an external field is applied orthogonal (the *x*-direction as shown in Figure 2.1) to the channel flow and drives analytes towards one of the walls, termed the sample accumulation or collection wall [23]. This field-induced transport (U) of analyte components is counteracted by their intrinsic translational diffusive flux (D) due to the resultant concentration gradient [24]. At steady state, the field-induced flux and diffusive flux are in equilibrium and the net analyte flux is zero. This produces an exponential concentration profile with a mean layer thickness or average distance from the collection wall (ℓ) as defined by $\ell = D/|U|$. The concentration profile is thus described as

$$\frac{c(x)}{c_0} = exp(-\frac{|U|}{D}x) = exp(-\frac{x}{\ell}) \tag{2.1}$$

where the concentration is highest near the accumulation wall (c_0) and decreases exponentially towards the opposite wall. The ratio of the mean layer thickness (ℓ) to channel width (w) gives rise to

$$\lambda = \frac{\ell}{w} = \frac{D}{|U|w} \tag{2.2}$$

where λ is the dimensionless retention parameter that forms the basis of all FFF retention equations. The mean layer thickness depends on both the diffusional and field-induced transports which results in each analyte component having a characteristic λ value based on its intrinsic diffusion coefficient and specific interaction with the field.

The retention parameter λ provides a direct relation between an analyte's physicochemical properties, the strength of the field, and the analyte's average location and velocity in the parabolic flow profile within the channel. Retention time (t_r) is dependent on the magnitude of the analyte's interaction with the applied field and the volumetric flow rate in the channel. An alternate metric of retention is the dimensionless retention ratio (R) which is defined as the ratio of the mean fluid velocity ($\langle v \rangle$) to the analyte migration velocity (v_p)

$$R = \frac{v_p}{< v >} = \frac{t^0}{t_r} \tag{2.3}$$

The retention ratio can also be written in terms of average analyte retention time (t_r) and void time (t^0). Taking into consideration the concentration profile (Equation 2.1) and substituting in a parabolic function for the velocity *v*, an expression for *R* in terms of λ can be produced yielding

$$R = 6\lambda\left(coth\frac{1}{2\lambda} - 2\lambda\right) \tag{2.4}$$

This is the fundamental and exact form of the retention equation for all FFF techniques. Various approximations of Equation 2.4 have been used [25] with the simplest form $R = 6\lambda$ being the most common. Deviations of these approximations from the exact expression can be seen in Figure 2.2 where *R* is plotted as a function of λ. The linear approximation $R = 6\lambda$ deviates < 4% for *R* below 0.1 but climbs to ~30% for $R = 0.6$. The quadratic relationship $R = 6\lambda - 12\lambda^2$ is accurate to less than 1% when $R < 0.6$ then increases to 3% for $R = 0.7$ and should not be used beyond 0.7 as the error increases rapidly. Likewise, the cubic approximation stays within an error of 1.5% for $R < 0.6$ with the error increasing to 7% at $R = 0.8$ and ~15% at $R = 0.9$. Due to this consideration when calculating physicochemical properties from λ for analytes with $R > 0.6$, it is important to use the exact form of the FFF retention equation.

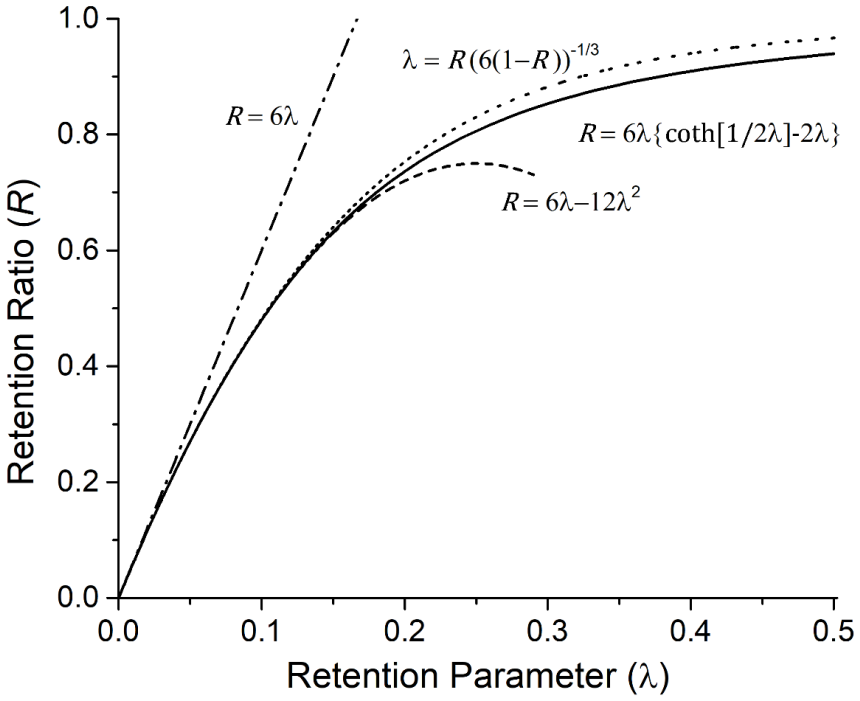

Figure 2.2. Comparison of linear, quadratic, and cubic approximations of the exact retention expression relating both dimensionless retention ratio (R) and retention parameter (λ).

2.1.1 Sample Relaxation and Overloading in FFF

2.1.1.1 Sample Relaxation

Sub-micrometer samples usually require no specific pretreatment besides the ability to form a stable suspension or solution. The absence of packing material permits the FFF analysis of analytes that would typically need filtration prior to chromatographic separation. When a sample is introduced into the FFF channel, two significant changes in concentration are observed. The sample is initially diluted as the concentrated plug enters the channel, field-induced transport then causes the sample components to concentrate and relax into distinct equilibrium distributions, e.g., ℓ_1, ℓ_2, in Figure 2.1. The amount of time needed for sample relaxation is dependent on the channel thickness (w), mean layer thickness of the analytes, and the field strength. A generalized relation for all FFF techniques is given by

$$\tau = \frac{w}{U} \quad or \quad \tau = \frac{\lambda w^2}{D} \tag{2.5}$$

where the relaxation time (τ) is the time necessary to establish the equilibrium concentration profile, and λ is the retention parameter specific to an FFF technique. As R and λ are based upon an exponential concentration gradient at steady state, the sample must be fully relaxed to ensure ideal behavior (i.e., minimal band broadening, expected retention times, well defined peak shapes, etc.). This may be achieved by routing the axial flow to bypass the channel, a process referred to as stop-flow, or by the introduction of an opposing flow which results in sample focusing. Additionally, the sample inlet can be positioned on the accumulation wall, as is now standard in commercial ThFFF channels. Frit-inlet FlFFF and frit-inlet asymmetrical FFF (FI-AF4) systems exploit an additional (high) flow in the channel inlet region which leads to rapid transport of the analyte to the accumulation wall [26], [27]. This modification allows continuous analysis of samples and eliminates the stop-flow (FlFFF) and focusing (AF4) steps when unwarranted sample loss due to adsorption on the accumulation wall is most likely to occur [28]. Resources for the systematic optimization of FFF conditions to improve selectivity and recovery are available in publications [29] and commercial software tools from Wyatt Technology and PostNova Analytics.

2.1.1.2 Sample Overloading

As analyte is injected into the channel, it first undergoes dilution followed by concentration until it reaches a steady-state exponential gradient concentration profile. Like chromatography, high concentrations may lead to increased plate heights and band broadening, which in turn influences data analysis (determination of molar mass, polydispersity index, etc.) if a molecular weight versus time calibration is used. At increasing concentrations, polymer solutions no longer behave as ideal systems at infinite dilution and exhibit deviant solution behavior (viscoelastic, rheological, etc.). The transition from dilute to semi dilute regime is well described by polymer solution theory [30]. As concentration increases, the distance between molecules is decreased which leads to chain overlap and entanglement. The onset of this regime transition is typified by the polymers critical overlap concentration c^* in Equation 2.6.

$$c^* = \frac{M_w}{N_A \rho (R_g)^3} \tag{2.6}$$

where M_w and R_g are the polymer's molecular weight and radius of gyration respectively, ρ is the solvent density, and N_A is Avogadro's number. As the relation of M_w and R_g for a given polymer-solvent system is dependent on the thermodynamic quality of the solvent, c^* is similarly

dependent on solvent quality. In FFF the effect of this excessive concentration manifests itself in the form of overloading [31]. For a sample to overload the concentration at the accumulation wall (c_0) must exceed the critical overlap concentration ($c_0 > c^*$). As discussed above, c_0 depends on the balance of the field-induced and intrinsic diffusion transports, a reasonable estimate can therefore be made

$$c_0 \cong \frac{c_{inj}}{\lambda} \tag{2.7}$$

where c_{inj} is the concentration injected and λ is the expected retention parameter for the analyte under the conditions to be used during analysis. If all necessary quantities are known, the appropriate concentration range to avoid overloading behavior may be determined prior to experimentation [32]. It should be noted that Equation 2.6 is dependent on the polymer molecular weight and polymer-solvent composition. In general, the critical concentration is higher in a poor solvent than in a good solvent. Likewise, polymers of high molecular weight will exhibit overloading at lower concentrations than polymers of low molecular weight.

Examination of retention time with respect to concentration provides an indication of the onset of overloading, specifically, when retention time begins to change as a function of concentration. In an empirical approach, the sample is analyzed at various mass loadings in the channel (by either varying injection loop volume or sample concentration) [33]. An example of an overloading study is shown in Figure 2.3A. This illustrates the overloading behavior of soluble polymers with the peak becoming broader as sample mass loading increases. At some critical mass loading, retention time shifts to later times which is typical for soluble polymer in organic solvents. Overloading behavior may vary depending on the analyte. Many particle systems, polyelectrolytes, polymers in aqueous systems, and biomacromolecules can display a decrease in retention time in overloaded conditions. For polymers, the presence of a pronounced shoulder or second peak is often attributed to the formation of entangled polymer aggregates [32]. The presence of broad peaks, peak shoulders, or second peaks is also common for polymers which are not completely solubilized. The dissolution process can be monitored by analyzing the sample at different time points (hours to days to weeks) after suspension in solvent, as illustrated by Figure 2.3B. As a rule of thumb, polymers < 1 MDa in a good solvent may take less than 24

hours to dissolve. For ultra-high molecular weight polymers, >1 MDa, or polymers in poor solvents, dissolution may take days or weeks at ambient temperatures.

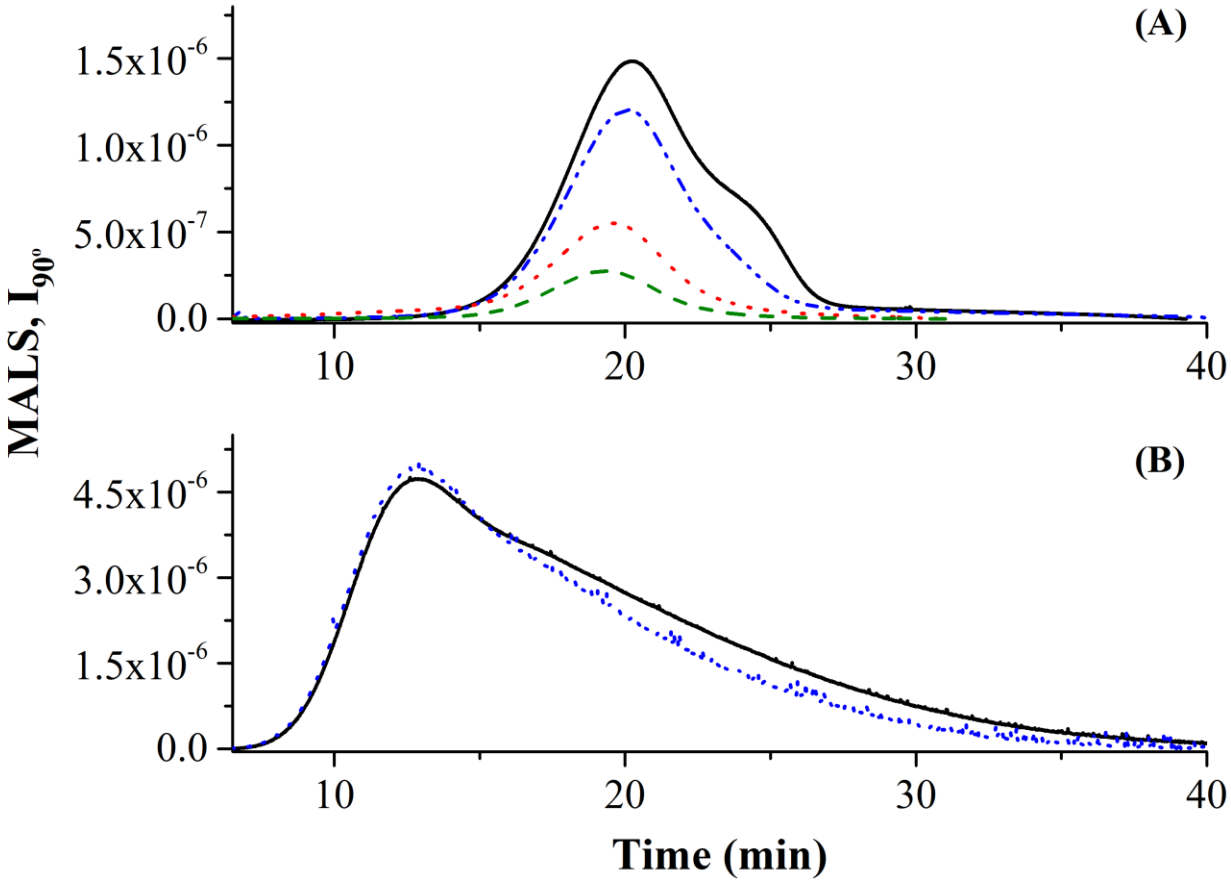

Figure 2.3. (A) Overloading behavior of 200 kDa polystyrene in THF with increasing concentration from 0.5 mg/mL to 4 mg/mL and 20 µL sample volume. (B) Black trace is an ultra-high molecular weight bottlebrush polymer which has been in solution for 24 hours and is not fully solubilized; the dotted trace is the same polymer which has been in solution for 1 week.

2.2 Flow FFF

The use of a crossflow of fluid as a 'field' to transport analytes to the accumulation wall gives rise to the technique known as flow field-flow fractionation (FlFFF) [34]. The flow field is appealing because the bulk movement of the crossflow interacts with all analyte species regardless of size, mass, charge, etc. In theory, flow FFF is applicable to any analyte provided a suitable semipermeable membrane that retains the analyte in the channel is available. This, and the simple separation mechanism, has helped make flow FFF the most widely used FFF technique today [35], [36]. In the following sections, theoretical and experimental aspects of flow FFF are discussed with emphasis on asymmetrical flow FFF (AF4) applications [37].

2.2.1 Retention Theory

Retention and separation in flow FFF follow the same general stages as described in Section 2.1. More specifically, the applied crossflow transports analytes by positive displacement (with no preference for size, shape, etc.) to the accumulation wall. The resulting higher concentration at the wall leads to a counteracting diffusion which transfers analyte molecules back towards the center of the channel at a rate that is related to their hydrodynamic size. A steady state equilibrium between these two transfer phenomena is eventually reached, generating exponential concentration profiles with different average thicknesses, ℓ_1, ℓ_2, etc., that are unique to each analyte species. Separation in flow FFF thus relies solely on differences in diffusion coefficients D of the analyte species. These differences in D are represented by different retention times that reflect separation.

The general equation for λ shown as Equation 2.2 can be rewritten specifically for flow FFF by substituting the specific expression for field-induced velocity, i.e., U is the crossflow velocity and is equal to $V_c\, w/V^0$, to obtain:

$$\lambda = \frac{D\, V^0}{V_c\, w^2} \tag{2.8}$$

where V^0, V_c and w are the channel void volume, the crossflow rate, and the channel thickness, respectively. Substitution of Equation 2.8 into the simplified form of Equation 2.4 where $R=6$□ yields

$$t_r \cong \frac{w^2\, V_c}{6\, D\, V_{out}} \tag{2.9}$$

where V_{out} equals V^0/t^0. Equation 2.9 applies only to symmetrical flow FFF and is modified as follows for AF4 [2]

$$t_r \cong \frac{w^2}{6\, D}\, ln\left(1 + \frac{V_c}{V_{out}}\right) \tag{2.10}$$

These simplified equations 2.9 and 2.10 are good approximations when $R < 0.1$ and clearly shows the relationship between t_r and D. However, more rigorous equations are available and should be used in experimental practice for sample characterization especially when R > 0.1 [38]. The D values can be transformed to a sphere equivalent hydrodynamic size using the

Stokes-Einstein equation $D = kT/3\pi\eta d_h$ where η is carrier liquid viscosity and d_h is hydrodynamic diameter. Thus, small size species elute first and size (or molecular weight) information including polydispersity can be directly obtained from measured retention times.

2.2.2 Instrumentation

Flow FFF systems includes pumps, a flow FFF channel, and one or more detectors to register the elution of analytes and additional characterization for molecular weight, size, etc. The flow FFF channel has multiple configurations including the symmetrical, asymmetrical, and hollow fiber channels shown in Figure 2.4. Currently, flow FFF devices are available from Postnova Analytics and Wyatt Technology.

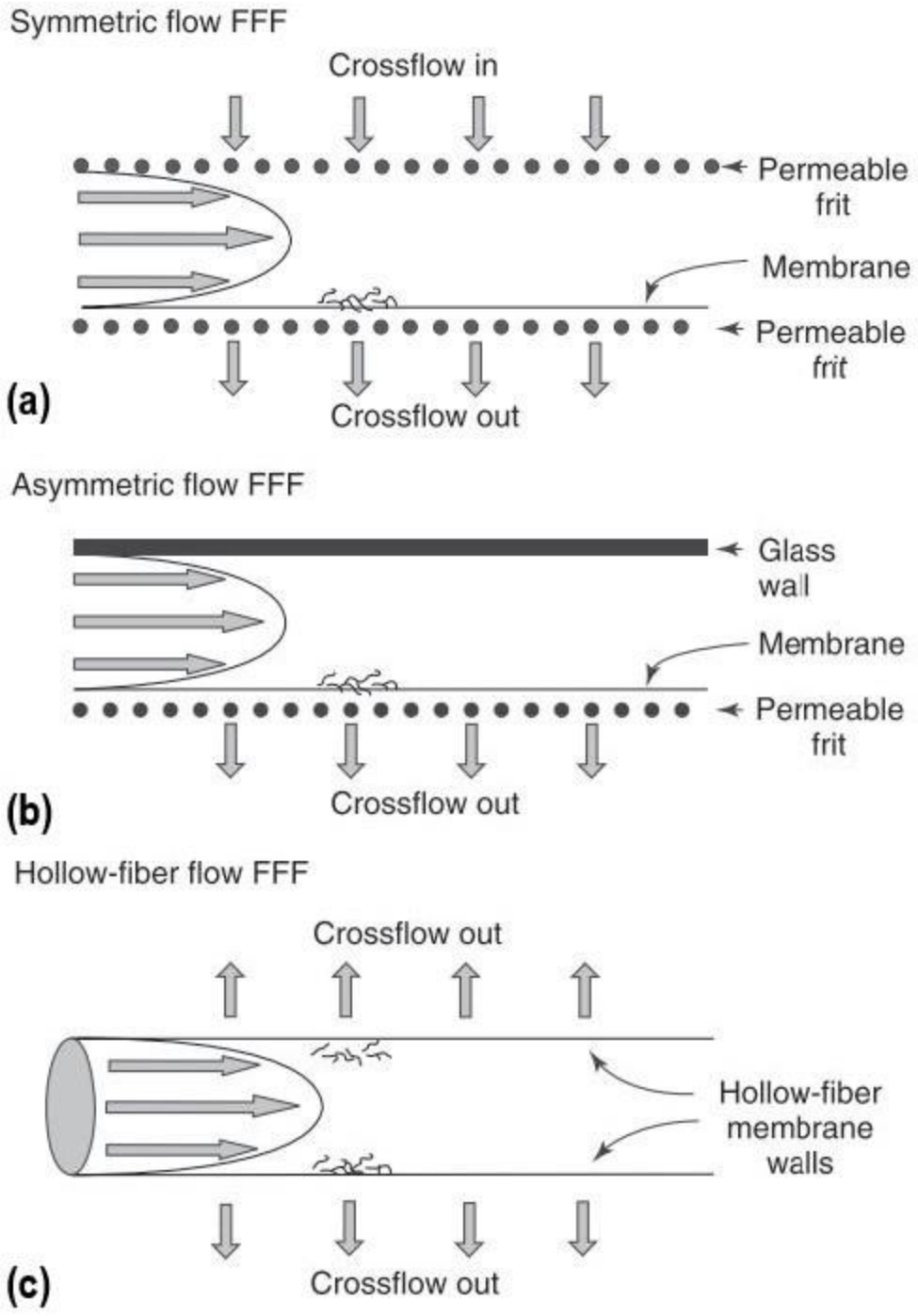

Figure 2.4. Different variants of flow FFF. (A) symmetrical flow FFF has a rectangular channel geometry with two permeable walls and was the original configuration, (B) asymmetrical flow FFF (AF4) also uses in a rectangular channel geometry but has only one permeable wall, and (C) hollow fiber flow FFF uses a hollow fiber membrane or ceramic tube. (Reprinted with permission from [39].)

The symmetrical flow FFF channel consists of two permeable walls made of porous ceramic frit where one wall is overlaid with a semi-permeable ultrafiltration membrane that acts as the sample accumulation wall. A spacer that defines the FFF channel is sandwiched between one frit wall and the membrane and the channel shape is rectangular with two triangular ends at the inlet and outlet [40]. In AF4, the upper wall frit is replaced by a non-porous material such as glass, which simplifies the setup [3]. The AF4 channel maintains the triangular end pieces at the inlet and outlet but has a trapezoidal shape with a narrower breadth at the outlet end. Since the flow at the inlet supplies both the channel flow and the crossflow, the channel flow rate continuously decreases towards the outlet (as one part is continuously exiting through the membrane). The trapezoidal channel shape increases the channel flow velocity in the direction of the channel outlet and results in more reasonable analysis time. The thickness of the spacer/FFF channel ranges from 50 to 500 μm, the channel length commonly lies in the 10 to 20 cm range, and the breadth between 1 to 2 cm.

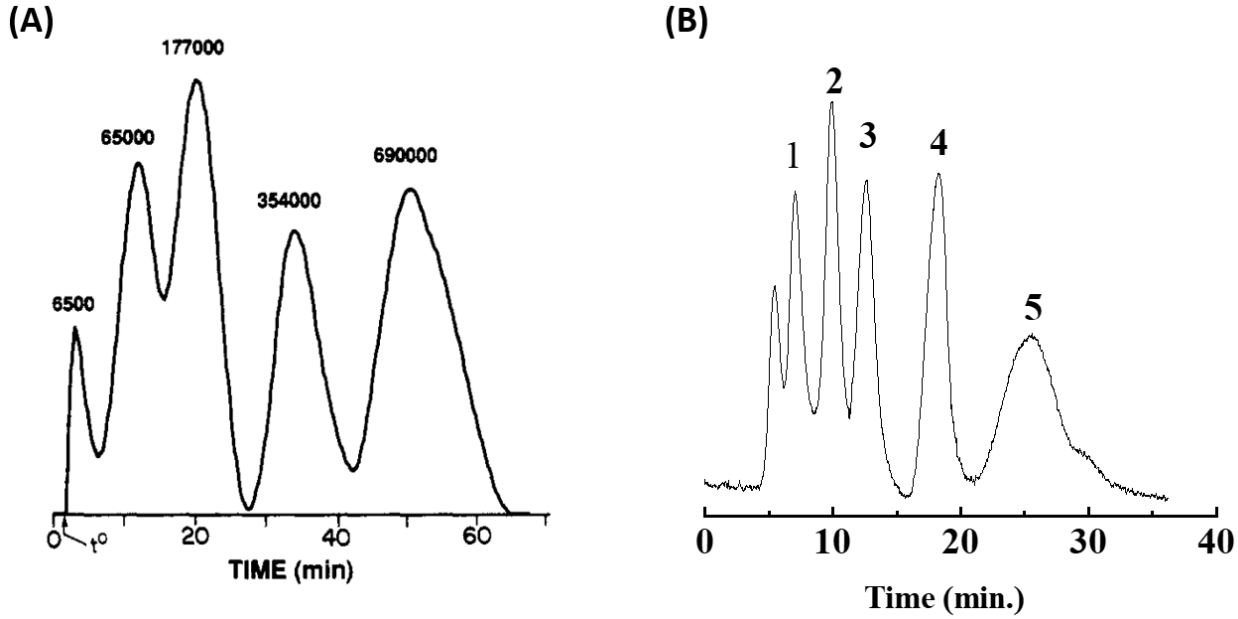

Figure 2.5. AF4 fractograms. (A) mixture of 5 μg each of polystyrene sulfonate (PSS) polymer standards in Tris buffer. (B) protein mixture: 1- carbonic anhydrase (29 kDa), 2- bovine serum albumin (66 kDa), 3- alcohol dehydrogenase (150 kDa), 4- apoferritin (444 kDa), and 5- thyroglobulin (669 kDa). (Reprinted with permission from [41] and [42])

Identification of an appropriate semi-permeable membrane is crucial in flow FFF experiments. Ideally, the membrane should not interact with the sample and its pore size should allow small molecules to flow out of the channel while retaining analytes. Several membranes

with different materials and nominal molecular weight cut-offs (MWCO) are currently available on the market (Table 2.1). Thus far, the most used are regenerated cellulose (RC) and polyether sulfone (PES) ultrafiltration membranes. An appropriate MWCO is usually one that is below the molecular weight (or size) of the smallest species of interest. The MWCO is determined using model proteins and specific conditions and is a nominal value only. Hence, sample loss may occur through the membrane if the analytes are a different shape and the FFF flow rates (channel pressures) are sufficiently high. The physicochemical properties of the sample can give useful indication what type of membrane material to choose (e.g., the hydrophilic RC is less likely to interfere with the fractionation of hydrophobic molecules than PES). Other variables such as flow rates and carrier composition, ionic strength, and pH may also impact membrane-sample interactions [35]. Preliminary experiments which evaluate and optimize membrane performance should be included in method development especially for new analyte types for which there is no prior flow FFF work [3], [43], [44].

Table 2.1. Selected examples of membrane chemistry and MWCO recently used in AF4 characterization of different samples.

Sample	Membrane chemistry	MWCO (kDa)	Reference
Metal-bearing colloids	PES	0.3	Cuss, *et al.* [45]
Gelatin nanoparticles	PES	1	Fraunhofer, *et al.* [46]
Trace metals and dissolved organic matter	PES	1	Wang, *et al.* [47]
Cereal β-glucan	PES	5, 10	Zielke, *et al.* [48]
Polymer emulsion	RC	5	Makan, *et al.* [49]
Complex polymers	RC	5	Pasch, *et al.* [50]
Cationic copolymer	RC	10	Perevyazko, *et al.*[51]
Gluten	RC	10	Mahroug, *et al.* [52]
Caseins	RC	10	Abbate, *et al.* [53]
PVA-g-PMMA nanoparticles	RC	12-14	Halamish, *et al.* [54]

2.2.3 Methodology

Several parameters can be adjusted to tune separation conditions for a given sample, such as membrane chemistry, MWCO, carrier composition, and flow rates. Such versatility has allowed AF4 to be applied to a wide range of samples from macromolecules (e.g., dendritic macromolecules [55], amphiphilic copolymers [56] and tannins [57]) to more complex assemblies (e.g., fullerene aggregates [58], cellulose [59], amylopectins and glycogen [60]) and up to entire bacterial cells [61]. Optimization of multiple variables can be challenging and time-consuming, however, a systematic approach as described below may expedite this process [62].

2.2.4 Solvent Selection

Flow FFF can be implemented with both organic and aqueous solvents [63]. Different channels optimized for either carrier compositions are available on the market and can easily be connected to the pump without the need for major changes in the setup. Organic solvents such as tetrahydrofuran (THF) and 1,2,4-trichlorobenzene (TCB) are used for the fractionation of synthetic polymers [49], [50], [64], [65] whereas aqueous carriers are more frequently employed in the analysis of natural and biopolymers (Table 2.2) [51,52,65–74]. In the latter case, dilute salt, or buffer solutions (in the 10 – 50 mM range) such as phosphate buffer (PBS), sodium nitrate ($NaNO_3$) or sodium chloride (NaCl) are typically used to provide biocompatible conditions and reduce electrostatic interactions between the analyte itself and between the analyte and the ultrafiltration membrane. Addition of NaN_3 in small concentrations (approx. 200 µg/L) is often beneficial to prevent microbial growth.

Table 2.2. Selected examples of carriers recently used in flow FFF characterization of different samples.

Sample	Carrier	Information sought	Reference
Complex polymers	TCB	Size and MW distributions	Pasch, *et al.* [50]
Branched and ultra-high molecular weight polyolefins	TCB	Size and MW distributions	Otte, *et al.* [64]
Polymer emulsions	THF	Size, MW, and gel content characterization	Makan, *et al.* [49]
Whey protein	45 mM NaCl	Aggregate size	de Guibert, *et al.* [73]
Starches from different sources	10 mM $NaNO_3$	Physicochemical and structural characterization	Fuentes, *et al.* [66], [67], [76]
Human plasma	50 mM PBS	Lipoprotein characterization	Bria, *et al.* [70]
PVA-g-PMMA nanoparticles	Deionized water	Characterization of self-assembly and nanostructures	Halamish, *et al.* [54]
Dextran	50 mM $NaNO_3$	Size characterization	Eckel, *et al.* [74]
Non-alcoholic beer	50 mM $NaNO_3$	Macromolecular characterization	Krebs, *et al.* [77]

Separation in aqueous phases requires the user to select appropriate pH and ionic strength for the analysis. These parameters should be tuned according to the sample characteristics (e.g., stability, solubility etc.). Low ionic strengths for instance, have been proven to adversely affect the separation of charged polymers by causing early-eluting, deformed peaks [78]. On the other hand, high ionic strengths may cause a decrease in the thickness of the electric double layer between analyte and membrane, which results in a closer approach of analytes to the channel wall and, eventually, in elongated retention times [79]. Similarly, the effect of carrier liquid pH should be considered as pH values in the range of the isoelectric point of the analyte may result in sample aggregation and/or precipitation [72], [80]. A careful balance between these two parameters, pH and ionic strength, results in an optimum separation.

2.2.4.1 Sample Preparation, Loading, and Overloading

A stable sample solution or suspension is an important criterion for successful analysis and has proven to be challenging for samples such as polysaccharides. Elevated temperatures, high pH, and organic solvents may be employed as long as the sample does not undergo degradation during the process [81].

Flow FFF techniques are generally employed for analytical purposes with small sample loads. Injection of excessive amounts of sample (i.e., overloading), may cause shifted retention times, skewed and broadened peaks and the introduction of artifact peaks [32]. Such effects arise in good solvents at analyte concentrations close to the so-called “semi-dilute” region. Other factors such as ionic strength and pH of the carrier liquid and the crossflow rate play a major role in overloading effects and should be carefully evaluated [78]. A detailed study on overloading effects in flow FFF methods is available which addresses both theoretical and experimental aspects [32]. In practice, overloading concentration may be ascertained by systematically injecting sample solutions with decreasing concentration until no changes in retention time and peak shapes/breadths occur.

2.2.4.2 Flow Rates and Sample Focusing in AF4

Control of the ratio of the crossflow rate to the outlet flow rate V_c/V_{out} is important to obtain an adequate fractionation. The crossflow rate is particularly important in order to optimize separation resolution and analysis time. Commercial AF4 instrumentation allows the user to apply constant (isocratic) cross flow rates and use program crossflow rate gradients to continuously decrease analyte retention during the analysis. This can be particularly beneficial when analyzing highly polydisperse samples as total run times can be shortened significantly. A gradient crossflow rate can also be useful as an initial step to probe the general size/MW range of components present in an unknown sample [3]. Crossflow rate programming utilizes two types of gradients: linear or exponential [82]. AF4 method development can now be done using commercial software tools offered by FFF instrument manufacturers.

An optimization strategy that addresses both separation and detection has been proposed [43]. The two additional parameters considered are the time required to separate two components differing by a factor of two in their MW (TREQ) and the ratio between analyte concentrations during the separation (DILF). When changing the crossflow rate, TREQ and DILF are affected in

opposite directions with an increase in the crossflow resulting in greater TREQ and improved separation. Detection sensitivity on the other hand, can be improved by enhancing the DILF through a reduction of the crossflow intensity.

Symmetrical flow FFF utilizes a stop-flow period during which the channel flow is routed to bypass the channel while the crossflow establishes steady state analyte layers at different average distances from the membrane accumulation wall. The stop-flow relaxation time in flow FFF techniques depends on the channel volume (V^0), the crossflow rate (V_c) and the time required to sweep sample from the injection valve through connecting tubing and into the channel according to Equation 2.11 [2]. Injection time is obtained dividing the volume of injection tubing (V^0_{tubing}) by the injection flow rate (V_{inj}). Approximately 20% more time is usually added as this has been observed to yield the best separation performance. The stop-flow time, τ, is thus calculated as

$$\tau \approx 1.2 \left(\frac{V^0}{V_c} + \frac{V^0_{tubing}}{V_{inj}} \right) \tag{2.11}$$

Equation 2.11 is also applicable to AF4 where analytes are relaxed to their equilibrium layers through a process termed "focusing". Focusing takes place at point *z* within the channel. Typically, *z* is located 2-5 cm downstream from the carrier inlet to avoid the flow inhomogeneities present near the inlet [3], [83]. Its coordinate can be set by adjusting flowrates according to

$$\frac{z}{L} = \frac{V_{in}}{V_{in} + V_{out}} \tag{2.12}$$

where L is the total channel length, V_{in} and V_{out} are the two opposing flowrates, coming respectively from the inlet and the outlet (Figure 2.6). The focusing time also takes in to account the time needed to fully load the sample into the AF4 channel.

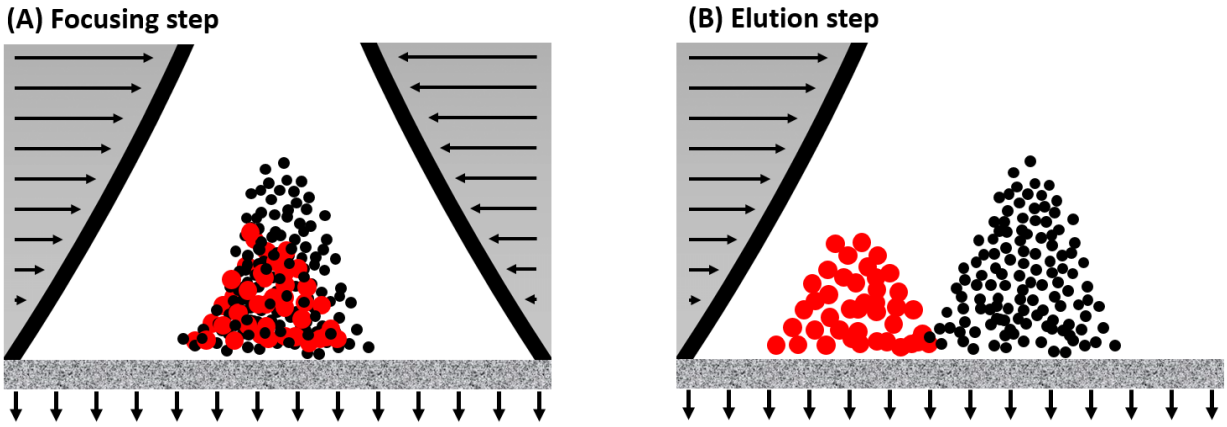

Figure 2.6. Schematic representation of an AF4 channel during the fractionation steps. (A) focusing/relaxation: Sample is introduced through the injection port, while two opposing carrier flows are pumped in from both the channel inlet and outlet. Fluid exits through the semipermeable membrane and porous frit wall while providing the essential crossflow that drives analytes to the accumulation wall. Upon relaxation, two different *D* (or size) species have two different mean layer thicknesses. (B) elution: A single flow of carrier fluid from the channel inlet serves as the source of both the crossflow and the channel flow. The latter carries analytes down the length of the channel towards the detector.

2.2.5 Advances in Flow FFF Instrumentation

2.2.5.1 High Temperature AF4

The development of ceramic membranes capable of withstanding temperatures above 130 °C has made it possible to develop high-temperature (HT) flow FFF methods [63]. Until recently the large MWCO displayed by such membranes caused important fractions of the sample to be lost through the accumulation wall, thereby significantly limiting their applicability [64]. Novel ceramic membranes with improved characteristics (i.e., 50 – 150 kDa MWCO) allowed HT-AF4 to be applied to a wider variety of samples. For instance, this technique was used to analyze high molar mass branched low-density polyolefins of high MW [65]. SEC with multiangle light scattering (MALS) and differential refractive index (dRI) detection displayed co-elution of long branched chains and linear analogues, which prevents a correct MW characterization of the sample [16]. Application of HT-AF4-MALS-dRI to the same sample showed a monotonic increase in MW and enabled the determination of MW distribution [64]. Although significant progress has been made in the fabrication of ceramic membranes, their large pores still constitute a major limitation to the applicability and the potential of HT-AF4 for polyolefin analyses.

2.2.5.2 Microstructured Membranes

Optimized experimental conditions are not always sufficient for successful fractionation of components with similar retention. Though resolution can be improved by increasing the channel thickness and/or the crossflow intensity, this may lead to detection and transmembrane pressure problems. The concept of micro-sized grooves at the accumulation wall was implemented in 1978 on ThFFF [84] and recently applied to AF4 [85]. AF4 results showed that microstructured membranes with grooves perpendicular to the direction of the carrier flow (Figure 2.7) induced a decrease in the zone velocity, which is stronger for larger molecules, thereby improving the resolution of the separation. It should be mentioned that due to the patterning process (i.e., hot embossing), membranes presented a slight increase in the MWCO. Future studies will therefore focus on the fabrication of microstructured membranes with lower MWCO as well as on the determination of the most effective groove structure.

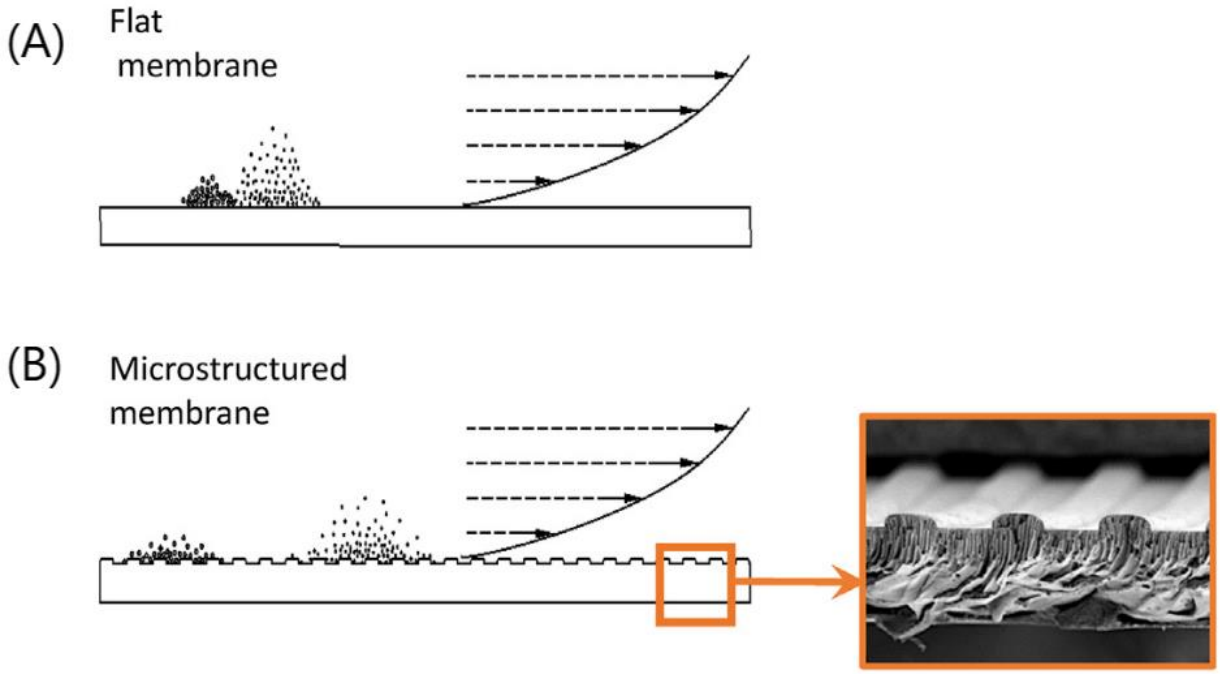

Figure 2.7. (A) Schematic representation of AF4 separation with flat microstructured membranes. (B) Electron microscopy image of microstructured membrane. (Reprinted with permission from [85].)

2.2.5.3 Semi-Preparative AF4

The applicability of analytical scale separation techniques is sometimes limited by the amount of sample produced (approximately 100 µg) [86]. Separation and purification of larger

amounts is sought when further off-line characterization is necessary or when fractions of substantial amount are needed for testing performance. Though chromatography methods are already available for preparative separation of molecules of a few nm in size [87], [88], for larger species this is not the case. Precipitation and ultracentrifugation (sometimes combined) are currently used for this purpose. These techniques are often time-consuming, require sample-specific conditions, and may induce irreversible aggregation in the sample. Semi-preparative AF4 (SP-AF4) can be performed by combining multiple channels in parallel or by increasing the dimensions of a single channel [70]. The former approach yields low sample amounts and is limited by variations in each channel membrane's properties (e.g., porosity, flux, and surface chemistry). Such irreproducibility has been proven to cause as much as a 56% increase in peak broadening [89]. Increasing the size of a single channel appears to be a more successful strategy. A recent study demonstrated the successful purification of significantly higher amounts of sample both in organic and aqueous carrier liquids. Thereby, sample loads as high as tens of mg, in the case of silica nanoparticles, could be fractionated while still retaining a satisfactory resolution [86] In the same study the relationships between channel breadth, sample load, and separation resolution were also investigated. Results show that wider channel breaths may enable the loading of higher sample quantities without causing overloading effects (Figure 2.8). The optimal focusing position for large sample loads, moreover, was determined to be as close to the channel inlet and near the broadest part of the channel.

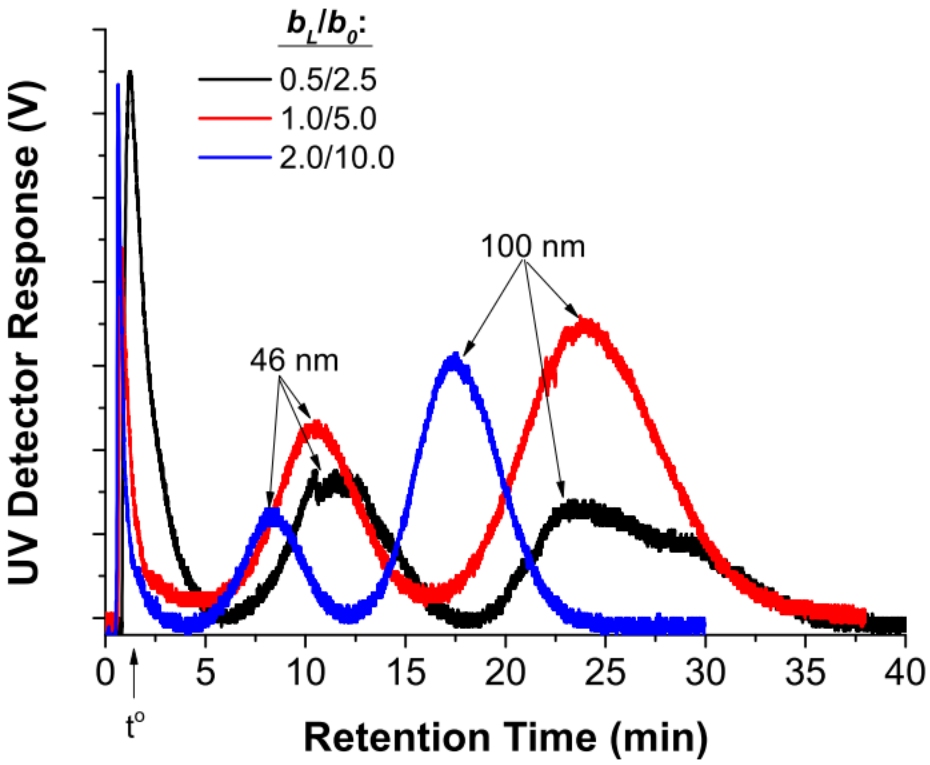

Figure 2.8. Fractograms of polystyrene latex beads (46 and 100 nm in diameter) obtained with channel of different dimensions. The respective values of b_L= minimum channel breadth and b_0 = maximum channel breadth are reported in the graph. (Reprinted with permission from [86].)

2.2.5.4 Miniaturized AF4

Some flow FFF applications require minimization of solvent and sample consumption as well as reduced analysis time. Such characteristics can be attained by the implementation of miniaturized AF4 (mAF4) [90]. The first study on the subject was published in 2004 [91] and was followed by several others addressing the separation of metal nanoparticles [90] and biopolymers (i.e., proteins and lipoproteins) [92]–[94]. It was only in 2017 however, that mAF4 performances were comprehensively and systematically studied, including the determination of important parameters such as sample recovery, limit of detection (LOD), and limit of quantification (LOQ) [95]. Results showed as much as a 50% reduction in solvent consumption and an 87.5% reduction in sample consumption. Moreover, LOD and LOQ could be halved compared to conventional AF4 channels, paving the way to the standardization of mAF4 as a method for trace analysis (e.g., detection of nanoparticles in environmental matrices). Such improvements though, come at a partial expense of peak resolution (Figure 2.9).

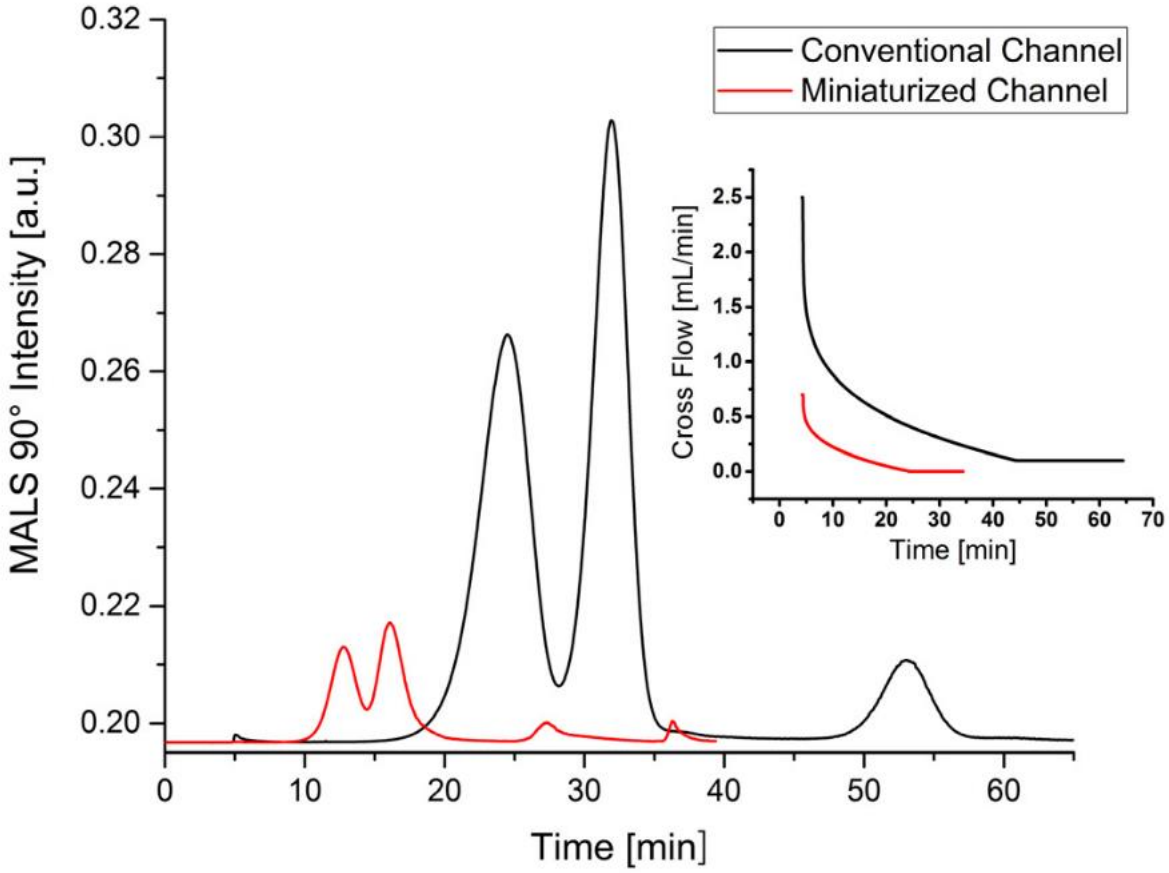

Figure 2.9. Comparison of fractograms of mixtures of polystyrene nanoparticles in a conventional (black) and a miniaturized (red) AF4 channel. Insert shows the crossflow profile utilized. (Reprinted with permission from [95].)

2.2.6 Applications

In this section selected applications of flow FFF are reported and discussed. The variety of examples described further confirms the versatility of flow FFF methods and their wide applicability.

2.2.6.1 Polymer Nanoparticles for Drug Delivery

Nanoparticles constituted of synthetic polymers are considered appealing systems for drug delivery and biomedical applications [96]. Dendrimers and polymersomes are among the most promising in this category and are chosen as examples for more detailed discussion in this section.

Dendrimers are characterized by a central core combined with a perfectly branched structure [55]. These macromolecules possess a high number of chain-ends available for modification and are able to load cargo molecules within their scaffold and/or on their surface. Furthermore, dendrimers feature good solubility, prolonged storage stability, and circulation safety. For these reasons they are intensively studied as drug delivery systems [97]. Several investigations where AF4 was applied to the characterization of dendrimers are available in the literature [97]–[101]. A 2010 study investigated the complexation capacity of poly(ethylene imine) functionalized with a maltose shell [102]. In this study Rose Bengal (RB) was chosen as a model of a drug because of its small and polar structure. Such characteristics allowed the uncomplexed fraction of RB to exit the AF4 channel via the ultrafiltration membrane, making its quantification straightforward. By doing so it was possible to derive the fraction of RB successfully complexed by dendrimers, and therefore to estimate their efficiency as drug carriers. This approach allowed a comprehensive characterization of the RB-dendrimer system in terms of size and MW. Different degrees of dendrimer modification were also tested in order to improve the stability of the complexes over time.

Another example of a promising drug delivery system is polymersomes (Psomes) [103], [104]. Psomes are vesicles constituted by amphiphilic synthetic block copolymers (BCPs). They display relevant advantages over their natural counterpart (i.e., liposomes), such as a higher mechanical and chemical stability [105]. Moreover, membrane properties can be tuned by changing the chemical composition of BCPs [103], [106]. It is possible to obtain stimuli-responsive vesicles by incorporating functional moieties [106]–[108]. The loading behavior of Psomes was investigated to compare two different strategies: the well-established *in situ* approach and post-loading [71]. In the former method, particle loading takes place during the assembly, while in the latter particles are loaded only after the assembly is completed. Diverse types of cargos were tested including gold nanoparticles, glycopolymer protein mimics, and two different enzymes. Coupled to light scattering detectors and electron microscopy techniques, AF4 allowed the precise determination of cargo location after loading. Results showed that despite a reduced selectivity toward the encapsulation of cargo inside the lumen of the vesicles, post-loading enables a more precise tuning of Psomes characteristics.

2.2.6.2 Macromolecules in Food and Beverages

AF4 is one of the few separation techniques applicable to the macromolecular characterization of highly polydisperse samples associated with food and beverages. For instance, it has been employed to analyze polysaccharides (e.g., starch and its derivatives) [26], [60], [66]–[68], [75], [76], [109]–[111], cellulose and pullulan [112], β-glucan [48], [69], [77], [113]–[116] and pectin [117]. Several studies on food proteins are also available in the literature, particularly concerning peptides in dairy [118] and cereal [119] products. Starch and glycogen were selected for a more detailed discussion in this section because of their key role in biological systems.

Starch and glycogen are highly branched homopolymers of glucose. The former is an energy reserve found in almost every part of plants and serves as a primary source of energy in animal feed. The latter serves primarily as a transient energy storage in animals, especially in muscle and liver cells [109]. The structure of these polysaccharides has important consequences on human health. Quickly digested starch molecules for instance, are known to increase blood glucose and insulin responses and to promote metabolic diseases including obesity and diabetes. Those featuring a slower digestion instead, can reduce the incidence of metabolic diseases and alleviate associated complications [120], [121]. Other studies focusing on glycogen found significant differences between the molecules synthesized by healthy and diabetic mice [122].

A comprehensive study addressed structural aspects of these two biopolymers with an interesting focus on possible implications on human health [109]. Investigations on how the structure of starch molecules evolves during *in vitro* and *in vivo* digestion and the structural differences between glycogen molecules synthesized by healthy and diabetic mice led to the formulation of new hypotheses on the subject, potentially paving the way to the discovery of novel drug targets for diabetes management. Understanding such processes may eventually lead to the discovery of new drug targets for diabetes management.

2.2.6.3 Proteins and Protein Aggregation

Proteins have been the target of AF4 investigations since the early days of this technique [17,69,71,93,122–129]. Important for the characterization of a protein is the analysis of its aggregation behavior [131]. Only recently however, was a systematic study done on the effect of AF4 experimental parameters on protein aggregates [132]. Two types of IgG with different MW were chosen as models. The effects of carrier fluid composition, injection shear stress, focusing,

and dilution-during-separation on aggregates stability were evaluated. Results showed significant differences in the aggregation behavior depending on the carrier composition. Furthermore, low MW proteins were found to be more prone to dissociation than their high MW counterparts, suggesting an aggregate-size dependent stability. Finally, it was shown that injecting the sample through a syringe can lead to slight changes in the sample size distribution, whereas the duration of the focusing step had no particular influence on the aggregation behavior of the proteins considered.

2.2.6.4 Environmental Pollution

Environmental pollution research is increasing worldwide. The presence of trace metals in aquatic environments is concerning due to its great potential for long-term accumulation in sediments and organisms [47]. Trace metals are often associated to a colloidal phase constituted by organic matter of different source, size, and composition [133]. Characterization of this heterogeneous phase is therefore important for its role in biogeochemical processes such as metal chelation and transportation of pollutants [134]. AF4 coupled to different detectors has been very successful in this kind of analyses, as it allows the simultaneous fractionation and characterization of polydisperse samples [135]–[138]. Until recently however, precise quantification of colloids below 1 kDa was not attainable due to the lack of appropriate ultrafiltration membranes and separation techniques. Solutions to overcome problems such as the high pressure associated with using low-MWCO membranes allowed the analysis of colloids using a 300 Da MWCO membrane [45], providing new information on organic matter. In particular, results indicated that a considerable fraction of trace metals may be associated with organic matter of less than 1 kDa, suggesting this low size of colloids to be much more abundant and ecologically significant than previously thought. Thereby, resolution and precise size distribution characterization of colloids in the lower size range were attained. The study also addresses the issues caused by using such small pore-sized membranes, including high transmembrane pressures, difficult calibration, and optimization of resolution and recovery.

2.3 Thermal Field-Flow Fractionation (ThFFF)

Thermodiffusion has been widely studied since its discovery by Ludwig [139] and Soret [140] over 100 years ago. While there is a comprehensive theory for thermophoresis in the gas phase [141], a theory for solution thermophoresis has eluded scientists. Despite lacking a fundamental understanding, this mass transport process was harnessed into an FFF separation

technique and the first results were reported in 1967 [142]. In ThFFF, a temperature gradient is applied as the 'external field' by heating one channel wall and cooling the other. In a typical polymer experiment, the analyte undergoes thermal diffusion (usually) towards the cold wall giving rise to a positive thermal diffusion coefficient (D_T). As the polymer concentration increases at the cold or sample accumulation wall, the analyte diffuses away from this region of high concentration by the process of Brownian diffusion, which is characterized by the diffusion coefficient (D). The ratio of these two fluxes, D_T and D, is known as the Soret coefficient (S_T) and is responsible for the positioning of analytes in the parabolic flow profile and their differential transport to the channel outlet. Before discussing the mechanisms, which govern retention in detail, it is important to note when it is appropriate to use ThFFF. Like other FFF techniques, it is well suited to study materials that may become physically trapped in a packed column or are sensitive to shear degradation and sample preparation (*e.g.*, ultrahigh MW polymers, complexes, and gels) [143]. In contrast to SEC-MALS where a U-shape profile is often observed in a plot of MW versus retention time [144], FFF demonstrates a monotonic increase with MWs extending as high as 10^8-10^9 Da [18], [145], [146]. ThFFF has also been shown to have higher molar mass selectivity than single-column SEC for polymers with molecular mass greater than 10^5 Da [147], [148]. Additionally, thermal diffusion's sensitivity to polymer-solvent interfaces makes ThFFF well suited for determining copolymer composition distributions [18], [149], [150]. More recently, D_T has been exploited to estimate architectural features as detailed in Section 2.4.5.2 of this chapter.

2.3.1 Analyte Retention

Analyte retention in ThFFF is governed by S_T, which is both mass (through D) and composition (through D_T) dependent. Separation of homopolymers occurs according to differences in D because D_T is constant. Like other FFF techniques, this results in the elution of low molar mass polymers (small size) followed by polymers of increasing mass (or size). ThFFF polymer separations typically occur in the normal mode with the exception of ultra-high molar mass polymers (>10^7 Da) [151] which are too large to undergo Brownian diffusion and thus separate in steric or hyperlayer mode. The relationship between polymer molar mass and D is generally well described; however, thermal diffusion is less well described. Since the introduction of ThFFF, there have been many investigative studies into the thermophoresis of polymers which have yielded some phenomenological descriptions [142], [152]–[154]. Low

molar mass (<1000 Da) polymers exhibit poor retention in ThFFF, thus thermal diffusion forced Rayleigh scattering experiments were used to examine the behavior of D_T at low masses. It was found that D_T of a polymer is independent of molar mass above some critical value, typically around 1000 Da [155], [156]. The magnitude of D_T is also dependent on the polymer-solvent system giving rise to composition-based separations and characterizations. These features of D_T make ThFFF an effective technique for analyzing complex polymers (*e.g.,* block copolymers). Assuming that the applied temperature gradient is linear across the thickness of the channel, the retention parameter (λ) can be represented by Equation 2.13.

$$\lambda = \frac{1}{S_T \Delta T} = \frac{D}{D_T \Delta T} \tag{2.13}$$

From λ, the retention ratio may be determined using a modified form of the general retention equation. This is shown in Equation 2.14 where ν is a correction for distortion of the parabolic flow profile due to a viscosity gradient induced by the temperature gradient [157], [158].

$$R = 6\lambda(\upsilon + (1 - 6\lambda\nu)\left[coth\frac{1}{2\lambda} - 2\lambda\right]) \tag{2.14}$$

If v is unknown for a solvent, its value can be calculated using known physical properties of the solvent (e.g., thermal conductivity, thermal expansion, and temperature-viscosity relationship). A reasonable estimate of v may also be made via comparison of existing non-parabolicity data to a solvents Andrade scaling factor (B). The scaling factor B may be determined by

$$\eta(T) = \eta_c \, e^{\left[B\left(\frac{1}{T} - \frac{1}{T_c}\right)\right]} \tag{2.15}$$

where η_c and T_c are the viscosity and temperature at the cold wall, respectively. An example of how to estimate v is shown in Figure 2.10.

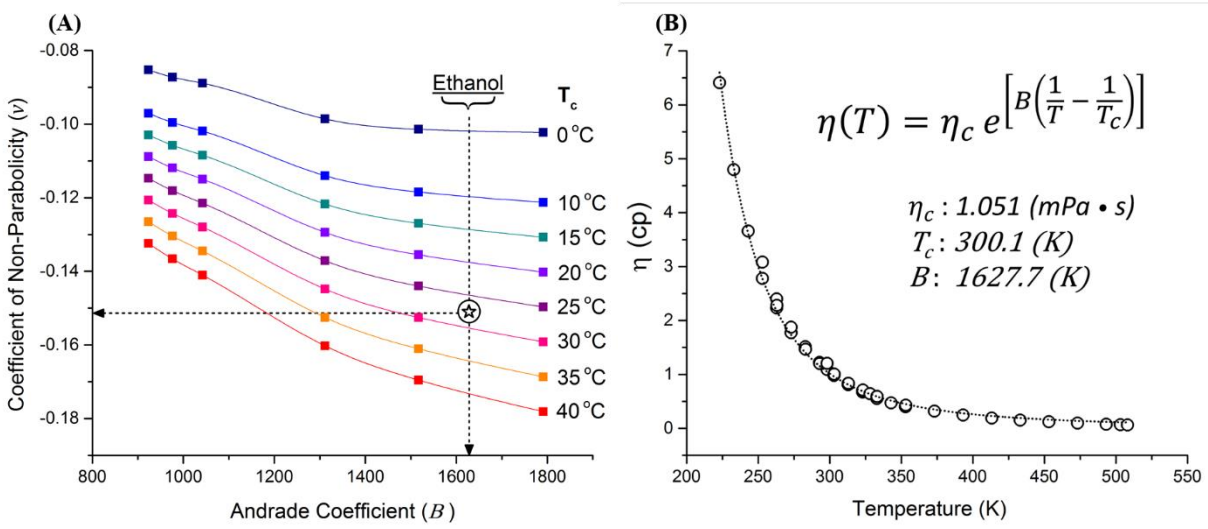

Figure 2.10. Variation of the *v*-parameter with respect to the Andrade scaling parameter (*B*) for various solvents. Note that curves were calculated for several cold wall temperatures (T_c) assuming a constant ΔT of 80 K and that variation of ΔT yields a new set of curves. A value for *v* (open star) was determined based on typical ThFFF conditions: T_c = 27°C, ΔT = 80 K, and *B* = 1627.7 K. Figure 2.10b depicts the temperature variation in viscosity for ethanol, an exponential decay in the form displayed allows for the determination of *B* used in Figure 2.10a.

Equations 2.13 and 2.14 allow accurate prediction of the retention ratio if D_T and *D* are known for the polymer-solvent system or if S_T is determined from a measured retention time. While *D* may be approximated through the well-known Stokes-Einstein relationship, D_T has no established theory. However, there are several competing predictive models which allow for the estimation of polymer D_T in polar and non-polar solvents [159]–[161]. These predictive models leverage physiochemical properties of the polymer-solvent system (e.g., thermal conductivity or polymer-solvent interaction parameter) to estimate D_T. Values calculated from predictive models vary in accuracy but have been shown to correctly predict trends in D_T [162]. These trends are highly useful in solvent selection, which at the moment is largely a trial-and-error approach. The experimental conditions which impact retention time include field strength, cold wall temperature, polymer-solvent interactions, and carrier fluid. The effect of each of these parameters and practical considerations are addressed in the following sections.

2.3.2 Methodology

2.3.2.1 Solvent Selection

The primary challenge of ThFFF polymer analysis is the selection of a suitable carrier fluid that will impart a sufficiently high D_T or S_T for analyte retention. Literature values for D_T

are available for well-studied polymers like PS and polyacrylates in a variety of solvents [152], [160], [162]. Commonly used solvent-polymer combinations are listed in Table 2.3. As with size (and thus D), D_T may change with respect to solvent and have dramatic effects on retention. It is also important to note that some polymer-solvent systems have D_T values too low to be measured and are often not reported. For polymers with unknown D_T, solvent selection is often done by a trial-and-error approach. The advent of predictive models has proven useful for estimating the D_T for a given polymer-solvent system but require inputs [156], [159]–[161], [163], [164] that may not be readily available. These inputs often include polymer and solvent properties or specific polymer-solvent interaction parameters. A comparison of two predictive models that were applied to polystyrene and polyacrylates may be found in literature [162]. Single-solvent systems simplify the interpretation of ThFFF fractograms and data from online detection schemes. However, in some cases binary solvents have been shown to double retention time of polymers [154], [165], [166]. The reverse case has also been shown where a binary solvent significantly decreases retention time which yielded some insight into the thermal diffusion mechanism [154]. It is hypothesized that if the 'good' solvent undergoes thermal diffusion in the same direction as the polymer, the resulting apparent D_T will be higher than that for the polymer alone.

An additional consideration in the solvent selection process is compatibility with the channel walls. Most ThFFF channels are coated with nickel or chromium [167] which may be degraded in aqueous or halogenated solvents. Sensitivity to these solvents is amplified at elevated temperatures and may result in channel surface pitting.

Table 2.3. List of common polymer-solvent combinations for ThFFF.

Sample	Common Solvents	Reference
Polystyrene	Tetrahydrofuran, Toluene, 2-Butanone, Ethyl Acetate, Cyclohexane	Kohler, *et al.*[168], Runyon, *et al.*[162]
Polyacrylates	Dioxane, 2-Butanone, Ethyl Acetate, Tetrahydrofuran, Acetone, Acetonitrile	Runyon, *et al.* [162], Greyling, *et al.*[169]
Polyisoprene	Tetrahydrofuran, Toluene, Benzene, Cyclohexane	Schimpf, *et al.*[152], Hiller, *et al.*[170]
Polybutadiene	Tetrahydrofuran	Pasch, *et al.*[50], Choi, *et al.*[18]

2.3.2.2 Field Strength

In ThFFF, the field strength is defined as the temperature gradient across the channel or *dT/dx*. Multiplying *dT/dx* by channel thickness *w* yields the temperature difference between the hot and cold walls (ΔT) [171]. Regardless of channel thickness, the retention ratio is dependent on ΔT and thus field strength is referred to as ΔT as written in Equation 2.13. This means that channels with different thicknesses but with the same ΔT will have equivalent retention ratios [171]. Field strengths typically range between 5 and 100 °C. In polymer analysis, the independence of D_T from molar mass simplifies field strength selection as separation of polymers with the same composition is only dependent on *D*. In a theta solvent, *D* decreases with the square root of molar mass and retention is inversely related to *D*. Thus, retention for a given polymer-solvent system may be optimized by the relationship between size, molar mass, and field strength. It is important to consider that this optimization is highly dependent on the polymer-solvent system as D_T and the relationship between *D* and molar mass may vary considerably.

In a typical experiment, the sample is first injected without a field to ensure a large measurable detector response. The injected sample may then be systematically diluted until an appropriate detector response is observed and the field strength is then increased to increase retention. The detector peak area in the absence of an applied field may be employed to calculate sample recovery [70]. It should also be noted that overloading concentrations change with field strength and polymer molar mass as indicated by Equation 2.7.

2.3.2.3 Temperature Field Programming

In the case of highly polydisperse mixtures, a constant field strength may lead to long analysis times. Like gradient elution chromatography, temperature field programming utilizes a high initial ΔT to retain low S_T components followed by a decrease in ΔT to hasten elution of highly retained (high S_T) components. The rate of field decay is limited by the cooling power of the recirculating chiller. Several mathematical functions have been developed for optimal programming field decay profiles and are discussed in the literature [2], [172]–[175]. The separation of 10^4 – 10^6 Da PS shown in Figure 2.11 uses the exponential decay function described by Equation 2.16 where t_1 is the hold time for initial field strength, *p* is the power of the decay, and t_a is the asymptotic time.

$$\Delta T(t) = \Delta T_0 (\frac{t_1 - t_a}{t - t_a})^p \qquad t \geq t_1 > t_a \tag{2.16}$$

Most separations are optimally performed where t_1 is approximately void time, p is set to 2, and where $t_a = -pt_1$ [174]. Molar mass calibration curves may be generated for programmed decay methods but there are potential pitfalls. Under high field strengths, large molar mass species will be more compressed against the cold wall which may exacerbate overloading effects. This can be accounted for by varying the injected sample amount and if retention time and peak shapes remain constant then overloading is not present. An additional concern is that the cold wall temperature may change. In the case of a field decay from a ΔT of 80 to 0, the cold wall temperature may decrease from 25 to 15 ^{o}C thus impacting both ΔT and D. These changes, along with detector drift, can impact data analysis and interpretation. Differential refractometers are especially sensitive to changes in pressure and temperature, in principle the latter may be easily accounted for. However, in practice this may prove to be more difficult and blank baseline subtractions should be utilized.

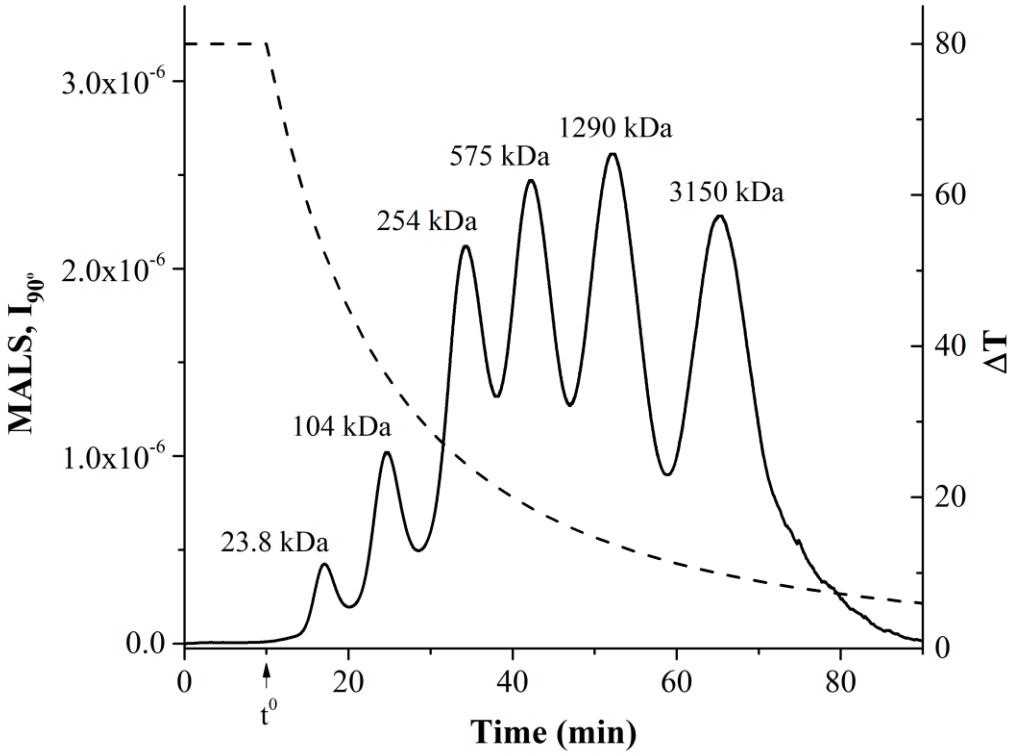

Figure 2.11. Programmed temperature field decay separation of PS standards (23.8, 104, 254, 575, 1290, and 3150 kDa) using Equation 2.13 where t_1 = 10, t_a = -20, p = 2. Carrier fluid is methyl ethyl ketone, t^0 = 10 min.

2.3.2.4 Cold Wall Temperature

As alluded to in the previous section, cold wall temperature may have a significant impact on retention as well as data analysis (due to the relationship between temperature, viscosity, and *D*). It was shown that a universal calibration curve may be generated which incorporates a correction for cold wall temperature [176]. This allows the transference of calibration curves between laboratories and instruments without the need to maintain an explicit cold wall temperature. This is especially important when dealing with samples at the upper limits of field strength where control over the cold wall temperature becomes difficult to maintain. Finally, it is good practice to report cold wall temperature in ThFFF experiments.

2.3.2.5 Flow Rate

A typical flow rate for ThFFF experiments is 0.2 mL/min. However, variation of this flow rate may be necessary to either reduce run time or increase fractionating power. Increasing the flow rate will decrease analysis time, but this will in turn reduce resolution. To obtain the most accurate molar mass distributions, lower flow rates should be used [2]. In some polymer-solvent systems there is a fine balance between sufficient concentration for detector response and overloading behavior. High molar mass polymers have a greater tendency to interact with channel walls due to the number of contact points between the wall and an individual chain. This may appear as overloading behavior and a modest increase in flow rate may reduce this effect as this can decrease contact time between the compressed polymer layer and the accumulation wall [2].

Unlike other FFF techniques, sample equilibrium layers are rapidly achieved in ThFFF so there is usually no need for the stop-flow relaxation used in sedimentation FFF or focusing time required in AF4.

2.3.3 Instrumentation

Thermal FFF systems are comprised of a pump, separation channel, and a series of detectors. The ThFFF channel is formed from two nickel-plated copper blocks separated by a spacer. The metal surface is polished to a mirror finish to provide a smooth surface for laminar flow. The hot block (top block on commercial channels) is heated by resistive heaters while the bottom block is cooled by a recirculating chiller. Holes are drilled into the cold block to form the inlet and outlet of the channel. Additional holes are drilled along the length of the hot and cold walls to accommodate temperatures probes which are used to monitor field strength. The two

blocks sandwich a polytetrafluoroethylene coated polyimide spacer whose thickness can vary between 50-400 μm. The channel geometry is dictated by the shape cut out of the spacer and is rectangular (breadth 1-2 cm) with triangular ends. These dimensions impact the sample loading capacity of the channel, where capacity increases with volume. Currently there is one commercial vendor for ThFFF instruments, Postnova Analytics. While organic solvents are most commonly used as carrier liquids, aqueous solutions have also been used over a range of ionic strengths and pH values. Care should be taken when using aqueous carrier liquids as the nickel plating may be adversely impacted.

Due to FFF's open channel design, high pressure pumps are generally not required even though they are used in commercial systems. It is common practice to add restriction tubing at the outlet to pressurize the channel (maximum of 14 bar for commercial instruments) and thereby increase the boiling point of the carrier fluid. Field strength (ΔT) is limited by the ability of the recirculating chiller to maintain a constant cold wall temperature and the ability to elevate solvent boiling point. Commercially available channels have a maximum ΔT of approximately 120. For polystyrene in toluene, with a D_T of approximately 10.3 $\mu m^2 s^{-1} K^{-1}$, low molar mass ($<10^3$ Da) polymers are poorly retained if standard ThFFF practice is employed. To lower the molar mass limit, binary solvents have been used – if one solvent also thermally diffuses in the same direction as the polymer, the resultant additive D_T (of both polymer and solvent) will lead to increased polymer retention and a lower MW limit [165], [166], [177]. With this binary solvent approach, 2600 Da and 4400 Da PS were retained and separated. Alternatively, a ThFFF channel was built to operate at 8 atmospheres of pressure and a ΔT of 158 [178]. This channel was used to separate a mixture of polystyrene (PS) standards with M_w ranging from 600 to 2100 Da.

2.3.4 Advances in ThFFF Instrumentation

2.3.4.1 Microfluidics

Thermophoresis has been used in microfluidics to focus particles [179], [180], polymerize catalytically active polymers [181], separate and characterize [182], [183], and study the mechanism of thermal diffusion [184], [185]. The prototypical microfluidic ThFFF analogs described in literature [182], [183] demonstrate the feasibility of this approach but their applications to polymers have been limited thus far.

2.3.4.2 Online Detection

In addition to commonly used detectors, there have been several advancements in online detection for ThFFF. Matrix assisted laser desorption ionization coupled to time-of-flight mass spectrometry (MALDI-TOF-MS) is a useful characterization technique that is challenged when applied to polydisperse samples. This is remedied by using a separation technique as a first stage to collect more monodisperse fractions that are subsequently prepared for off-line MALDI-TOF-MS characterization. This time consuming and tedious process was improved by the development of an oscillating capillary nebulizer (OCN) that continuously deposited separated polymers on a MALDI plate [186]. The analytes deposited on the plate were analyzed by a MALDI-TOF-MS equipped with a nitrogen (337 nm) and a frequency tripled Nd:YAG laser (355 nm). The former was used for MW < ~15 kDa and the latter for MWs as high as ~100 kDa, both with all-trans retinoic acid as the matrix and silver trifluoroacetate as the cationization agent. The distance between the OCN tip and MALDI plate was important for complete solvent evaporation and the matrix film thickness also had an important role in attaining a desirable signal-to-noise ratio. Fractions were collected continuously (which yields a continuous distribution) on the MALDI plate.

Nuclear magnetic resonance (NMR) is another powerful tool which can provide detailed information about molecular structure and is used for off-line analysis of fractions collected from separation techniques. NMR was coupled to ThFFF to analyze a triblock polymer comprised of poly(t-butyl methacrylate), poly(2-vinylpyridine), and polybutadiene [187]. Analysis of this copolymer by liquid chromatography is hindered by non-ideal interactions between the polar polymer and stationary phase. Furthermore, ThFFF separates polymers compositionally which may allow for more accurate compositional analysis than by SEC-NMR analysis [170]. However, two copolymers of different composition and molar mass with the same S_T will coelute. This was shown in a direct comparison of ThFFF-NMR and SEC-NMR, where the compositional sensitivity of ThFFF improved separation for one copolymer and resulted in coelution of another [170].

Fourier transform infrared spectroscopy (FTIR) is another compositionally sensitive technique that has been traditionally used in off-line analysis. Its coupling with a separation technique has been inhibited by the need for thin and mechanically strong flow cells. To circumvent this, a flow cell based on attenuated total reflectance was built and optimized for

SEC of PS and PMMA [188]. Optimization proved to be a lengthy and tedious process but yielded a 9000-fold improvement over initial signal-to-noise ratios and minor components down to five mol % could be detected. This instrumentation was later developed for use in ThFFF where it was utilized to quantitatively analyze copolymer blends of PS and PMMA [189]. The results of this work, seen in Figure 2.12, illustrate the usefulness of this coupling as data was converted to weight percent of their respective components.

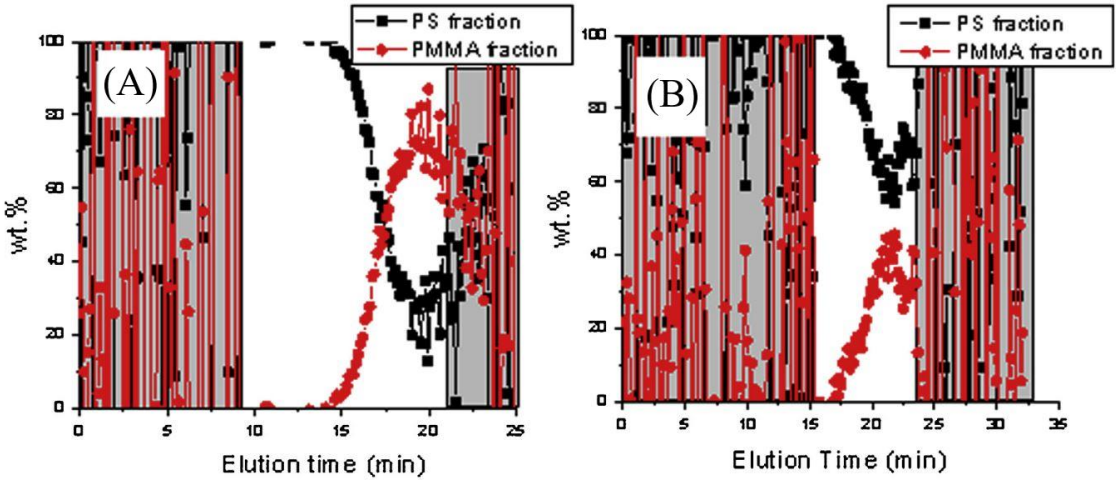

Figure 2.12. FTIR data collected from online fractionation of PS-PMMA copolymer blends by ThFFF. ΔT = 60 K, T_c = 25°C, and flow rate = 0.3 mL/min. (Reprinted with permission from [189])

2.3.5 Applications

2.3.5.1 Composition

ThFFF is particularly attractive for polymer analysis because thermal diffusion varies with polymer-solvent composition. This allows for the separation of heterogeneous polymers by their respective compositions and molar masses. There are many examples of this being leveraged to characterize copolymers [18], [149], [152], [190]–[192]. This body of work showed that a relationship between D_T of a copolymer and D_T of the individual homopolymers can be elucidated, provided a nonselective solvent for both polymers was used as the carrier liquid. This relationship is shown in Equation 2.17, where x_a and x_b represent the mole fraction of components A, and B.

$$(D_T)_{A-B} = x_a(D_T)_a + x_b(D_T)_b \tag{2.17}$$

Polymer composition may be determined from known D_T for homopolymer components and online concentration detectors. This work was expanded to characterize a terpolymer comprised of PS, PMMA, and poly(t-butyl acrylate) [190]. To analytically solve for the three unknown mole fractions, three equations which allow for their independent solution are required. The concentration of PS was determined from measured absorbance at 254 nm. Similar to Equation 17, the relationship between the incremental change in refractive index with respect to concentration (*dn/dc*) of a complex polymer [193] is well known and is shown in Equation 2.18.

$$(\frac{dn}{dc})_{A-B-C} = x_a(\frac{dn}{dc})_a + x_b(\frac{dn}{dc})_b + x_c(\frac{dn}{dc})_c \quad (2.18)$$

These three relationships were used to estimate the mole fractions of each component across the elution profile of the terpolymer. The mole fraction versus time plot in Figure 2.13 shows the compositional variation of the terpolymer eluting from the ThFFF channel. Furthermore, this sample also contained a PS-PtBA diblock copolymer component that eluted at ~7 mins whose presence was not evident from NMR analysis of the as-synthesized polymer. These results provide a detailed composition distribution which can yield invaluable insight into polymerization kinetics or be used in quality control. Note that to perform this analysis for a given polymer-solvent system, it must be possible to determine concentration for two of the three components. In some systems, UV detection may not be accessible due to the strong UV absorbance of a solvent or weak absorbance of a polymer. This process may be considered more routine for a two-component system, as dRI is reliable in a wide array of solvents.

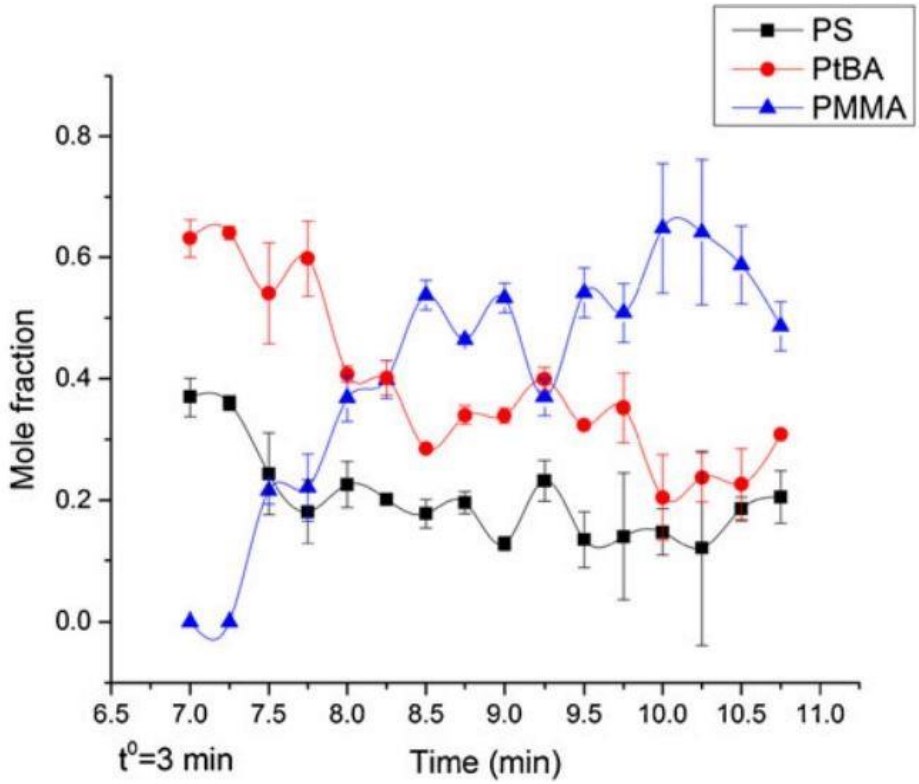

Figure 2.13. Mole fraction component analysis of terpolymer comprised of PS, PMMA, and poly(tert-butyl acrylate) (PtBA). (Reprinted with permission from [190])

2.3.5.2 Architecture

In addition to composition, ThFFF has been developed to characterize architectural features of polymer chains. This is achieved through the Soret contraction factor (*g"*), defined as the ratio of the branched polymer S_T to a linear polymer S_T [194].

$$g" = \frac{S_{T_{br}}}{S_{T_{lin}}} \tag{2.19}$$

Like other contraction factors related to viscometry and light scattering [195], *g"* relies on the fact that branched polymers exhibit a contraction in size relative to a linear polymer of equivalent mass. A linear polymer has a *g"* of one and an increase in the number of branching sites should cause this value to decrease. Qualitatively, the degree of contraction may be used to describe the relative amount of branching. In a well characterized system, it is feasible to create a calibration curve based on *g"* and some relevant parameter (*e.g.*, degree of branching determined via NMR). One such example was the analysis of a series of branched polyesters [196]. This work leveraged a polyester library synthesized through strategies which allowed for controlled

degrees of branching via protected and unprotected multifunctional monomers. Analysis of the branched polymers yielded the numerator of Equation 2.19 through the measured retention times. To approximate the denominator, a calibration curve of S_T with respect to molar mass was created to determine S_T of a linear analog (one which mimics the polymer-solvent interactions of the branched system) at an equivalent molar mass. Ideally, a calibration curve would be created by the analysis of a series of linear polymers with increasing molar masses. If this is impractical, it may be substituted for a linear sample with broad polydispersity [197]. In situations where no linear analog is available, S_T of a linear polymer may be approximated [198] or estimated through predictive models and the Stokes-Einstein equation. From the measured $S_{T,br}$ and calculated $S_{T,lin}$, g'' was determined across the elution profile to yield branching distributions. Data for this analysis may be seen in Figure 2.14 where log (g'') is plotted with respect to the differential number fraction. It is interesting that some polymers were observed to have a contraction factor greater than one. Fractions were collected and analyzed by MALDI-TOF-MS which confirmed that these were cyclic polymers. The mechanism that causes g'' for these cyclic polyesters to be greater than one is currently unknown. Another interesting feature of this paper is that a correlation between D_T and degree of branching was observed in tetrahydrofuran but not cyclohexane.

In an early publication, D_T was shown to be independent of molar mass and architecture (specifically branching for polystyrene in ethylbenzene) [153]. There have since been several literature examples where D_T was shown to fluctuate with microstructure [169] and branching [196], [198]. The first of these publications demonstrates the feasibility of characterizing microstructure (tacticity) of PMMA polymers in various solvents [169]. The fractionation of polymers by tacticity was validated by off-line NMR analysis of collected fractions. This work leveraged the availability of catalytically polymerized PMMA, which produces polymers with minimal to no dispersity in microstructure. In some polymer-solvent combinations there was no change in D_T and the magnitude of this change varied with solvent. Currently, it is not clear what the mechanism is for this phenomenon. Nevertheless, it is important to note that fractionation by microstructure is possible through ThFFF and solvent selection may greatly alter resolution. As with branching, changes in D_T may be observed in some solvents but not others.

The low shear stress in an FFF channel is an appealing characteristic when analyzing complexes and assemblies which are susceptible to shear degradation in a packed

chromatography column. In a recent example, block copolymers comprised of polybutadiene and PS which formed self-assembled micelles were characterized by ThFFF [191]. In a single analysis, multidetector ThFFF separated micelles according to corona composition and provided comprehensive information on important micelle characteristics (such as size, molar mass, and corona composition).

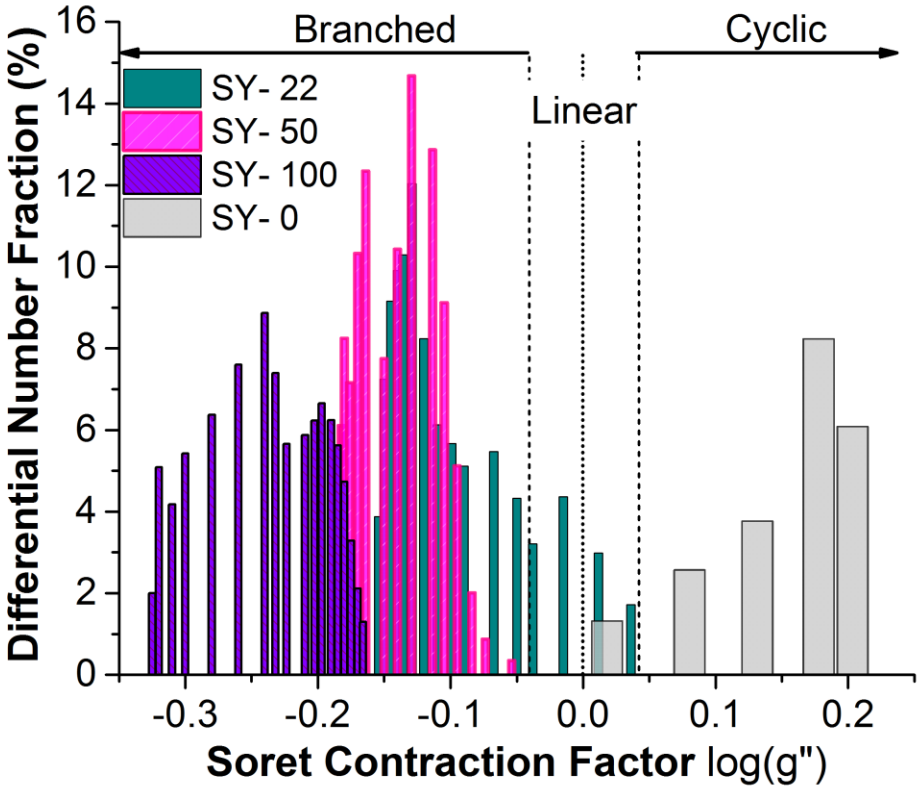

Figure 2.14. Distribution of g" within each sample where SY-# indicates the degree of branching as determined by NMR. The dashed lines represent error for the linear region. (Reprinted with permission from [196])

2.3.5.3 Microgels

FFF techniques share the advantage of an open channel design and ability to analyze samples over large molar mass range (10^3-10^8 Da). These traits provide an opportunity to study microgels which often range widely in molar mass and are filtered prior to injection into chromatography columns. ThFFF has been used to determine gel content [199] and molar mass of filtered and unfiltered microgels [18], [143], [146], [200]. The fractograms in Figure 2.15 illustrate the difference in both molar mass and RMS radius of a filtered and unfiltered microgel.

The filtered sample exhibits lower molar mass and RMS radius when compared to unfiltered. The light scattering intensity and dRI signal showed significant loss of both high molar mass ($>10^6$ Da) polymers and soluble lower molar mass polymers for the filtered sample. It was also demonstrated that sample dissolution should extend beyond 24 hours as there were subtle differences in molar mass over time [146].

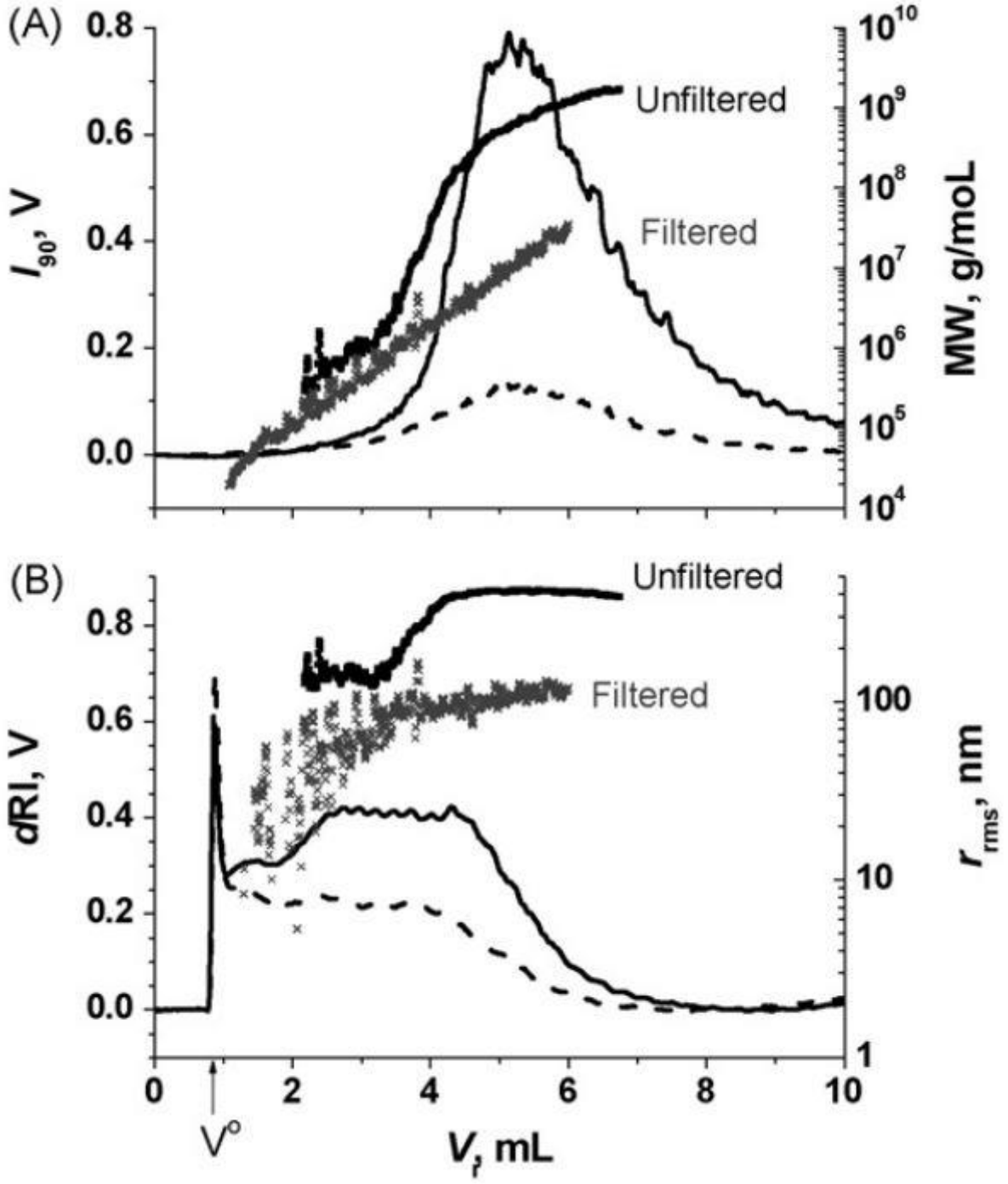

Figure 2.15. ThFFF-MALS analysis of unfiltered and filtered PVAc10 (poly (vinyl acetate)). The filter was 0.5 μm pore-size. (A) Intensity at 90° angle (I_{90}) fractograms and molar masses and (B) dRI fractograms and r_{rms}. Solid and dashed lines represent the fractograms of unfiltered and filtered PVAc10, respectively. The black and gray lines correspond to MW or r_{rms} of the unfiltered and filtered PVAc10, respectively. (Reprinted with permission from [146]).

2.4 Summary

Field-flow fractionation (FFF) has grown in popularity because of the benefits derived from an open channel design, diverse external fields that separate according to different physicochemical properties, availability of retention theory for normal mode separations, and high separation resolution. Polymers spanning a large range (~10^3 to ~10^8 Da), complexes, aggregates, and microgels can be separated and analyzed with minimal sample preparation, shear stress and sample loss. These features enable a comprehensive view of the sample system as changes in protein monomers and aggregates (or soluble polymers and microgels) are simultaneously monitored. Different fields separate according to different physicochemical properties and hence different information may be obtained. For example, the crossflow field produces fractograms whose retention time axis can be converted to diffusion coefficient or hydrodynamic size using FFF theory while a temperature gradient field yields information about composition, tacticity, and branching. Quite importantly, FFF coupled with multiple detectors, e.g., light scattering, mass spectrometry, is demonstrated as a versatile platform that combines desirable capabilities of multiple orthogonal analytical techniques. This chapter introduces the principles, applications, and advances of flow and thermal FFF for polymer separations and characterization.-Growth in the development and application of FFF techniques is expected as new complex polymers are synthesized and questions arise about structure-composition-function relationships and the importance of distributions in multiple properties.

2.5 Acknowledgements

The authors acknowledge the support of the National Science Foundation (CHE-1808805).

2.6 Bibliography

[1] J. C. Giddings, “A New Separation Concept Based on a Coupling of Concentration and Flow Nonuniformities,” *Separation Science*, vol. 1, no. 1, pp. 123–125, 1966, doi: 10.1080/01496396608049439.

[2] M. E. Schimpf, K. Caldwell, and J. C. Giddings, *Field-Flow Fractionation Handbook*. John Wiley & Sons, 2000.

[3] S. K. R. Williams and K. D. Caldwell, *Field-Flow Fractionation in Biopolymer Analysis*. Vienna: Springer Vienna, 2012. doi: 10.1007/978-3-7091-0154-4.

[4] S. K. R. Williams, J. R. Runyon, and A. A. Ashames, “Field-flow fractionation: Addressing the nano challenge,” *Anal Chem*, vol. 83, no. 3, pp. 634–642, 2011, doi: 10.1021/ac101759z.

[5] F. A. Messaud, R. D. Sanderson, J. R. Runyon, T. Otte, H. Pasch, and S. K. R. Williams, "An overview on field-flow fractionation techniques and their applications in the separation and characterization of polymers," *Progress in Polymer Science (Oxford)*, vol. 34, no. 4. Elsevier Ltd, pp. 351–368, 2009. doi: 10.1016/j.progpolymsci.2008.11.001.

[6] M. Baalousha, B. Stolpe, and J. R. Lead, "Flow field-flow fractionation for the analysis and characterization of natural colloids and manufactured nanoparticles in environmental systems: A critical review," *J Chromatogr A*, vol. 1218, no. 27, pp. 4078–4103, 2011, doi: 10.1016/j.chroma.2011.04.063.

[7] P. M. Shiundu and S. K. R. Williams, "Thermal Field-Flow Fractionation for Particle Analysis: Opportunities and Challenges," pp. 185–198, 2004, doi: 10.1021/bk-2004-0881.ch012.

[8] C. Mélin *et al.*, "Cancer stem cell sorting from colorectal cancer cell lines by sedimentation field flow fractionation," *Anal Chem*, vol. 84, no. 3, pp. 1549–1556, 2012, doi: 10.1021/ac202797z.

[9] B. Roda *et al.*, "Field-flow fractionation in bioanalysis: A review of recent trends," *Anal Chim Acta*, vol. 635, no. 2, pp. 132–143, 2009, doi: 10.1016/j.aca.2009.01.015.

[10] J. C. Giddings, F. J. F. Yang, and M. N. Myers, "Sedimentation Field-Flow Fractionation," *Anal Chem*, vol. 46, no. 13, pp. 1917–1924, 1974, doi: 10.1021/ac60349a046.

[11] J. C. Giddings, L. Cited, F. J. Yang, and M. N. Myers, "Theoretical and experimental characterization of flow field-flow fractionation," *Anal Chem*, vol. 48, no. 8, 1976, doi: 10.1021/ac50002a016.

[12] K. D. Caldwell, L. F. Kesner, M. N. Myers, and J. C. Giddings, "Electrical Field-Flow Fractionation of Proteins," *Science (1979)*, vol. 176, no. 4032, pp. 296–298, 1972, doi: 10.1126/science.176.4032.296.

[13] T. M. Vickrey and J. A. Garcia-Ramirez, "Magnetic Field-Flow Fractionation: Theoretical Basis," *Sep Sci Technol*, vol. 15, no. 6, pp. 1297–1304, 1980, doi: 10.1080/01496398008068506.

[14] J. M. Davis and J. C. Giddings, "Feasibility Study of Dielectrical Field-Flow Fractionation," *Sep Sci Technol*, vol. 21, no. 9, pp. 969–989, 1986, doi: 10.1080/01496398608058390.

[15] V. L. Kononenko, J. C. Giddings, and M. N. Myers, "On the possibility of photophoretic field-flow fractionation," *Journal of Microcolumn Separations*, vol. 9, no. 4, pp. 321–327, Jan. 1997, doi: 10.1002/(SICI)1520-667X(1997)9:4<321::AID-MCS10>3.0.CO;2-9.

[16] T. Otte, T. Klein, R. Brüll, T. Macko, and H. Pasch, "Study of the abnormal late co-elution phenomenon of low density polyethylene in size exclusion chromatography using high temperature size exclusion chromatography and high temperature asymmetrical flow field-flow fractionation," *J Chromatogr A*, vol. 1218, no. 27, pp. 4240–4248, 2011, doi: 10.1016/j.chroma.2011.01.009.

[17] M. I. Malik and H. Pasch, “Field-flow fractionation: New and exciting perspectives in polymer analysis,” *Prog Polym Sci*, vol. 63, pp. 42–85, 2016, doi: 10.1016/j.progpolymsci.2016.03.004.

[18] Y. J. Choi, S. T. Kim, S. H. Lee, A.-J. Kim, G. Kwag, and S. Lee, “Molecular characterization of solution styrene-butadiene rubber: Thermal field-flow fractionation/multi-angle light scattering studies,” *J Chromatogr A*, vol. 1314, pp. 306–312, Nov. 2013, doi: 10.1016/j.chroma.2013.09.037.

[19] J. C. Giddings and M. N. Myers, “Steric Field-Flow Fractionation: A New Method for Separating 1 to 100 μm Particles,” *Sep Sci Technol*, vol. 13, no. 8, pp. 637–645, Oct. 1978, doi: 10.1080/01496397808057119.

[20] J. C. Giddings, “Hyperlayer Field-Flow Fractionation,” *Sep Sci Technol*, vol. 18, no. 8, pp. 765–773, Jun. 1983, doi: 10.1080/01496398308068578.

[21] M. Martin and P. S. Williams, “Theoretical Basis of Field-Flow Fractionation,” in *Theoretical Advancement in Chromatography and Related Separation Techniques*, Dordrecht: Springer Netherlands, 1992, pp. 513–580. doi: 10.1007/978-94-011-2686-1_18.

[22] J. C. Giddings, “The conceptual basis of field-flow fractionation,” *J Chem Educ*, vol. 50, no. 10, p. 667, Oct. 1973, doi: 10.1021/ed050p667.

[23] J. C. Giddings, “Field-Flow Fractionation of Polymers: One-phase Chromatography,” *Pure & Appl. Chem.*, vol. 51, no. 7, pp. 1459–1471, 1979, doi: 10.1351/pac197951071459.

[24] J. C. Giddings, “Displacement and Dispersion of Particles of Finite Size in Flow Channels with Lateral Forces. Field-Flow Fractionation and Hydrodynamic Chromatography,” *Sep Sci Technol*, vol. 13, no. 3, pp. 241–254, Mar. 1978, doi: 10.1080/01496397808060222.

[25] E. Grushka, K. D. Caldwell, M. N. Myers, and J. C. Giddings, “Field Flow Fractionation,” *Separation and Purification Methods*, vol. 2, no. 1, pp. 127–151, Jan. 1973, doi: 10.1080/03602547408068793.

[26] C. Fuentes, J. Choi, C. Zielke, J. M. Peñarrieta, S. Lee, and L. Nilsson, “Comparison between conventional and frit-inlet channels in separation of biopolymers by asymmetric flow field-flow fractionation,” *Analyst*, vol. 144, no. 15, pp. 4559–4568, Jul. 2019, doi: 10.1039/C9AN00466A.

[27] M. Ali, E. Hwang, I.-H. Cho, and M. H. Moon, “Characterization of sodium hyaluronate blends using frit inlet asymmetrical flow field-flow fractionation and multiangle light scattering.,” *Anal Bioanal Chem*, vol. 402, no. 3, pp. 1269–76, Jan. 2012, doi: 10.1007/s00216-011-5531-0.

[28] U. Till *et al.*, “Frit inlet field-flow fractionation techniques for the characterization of polyion complex self-assemblies,” *J Chromatogr A*, vol. 1481, pp. 101–110, Jan. 2017, doi: 10.1016/j.chroma.2016.12.050.

[29] J. Gigault, J. M. Pettibone, C. Schmitt, and V. A. Hackley, “Rational strategy for characterization of nanoscale particles by asymmetric-flow field flow fractionation: A tutorial,” *Anal Chim Acta*, vol. 809, pp. 9–24, Jan. 2014, doi: 10.1016/j.aca.2013.11.021.

[30] W. Graessley, “Polymer chain dimensions and the dependence of viscoelastic properties on concentration, molecular weight and solvent power,” *Polymer (Guildf)*, vol. 21, no. 3, pp. 258–262, Mar. 1980, doi: 10.1016/0032-3861(80)90266-9.

[31] M. Martin and F. Feuillebois, “Onset of sample concentration effects on retention in field-flow fractionation,” *J Sep Sci*, vol. 26, no. 6–7, pp. 471–479, May 2003, doi: 10.1002/jssc.200390063.

[32] K. D. Caldwell, S. L. Brimhall, Y. Gao, and J. C. Giddings, “Sample overloading effects in polymer characterization by field-flow fractionation,” *J Appl Polym Sci*, vol. 36, no. 3, pp. 703–719, Jul. 1988, doi: 10.1002/app.1988.070360319.

[33] W.-J. Cao, M. N. Myers, R. S. Williams, and J. C. Giddings, “Sample Mass Effects on Thermal Field-Flow Fractionation Retention and Universal Calibration,” *International Journal of Polymer Analysis and Characterization*, vol. 4, no. 5, pp. 407–433, Sep. 1998, doi: 10.1080/10236669808009726.

[34] J. Giddings, F. Yang, and M. Myers, “Flow Field-Flow Fractionation: A Versatile New Separation Method,” *Science (1979)*, vol. 193, no. 4259, pp. 1244–1245, 1976, doi: 10.1126/science.959835.

[35] G. Yohannes, M. Jussila, K. Hartonen, and M. Riekkola, “Asymmetrical flow field-flow fractionation technique for separation and characterization of biopolymers and bioparticles,” *J Chromatogr A*, vol. 1218, no. 27, pp. 4104–4116, 2011, doi: 10.1016/j.chroma.2010.12.110.

[36] M. Wagner, S. Holzschuh, A. Traeger, A. Fahr, and U. S. Schubert, “Asymmetric flow field-flow fractionation in the field of nanomedicine,” *Anal Chem*, vol. 86, no. 11, pp. 5201–5210, 2014, doi: 10.1021/ac501664t.

[37] K.-G. Wahlund and J. C. Giddings, “Properties of an asymmetrical flow field-flow fractionation channel having one permeable wall,” *Anal Chem*, vol. 59, no. 9, pp. 1332–1339, May 1987, doi: 10.1021/ac00136a016.

[38] K.-G. Wahlund, “Flow field-flow fractionation: Critical overview,” *J Chromatogr A*, vol. 1287, pp. 97–112, Apr. 2013, doi: 10.1016/j.chroma.2013.02.028.

[39] S. K. R. Williams, M.-A. Benincasa, W. C. Smith, and J. D. Oliver, “Field-Flow Fractionation in Analysis of Polymers and Rubbers,” in *Encyclopedia of Analytical Chemistry*, Chichester, UK: John Wiley & Sons, Ltd, 2016, pp. 1–33. doi: 10.1002/9780470027318.a2008.pub3.

[40] S. Phuntsho, H. K. Shon, S. Vigneswaran, and J. Cho, “Assessing membrane fouling potential of humic acid using flow field-flow fractionation,” *J Memb Sci*, vol. 373, no. 1–2, pp. 64–73, 2011, doi: 10.1016/j.memsci.2011.02.046.

[41] M. A. Benincasa and J. C. Giddings, “Separation and Molecular Weight Distribution of Anionic and Cationic Water-Soluble Polymers by Flow Field-Flow Fractionation,” *Anal Chem*, vol. 64, no. 7, pp. 790–798, 1992, doi: 10.1021/ac00031a016.

[42] D. Kang and M. H. Moon, “Hollow Fiber Flow Field-Flow Fractionation of Proteins Using a Microbore Channel,” *Anal Chem*, vol. 77, no. 13, pp. 4207–4212, Jul. 2005, doi: 10.1021/ac050301x.

[43] R. N. Qureshi and W. T. Kok, “Optimization of asymmetrical flow field-flow fractionation,” *LCGC North America*, vol. 29, no. 1, pp. 76–83, 2011.

[44] M. E. Schimpf, K. Caldwell, and J. C. Giddings, *Field-Flow Fractionation Handbook*. John Wiley & Sons, 2000.

[45] C. W. Cuss, I. Grant-Weaver, and W. Shotyk, “AF4-ICPMS with the 300 da Membrane to Resolve Metal-Bearing ‘colloids’ < 1 kDa: Optimization, Fractogram Deconvolution, and Advanced Quality Control,” *Anal Chem*, vol. 89, no. 15, pp. 8027–8035, 2017, doi: 10.1021/acs.analchem.7b01427.

[46] W. Fraunhofer, G. Winter, and C. Coester, “Asymmetrical Flow Field-Flow Fractionation and Multiangle Light Scattering for Analysis of Gelatin Nanoparticle Drug Carrier Systems,” *Anal Chem*, vol. 76, no. 7, pp. 1909–1920, 2004, doi: 10.1021/ac0353031.

[47] W. Wang, M. Chen, L. Guo, and W. Wang, “Size partitioning and mixing behavior of trace metals and dissolved organic matter in a South China estuary,” *Science of the Total Environment*, vol. 603–604, pp. 434–444, 2017, doi: 10.1016/j.scitotenv.2017.06.121.

[48] C. Zielke, C. Teixeira, H. Ding, S. Cui, M. Nyman, and L. Nilsson, “Analysis of β-glucan molar mass from barley malt and brewer’s spent grain with asymmetric flow field-flow fractionation (AF4) and their association to proteins,” *Carbohydr Polym*, vol. 157, pp. 541–549, 2017, doi: 10.1016/j.carbpol.2016.10.045.

[49] A. C. Makan, R. P. Williams, and H. Pasch, “Field Flow Fractionation for the Size, Molar Mass, and Gel Content Analysis of Emulsion Polymers for Water-Based Coatings,” *Macromol Chem Phys*, vol. 217, no. 18, pp. 2027–2040, 2016, doi: 10.1002/macp.201600208.

[50] H. Pasch, A. C. Makan, H. Chirowodza, N. Ngaza, and W. Hiller, “Analysis of complex polymers by multidetector field-flow fractionation Field-Flow Fractionation,” *Anal Bioanal Chem*, vol. 406, no. 6, pp. 1585–1596, 2014, doi: 10.1007/s00216-013-7308-0.

[51] I. Perevyazko, A. Trützschler, A. Gubarev, and E. Lebedeva, “Absolute characteristics and conformation of cationic polymers by hydrodynamic approaches : Poly (AEMA- co -MAEMA- co -DMAEMA) stat copolymers,” *Eur Polym J*, vol. 97, no. August, pp. 347–355, 2017, doi: 10.1016/j.eurpolymj.2017.10.024.

[52] H. Mahroug *et al.*, “How microwave treatment of gluten affects its toxicity for celiac patients? A study on the effect of microwaves on the structure, conformation, functionality and immunogenicity of gluten,” *Food Chem*, vol. 297, no. February, p. 124986, Nov. 2019, doi: 10.1016/j.foodchem.2019.124986.

[53] R. A. Abbate *et al.*, “Asymmetric flow field flow fractionation for the investigation of caseins cross-linked by microbial transglutaminase,” *Food Hydrocoll*, vol. 92, no. January, pp. 117–124, 2019, doi: 10.1016/j.foodhyd.2019.01.043.

[54] H. M. Halamish *et al.*, “Self-assembly and nanostructure of poly(vinyl alcohol)-graft-poly(methyl methacrylate) amphiphilic nanoparticles,” *J Colloid Interface Sci*, vol. 553, pp. 512–523, 2019, doi: 10.1016/j.jcis.2019.06.047.

[55] A. Lederer, S. Boye, and D. Appelhans, “Advanced AF4 characterization of dendritic biomacromolecules, their self-assembly, and hybrid formation,” *ACS Symposium Series*, vol. 1281, pp. 171–187, 2018, doi: 10.1021/bk-2018-1281.ch009.

[56] B. Wittgren, K.-G. Wahlund, H. Dérand, and B. Wesslén, “Aggregation behavior of an amphiphilic graft copolymer in aqueous medium studied by asymmetrical flow field-flow fractionation,” *Macromolecules*, vol. 29, no. 1, pp. 268–276, 1996, doi: 10.1021/ma950837s.

[57] A. Vernhet, S. Dubascoux, B. Cabane, H. Fulcrand, E. Dubreucq, and C. Poncet-Legrand, “Characterization of oxidized tannins: Comparison of depolymerization methods, asymmetric flow field-flow fractionation and small-angle X-ray scattering,” *Anal Bioanal Chem*, vol. 401, no. 5, pp. 1563–1573, 2011, doi: 10.1007/s00216-011-5076-2.

[58] C. W. Isaacson and D. Bouchard, “Asymmetric flow field flow fractionation of aqueous C60 nanoparticles with size determination by dynamic light scattering and quantification by liquid chromatography atmospheric pressure photo-ionization mass spectrometry,” *J Chromatogr A*, vol. 1217, no. 9, pp. 1506–1512, 2010, doi: 10.1016/j.chroma.2009.12.060.

[59] M. Andersson, B. Wittgren, and K.-G. Wahlund, “Ultrahigh molar mass component detected in ethylhydroxyethyl cellulose by asymmetrical flow field-flow fractionation coupled to multiangle light scattering,” *Anal Chem*, vol. 73, no. 20, pp. 4852–4861, 2001, doi: 10.1021/ac0104734.

[60] A. Rolland-Sabaté, P. Colonna, M. G. Mendez-Montealvo, and V. Planchot, “Branching features of amylopectins and glycogen determined by asymmetrical flow field flow fractionation coupled with multiangle laser light scattering,” *Biomacromolecules*, vol. 8, no. 8, pp. 2520–2532, 2007, doi: 10.1021/bm070024z.

[61] H. Lee, S. K. R. Williams, K. L. Wahl, and N. B. Valentine, “Analysis of whole bacterial cells by flow field-flow fractionation and matrix-assisted laser desorption/ionization time-of-flight mass spectrometry,” *Anal Chem*, vol. 75, no. 11, pp. 2746–2752, 2003, doi: 10.1021/ac020698u.

[62] W. Fraunhofer and G. Winter, “The use of asymmetrical flow field-flow fractionation in pharmaceutics and biopharmaceutics,” *European Journal of Pharmaceutics and Biopharmaceutics*, vol. 58, no. 2, pp. 369–383, 2004, doi: 10.1016/j.ejpb.2004.03.034.

[63] M. E. Miller and J. C. Giddings, “Development of a Universal Separator: Characterization of Macromolecular and Particulate Material by Aqueous and Nonaqueous Flow FFF at Ambient and Elevated Operating Temperatures,” *Journal of Microcolumn Separations*,

vol. 10, no. 1, pp. 75–78, 1998, doi: 10.1002/(SICI)1520-667X(1998)10:1<75::AID-MCS10>3.0.CO;2-L.

[64] T. Otte *et al.*, "Characterization of branched ultrahigh molar mass polymers by asymmetrical flow field-flow fractionation and size exclusion chromatography," *J Chromatogr A*, vol. 1218, pp. 4257–4267, 2011, doi: 10.1016/j.chroma.2010.12.072.

[65] T. Otte, R. Brüll, T. Macko, H. Pasch, and T. Klein, "Optimisation of ambient and high temperature asymmetric flow field-flow fractionation with dual/multi-angle light scattering and infrared/refractive index detection," *J Chromatogr A*, vol. 1217, no. 5, pp. 722–730, 2010, doi: 10.1016/j.chroma.2009.12.014.

[66] C. Fuentes, D. Perez-Rea, B. Bergenståhl, S. Carballo, M. Sjöö, and L. Nilsson, "Physicochemical and structural properties of starch from five Andean crops grown in Bolivia," *Int J Biol Macromol*, vol. 125, pp. 829–838, 2019, doi: 10.1016/j.ijbiomac.2018.12.120.

[67] C. Fuentes *et al.*, "Characterization of non-solvent precipitated starch using asymmetrical flow field-flow fractionation coupled with multiple detectors," *Carbohydr Polym*, vol. 206, no. July 2018, pp. 21–28, 2019, doi: 10.1016/j.carbpol.2018.10.100.

[68] W. Zhang *et al.*, "Study on the retrogradation behavior of starch by asymmetrical flow field-flow fractionation coupled with multiple detectors," *Food Chem*, vol. 277, no. November 2018, pp. 674–681, 2019, doi: 10.1016/j.foodchem.2018.11.033.

[69] K. Korompokis, L. Nilsson, and C. Zielke, "The effect of in vitro gastrointestinal conditions on the structure and conformation of oat β-glucan," *Food Hydrocoll*, vol. 77, pp. 659–668, 2018, doi: 10.1016/j.foodhyd.2017.11.007.

[70] C. R. M. Bria *et al.*, "Asymmetrical flow field-flow fractionation for improved characterization of human plasma lipoproteins," *Anal Bioanal Chem*, vol. 411, no. 3, pp. 777–786, 2019, doi: 10.1007/s00216-018-1499-3.

[71] H. Gumz *et al.*, "Toward Functional Synthetic Cells: In-Depth Study of Nanoparticle and Enzyme Diffusion through a Cross-Linked Polymersome Membrane," *Advanced Science*, vol. 6, no. 7, 2019, doi: 10.1002/advs.201801299.

[72] M. Marioli and W. Th. Kok, "Recovery, overloading, and protein interactions in asymmetrical flow field-flow fractionation," *Anal Bioanal Chem*, 2019, doi: 10.1007/s00216-019-01673-w.

[73] D. de Guibert *et al.*, "Flow process and heating conditions modulate the characteristics of whey protein aggregates.," *J Food Eng*, vol. 264, no. March 2019, p. 109675, Jan. 2020, doi: 10.1016/j.jfoodeng.2019.07.022.

[74] V. P. L. Eckel, R. F. Vogel, and F. Jakob, "In situ production and characterization of cloud forming dextrans in fruit-juices," *Int J Food Microbiol*, vol. 306, no. March, p. 108261, 2019, doi: 10.1016/j.ijfoodmicro.2019.108261.

[75] P. Guo, W. Wang, S. Dai, S. Shen, W. Zhang, and Y. Lian, "Ultrasound-assisted dissolution and characterization of maize starch using asymmetrical flow field-flow

fractionation coupled with multiple detectors," *Microchemical Journal*, vol. 150, no. July, p. 104092, 2019, doi: 10.1016/j.microc.2019.104092.

[76] C. Fuentes, R. Castañeda, F. Rengel, J. M. Peñarrieta, and L. Nilsson, "Characterization of molecular properties of wheat starch from three different types of breads using asymmetric flow field-flow fractionation (AF4)," *Food Chem*, vol. 298, no. April, 2019, doi: 10.1016/j.foodchem.2019.125090.

[77] G. Krebs, M. Müller, T. Becker, and M. Gastl, "Characterization of the macromolecular and sensory profile of non-alcoholic beers produced with various methods," *Food Research International*, vol. 116, no. August 2018, pp. 508–517, 2019, doi: 10.1016/j.foodres.2018.08.067.

[78] J. E. G. J. Wijnhoven, J. P. Koorn, H. Poppe, and W. T. Kok, "Influence of injected mass and ionic strength on retention of water-soluble polymers and proteins in hollow-fibre flow field-flow fractionation," *J Chromatogr A*, vol. 732, no. 2, pp. 307–315, 1996, doi: 10.1016/0021-9673(95)01263-X.

[79] M. H. Moon, I. Park, and Y. Kim, "Size characterization of liposomes by flow field-flow fractionation and photon correlation spectroscopy: Effect of ionic strength and pH of carrier solutions," *J Chromatogr A*, vol. 813, no. 1, pp. 91–100, 1998, doi: 10.1016/S0021-9673(98)00325-2.

[80] A. Litzén and K. G. Wahlund, "Effects of temperature, carrier composition and sample load in asymmetrical flow field-flow fractionation," *J Chromatogr A*, vol. 548, no. C, pp. 393–406, 1991, doi: 10.1016/S0021-9673(01)88622-2.

[81] L. Nilsson, "Separation and characterization of food macromolecules using field-flow fractionation: A review," *Food Hydrocoll*, vol. 30, no. 1, pp. 1–11, 2013, doi: 10.1016/j.foodhyd.2012.04.007.

[82] J. J. Kirkland, C. H. Dilks, S. W. Rementer, and W. W. Yau, "Asymmetric-channel flow field-flow fractionation with exponential force-field programming," *J Chromatogr A*, vol. 593, no. 1–2, pp. 339–355, 1992, doi: 10.1016/0021-9673(92)80303-C.

[83] K. G. Wahlund and A. Litzén, "Application of an asymmetrical flow field-flow fractionation channel to the separation and characterization of proteins, plasmids, plasmid fragments, polysaccharides and unicellular algae," *J Chromatogr A*, vol. 461, no. C, pp. 73–87, 1989, doi: 10.1016/S0021-9673(00)94276-6.

[84] J. C. Giddings, L. K. Smith, and M. N. Myers, "Surface Barriers for Retention Enhancement in Field-Flow Fractionation," *Sep Sci Technol*, vol. 13, no. 4, pp. 367–385, 1978, doi: 10.1080/01496397808057108.

[85] M. Marioli, B. Kavurt, D. Stamatialis, and W. T. Kok, "Application of microstructured membranes for increasing retention, selectivity and resolution in asymmetrical flow field-flow fractionation," *J Chromatogr A*, vol. 1605, p. 360347, 2019, doi: 10.1016/j.chroma.2019.07.001.

[86] C. R. M. Bria, P. W. Skelly, J. R. Morse, R. E. Schaak, and S. K. R. Williams, "Semi-preparative asymmetrical flow field-flow fractionation: A closer look at channel

dimensions and separation performance," *J Chromatogr A*, vol. 1499, pp. 149–157, May 2017, doi: 10.1016/j.chroma.2017.03.017.

[87] S. Knoppe, J. Boudon, I. Dolamic, A. Dass, and B. Thomas, "Size Exclusion Chromatography for Semipreparative Scale," *Anal Chem*, vol. 38, pp. 5056–5061, 2011, doi: 10.1021/ac200789v.

[88] Y. Chen, C. T. Mant, and R. S. Hodges, "Preparative reversed-phase high-performance liquid chromatography collection efficiency for an antimicrobial peptide on columns of varying diameters (1mm to 9.4mm I.D.)," *J Chromatogr A*, vol. 1140, no. 1–2, pp. 112–120, Jan. 2007, doi: 10.1016/j.chroma.2006.11.052.

[89] J. Y. Lee, K. H. Kim, and M. H. Moon, "Evaluation of multiplexed hollow fiber flow field-flow fractionation for semi-preparative purposes," *J Chromatogr A*, vol. 1216, no. 37, pp. 6539–6542, 2009, doi: 10.1016/j.chroma.2009.07.044.

[90] D. Müller, S. Cattaneo, F. Meier, R. Welz, and A. J. de Mello, "Nanoparticle separation with a miniaturized asymmetrical flow field-flow fractionation cartridge," *Front Chem*, vol. 3, no. JUL, pp. 1–6, 2015, doi: 10.3389/fchem.2015.00045.

[91] D. Kang and M. H. Moon, "Miniaturization of frit inlet asymmetrical flow field-flow fractionation," *Anal Chem*, vol. 76, no. 13, pp. 3851–3855, 2004, doi: 10.1021/ac0496704.

[92] K. H. Kim and M. H. Moon, "Chip-type asymmetrical flow field-flow fractionation channel coupled with mass spectrometry for top-down protein identification," *Anal Chem*, vol. 83, no. 22, pp. 8652–8658, 2011, doi: 10.1021/ac202098b.

[93] I. Yang, K. H. Kim, J. Y. Lee, and M. H. Moon, "On-line miniaturized asymmetrical flow field-flow fractionation-electrospray ionization-tandem mass spectrometry with selected reaction monitoring for quantitative analysis of phospholipids in plasma lipoproteins," *J Chromatogr A*, vol. 1324, pp. 224–230, 2014, doi: 10.1016/j.chroma.2013.11.035.

[94] M. H. Moon, "Flow field-flow fractionation: Recent applications for lipidomic and proteomic analysis," *TrAC - Trends in Analytical Chemistry*, vol. 118, pp. 19–28, 2019, doi: 10.1016/j.trac.2019.05.024.

[95] Z. You, F. Meier, and S. Weidner, "Comparison of Miniaturized and Conventional Asymmetrical Flow Field-Flow Fractionation (AF4) Channels for Nanoparticle Separations," *Separations*, vol. 4, no. 1, p. 8, 2017, doi: 10.3390/separations4010008.

[96] A. Zattoni, B. Roda, F. Borghi, V. Marassi, and P. Reschiglian, "Flow field-flow fractionation for the analysis of nanoparticles used in drug delivery," *J Pharm Biomed Anal*, vol. 87, pp. 53–61, 2014, doi: 10.1016/j.jpba.2013.08.018.

[97] A. Szulc *et al.*, "Maltose modified poly(propylene imine) dendrimers as potential carriers of nucleoside analog 5′-triphosphates.," *Int J Pharm*, vol. 495, no. 2, pp. 940–947, 2015, doi: 10.1016/j.ijpharm.2015.09.065.

[98] S. Boye *et al.*, "PH-triggered aggregate shape of different generations lysine-dendronized maleimide copolymers with maltose shell," *Biomacromolecules*, vol. 13, no. 12, pp. 4222–4235, 2012, doi: 10.1021/bm301489s.

[99] B. Voit and D. Appelhans, “Glycopolymers of various architectures-more than mimicking nature,” *Macromol Chem Phys*, vol. 211, no. 7, pp. 727–735, 2010, doi: 10.1002/macp.201000007.

[100] M. Gorzkiewicz, D. Appelhans, S. Boye, A. Lederer, B. Voit, and B. Klajnert-Maculewicz, “Effect of the Structure of Therapeutic Adenosine Analogues on Stability and Surface Electrostatic Potential of their Complexes with Poly(propyleneimine) Dendrimers,” *Macromol Rapid Commun*, vol. 1900181, p. 1900181, 2019, doi: 10.1002/marc.201900181.

[101] E. R. Gillies and J. M. J. Fréchet, “Dendrimers and dendritic polymers in drug delivery,” *Drug Discov Today*, vol. 10, no. 1, pp. 35–43, 2005, doi: 10.1016/S1359-6446(04)03276-3.

[102] S. Boye, N. Polikarpov, D. Appelhans, and A. Lederer, “An alternative route to dye-polymer complexation study using asymmetrical flow field-flow fractionation,” *J Chromatogr A*, vol. 1217, no. 29, pp. 4841–4849, 2010, doi: 10.1016/j.chroma.2010.05.036.

[103] J. Gaitzsch, D. Appelhans, L. Wang, G. Battaglia, and B. Voit, “Synthetic bio-nanoreactor: Mechanical and chemical control of polymersome membrane permeability,” *Angewandte Chemie - International Edition*, vol. 51, no. 18, pp. 4448–4451, 2012, doi: 10.1002/anie.201108814.

[104] T. Anajafi and S. Mallik, “Polymersome-based drug-delivery strategies for cancer therapeutics,” *Ther Deliv*, vol. 6, no. 4, pp. 521–534, 2015, doi: 10.4155/tde.14.125.Polymersome-based.

[105] B. M. Discher *et al.*, “Polymersomes: Tough vesicles made from diblock copolymers,” *Science (1979)*, vol. 284, no. 5417, pp. 1143–1146, May 1999, doi: 10.1126/science.284.5417.1143.

[106] B. Iyisan *et al.*, “Dynamic Docking and Undocking Processes Addressing Selectively the Outside and Inside of Polymersomes,” *Macromol Rapid Commun*, vol. 38, no. 21, pp. 1–8, 2017, doi: 10.1002/marc.201700486.

[107] D. Gräfe, J. Gaitzsch, D. Appelhans, and B. Voit, “Cross-linked polymersomes as nanoreactors for controlled and stabilized single and cascade enzymatic reactions,” *Nanoscale*, vol. 6, no. 18, pp. 10752–10761, 2014, doi: 10.1039/c4nr02155j.

[108] V. Balasubramanian, B. Herranz-Blanco, P. V. Almeida, J. Hirvonen, and H. A. Santos, “Multifaceted polymersome platforms: Spanning from self-assembly to drug delivery and protocells,” *Prog Polym Sci*, vol. 60, pp. 51–85, 2016, doi: 10.1016/j.progpolymsci.2016.04.004.

[109] R. G. Gilbert, A. C. Wu, M. A. Sullivan, G. E. Sumarriva, N. Ersch, and J. Hasjim, “Improving human health through understanding the complex structure of glucose polymers,” *Anal Bioanal Chem*, vol. 405, no. 28, pp. 8969–8980, Nov. 2013, doi: 10.1007/s00216-013-7129-1.

[110] H. Dou, B. Zhou, H. D. Jang, and S. Lee, “Study on antidiabetic activity of wheat and barley starch using asymmetrical flow field-flow fractionation coupled with multiangle light scattering,” *J Chromatogr A*, vol. 1340, pp. 115–120, 2014, doi: 10.1016/j.chroma.2014.03.014.

[111] L. A. Bello-Perez, E. Agama-Acevedo, M. Lopez-Silva, and J. Alvarez-Ramirez, “Molecular characterization of corn starches by HPSEC-MALS-RI: A comparison with AF4-MALS-RI system,” *Food Hydrocoll*, vol. 96, no. January, pp. 373–376, 2019, doi: 10.1016/j.foodhyd.2019.04.067.

[112] M. Leeman, K.-G. Wahlund, and B. Wittgren, “Programmed cross flow asymmetrical flow field-flow fractionation for the size separation of pullulans and hydroxypropyl cellulose,” *J Chromatogr A*, vol. 1134, no. 1–2, pp. 236–245, 2006, doi: 10.1016/j.chroma.2006.08.065.

[113] J. R. Runyon, L. Nilsson, J. Alftrén, and B. Bergenståhl, “Characterization of oat proteins and aggregates using asymmetric flow field-flow fractionation,” *Anal Bioanal Chem*, vol. 405, no. 21, pp. 6649–6655, 2013, doi: 10.1007/s00216-013-7115-7.

[114] J. Choi, C. Zielke, L. Nilsson, and S. Lee, “Characterization of the molar mass distribution of macromolecules in beer for different mashing processes using asymmetric flow field-flow fractionation (AF4) coupled with multiple detectors,” *Anal Bioanal Chem*, vol. 409, no. 19, pp. 4551–4558, 2017, doi: 10.1007/s00216-017-0393-8.

[115] C. Zielke, Y. Lu, and L. Nilsson, “Aggregation and microstructure of cereal β-glucan and its association with other biomolecules,” *Colloids Surf A Physicochem Eng Asp*, vol. 560, no. August 2018, pp. 402–409, 2019, doi: 10.1016/j.colsurfa.2018.10.042.

[116] C. Zielke, A. Stradner, and L. Nilsson, “Characterization of cereal β-glucan extracts: Conformation and structural aspects,” *Food Hydrocoll*, vol. 79, pp. 218–227, 2018, doi: 10.1016/j.foodhyd.2017.12.036.

[117] H. Thielking and W. M. Kulicke, “Determination of the Structural Parameters of Aqueous Polymer Solutions in the Molecular, Partially Aggregated, and Particulate States by Means of FFFF / MALLS,” *Journal of Microcolumn Separations*, vol. 10, no. 1, pp. 51–56, 1998, doi: 10.1002/(SICI)1520-667X(1998)10:1<51::AID-MCS7>3.0.CO;2-Y.

[118] D. Y. Kang, J. M. Moon, and S. Lee, “Comparison of size-exclusion chromatography and flow field-flow fractionation for separation of whey proteins,” *Bull Korean Chem Soc*, vol. 32, no. 4, pp. 1315–1320, 2011, doi: 10.5012/bkcs.2011.32.4.1315.

[119] L. Daqiq, C. M. Fellows, F. Bekes, and E. Lees, “Methodologies for symmetrical-flow field-flow fractionation analyses of polymeric glutenin,” *J Texture Stud*, vol. 38, no. 2, pp. 273–296, 2007, doi: 10.1111/j.1745-4603.2007.00098.x.

[120] U. Lehmann and F. Robin, “Slowly digestible starch e its structure and health implications : a review,” *Trends in Foos Science and Technology*, vol. 18, pp. 346–355, 2007, doi: 10.1016/j.tifs.2007.02.009.

[121] K. L. Johnston, E. L. Thomas, J. D. Bell, G. S. Frost, and M. D. Robertson, "Metabolism resistant starch improves insulin sensitivity in metabolic syndrome," *Diabetic Medicine*, no. 27, pp. 391–397, 2010, doi: 10.1111/j.1464-5491.2010.02923.x.

[122] M. A. Sullivan *et al.*, "Molecular Structural Differences between Type-2-Diabetic and Healthy Glycogen," *Biomacromolecules*, no. 12, pp. 1983–1986, 2011, doi: 10.1021/bm2006054.

[123] R. Bansal, S. Gupta, and A. S. Rathore, "Analytical Platform for Monitoring Aggregation of Monoclonal Antibody Therapeutics," pp. 1–11, 2019.

[124] R. G. Melton, "Preparation and purification of antibody-enzyme conjugates for therapeutic applications," *Adv Drug Deliv Rev*, vol. 22, no. 3, pp. 289–301, 1996, doi: 10.1016/S0169-409X(96)00447-4.

[125] L. Pitkänen, T. Sontag-Strohm, and P. Kanerva, "Enhanced separation and characterization of gluten polymers by asymmetrical flow field-flow fractionation coupled with multiple detectors," *J Cereal Sci*, vol. 59, no. 2, pp. 126–131, 2014, doi: 10.1016/j.jcs.2013.11.009.

[126] J. Y. Lee, D. Choi, C. Johan, and M. H. Moon, "Improvement of lipoprotein separation with a guard channel prior to asymmetrical flow field-flow fractionation using fluorescence detection," *J Chromatogr A*, vol. 1218, no. 27, pp. 4144–4148, 2011, doi: 10.1016/j.chroma.2010.11.079.

[127] S. Schachermeyer, J. Ashby, and W. Zhong, "Aptamer – protein binding detected by asymmetric flow field flow fractionation," *J Chromatogr A*, vol. 1295, pp. 107–113, 2013, doi: 10.1016/j.chroma.2013.04.063.

[128] K. Rebolj, D. Pahovnik, and E. Žagar, "Characterization of a protein conjugate using an asymmetrical-flow field-flow fractionation and a size-exclusion chromatography with multi-detection system," *Anal Chem*, vol. 84, no. 17, pp. 7374–7383, 2012, doi: 10.1021/ac3010378.

[129] M. Wolff *et al.*, "Quantitative thermophoretic study of disease-related protein aggregates.," *Sci Rep*, vol. 6, no. February, p. 22829, 2016, doi: 10.1038/srep22829.

[130] J. Ashby, S. Schachermeyer, Y. Duan, L. A. Jimenez, and W. Zhong, "Probing and quantifying DNA – protein interactions with asymmetrical flow field-flow fractionation," *J Chromatogr A*, vol. 1358, pp. 217–224, 2014, doi: 10.1016/j.chroma.2014.07.002.

[131] M. Leeman, M. Storm, and L. Nilsson, "Practical applications of asymmetrical flow field-flow fractionation: A review," *LC-GC North America*, vol. 34, no. 1, pp. 56–65, 2016.

[132] C. R. M. Bria and S. K. R. Williams, "Impact of asymmetrical flow field-flow fractionation on protein aggregates stability," *J Chromatogr A*, vol. 1465, pp. 155–164, 2016, doi: 10.1016/j.chroma.2016.08.037.

[133] Z. Zhou and L. Guo, "A critical evaluation of an asymmetrical flow field-flow fractionation system for colloidal size characterization of natural organic matter," *J Chromatogr A*, vol. 1399, pp. 53–64, 2015, doi: 10.1016/j.chroma.2015.04.035.

[134] S. Tak, B. Yang, J. Kim, J. Park, and M. Hee, “Combining asymmetrical flow field-flow fractionation with on- and off-line fluorescence detection to examine biodegradation of riverine dissolved and particulate organic matter,” *J Chromatogr A*, vol. 1409, pp. 218–225, 2015, doi: 10.1016/j.chroma.2015.07.074.

[135] F. Laborda, E. Bolea, and J. R. Castillo, “Study of the size-based environmental availability of metals associated to natural organic matter by stable isotope exchange and quadrupole inductively coupled plasma mass spectrometry coupled to asymmetrical flow field flow fractionation,” *J Chromatogr A*, vol. 1218, no. 27, pp. 4199–4205, 2011, doi: 10.1016/j.chroma.2011.01.076.

[136] H. Luan and T. M. Vadas, “Size characterization of dissolved metals and organic matter in source waters to streams in developed landscapes,” *Environmental Pollution*, vol. 197, pp. 76–83, 2015, doi: 10.1016/j.envpol.2014.12.004.

[137] T. Saito, T. Hamamoto, T. Mizuno, T. Iwatsuki, and S. Tanaka, “Comparative study of granitic and sedimentary groundwater colloids by flow-field flow fractionation coupled with ICP-MS,” *J Anal At Spectrom*, vol. 30, no. 6, pp. 1229–1236, 2015, doi: 10.1039/c5ja00088b.

[138] B. Stolpe, L. Guo, A. M. Shiller, and G. R. Aiken, “Abundance, size distributions and trace-element binding of organic and iron-rich nanocolloids in Alaskan rivers, as revealed by field-flow fractionation and ICP-MS,” *Geochim Cosmochim Acta*, vol. 105, pp. 221–239, 2013, doi: 10.1016/j.gca.2012.11.018.

[139] C. F. W. Ludwig, “Diffusion zwischen ungleich erwärmten Orten gleich zusammengesetzter Lösungen,” *Sitzungsberichte der Akademie der Wissenschaften der mathematisch-naturwissenschaftliche Klasse (Wien)*, vol. 20, p. 539, 1856.

[140] E. Bouty, “CH. SORET. — Sur l’état d’équilibre que prend, au point de vue de sa concentration, une dissolution saline primitivement homogène, dont deux parties sont portées à des températures différentes; Archives de Genève, 3e periode, t. II, p. 48; 1879,” *Journal de Physique Théorique et Appliquée*, vol. 9, no. 1, pp. 331–332, 1880, doi: 10.1051/jphystap:018800090033101.

[141] G. E. Uhlenbeck, “The Mathematical Theory of Non-uniform Gases. By S. Chapman and T. G. Cowling.,” *J Phys Chem*, vol. 45, no. 5, pp. 876–877, May 1941, doi: 10.1021/j150410a017.

[142] G. H. Thompson, M. N. Myers, and J. C. Giddings, “An Observation of a Field-Flow Fractionation Effect with Polystyrene Samples,” *Separation Science*, vol. 2, no. 6, pp. 797–800, 1967, doi: 10.1080/01496396708049739.

[143] S. Lee and C. Giddings, “Application of thermal field-flow fractionation for characterization of industrial polymers,” *Journal of Microcolumn Separations*, vol. 9, no. 4, pp. 281–286, Jan. 1997, doi: 10.1002/(SICI)1520-667X(1997)9:4<281::AID-MCS5>3.0.CO;2-Y.

[144] E. P. C. Mes, H. de Jonge, T. Klein, R. R. Welz, and D. T. Gillespie, “Characterization of high molecular weight polyethylenes using high temperature asymmetrical flow field-flow fractionation with on-line infrared, light scattering, and viscometry detection,” *J*

Chromatogr A, vol. 1154, no. 1–2, pp. 319–330, 2007, doi: 10.1016/j.chroma.2007.03.116.

[145] Y. S. Gao, K. D. Caldwell, M. N. Myers, and J. C. Giddings, "Extension of Thermal Field-Flow Fractionation to Ultrahigh (20 X 106) Molecular Weight Polystyrenes," *Macromolecules*, vol. 18, no. 6, pp. 1272–1277, 1985, doi: 10.1021/ma00148a039.

[146] D. Lee and S. K. R. Williams, "Thermal field-flow fractionation and multiangle light scattering of polyvinyl acetate with broad polydispersity and ultrahigh molecular weight microgel components," *J Chromatogr A*, vol. 1217, no. 10, pp. 1667–1673, 2010, doi: 10.1016/j.chroma.2010.01.035.

[147] J. J. Gunderson and J. C. Giddings, "Comparison of polymer resolution in thermal field-flow fractionation and size-exclusion chromatography," *Anal Chim Acta*, vol. 189, no. C, pp. 1–15, 1986, doi: 10.1016/S0003-2670(00)83710-1.

[148] J. C. Giddings, Y. H. Yoon, and M. N. Myers, "Evaluation and Comparison of Gel Permeation Chromatography and Thermal Field-Flow Fractionation for Polymer Separations," *Anal Chem*, vol. 47, no. 1, pp. 126–131, 1975, doi: 10.1021/ac60351a035.

[149] J. R. Runyon and S. K. R. Williams, "Composition and molecular weight analysis of styrene-acrylic copolymers using thermal field-flow fractionation," *J Chromatogr A*, vol. 1218, no. 38, pp. 6774–6779, 2011, doi: 10.1016/j.chroma.2011.07.076.

[150] K. H. Cho, Y. H. Park, S. J. Jeon, W. S. Kim, and D. W. Lee, "Retention behavior of copolymers in thermal field-flow fractionation and gel permeation chromatography," *J Liq Chromatogr Relat Technol*, vol. 20, no. 16–17, pp. 2741–2756, 1997, doi: 10.1080/10826079708005590.

[151] J. C. Giddings, S. Li, P. S. Williams, and M. E. Schimpf, "High speed separation of ultra-high-molecular-weight polymers by thermal/hyperlayer field-flow fractionation," *Die Makromolekulare Chemie, Rapid Communications*, vol. 823, no. 9, pp. 817–823, 1988, doi: https://doi.org/10.1002/marc.1988.030091207.

[152] M. E. Schimpf and J. C. Giddings, "Characterization of thermal diffusion of copolymers in solution by thermal field-flow fractionation," *J Polym Sci B Polym Phys*, vol. 28, no. 13, pp. 2673–2680, Dec. 1990, doi: 10.1002/polb.1990.090281313.

[153] J. C. Giddings and M. E. Schimpf, "Characterization of Thermal Diffusion in Polymer Solutions by Thermal Field-Flow Fractionation: Effects of Molecular Weight and Branching," *Macromolecules*, vol. 20, no. 7, pp. 1561–1563, 1987, doi: 10.1021/ma00173a022.

[154] C. A. Rue and M. E. Schimpf, "Thermal Diffusion in Liquid Mixtures and Its Effect on Polymer Retention in Thermal Field-Flow Fractionation," *Anal Chem*, vol. 66, pp. 4054–4062, Jun. 1994, doi: 10.1021/ac00094a030.

[155] D. Stadelmaier and W. Köhler, "Thermal diffusion of dilute polymer solutions: The role of chain flexibility and the effective segment size," *Macromolecules*, vol. 42, no. 22, pp. 9147–9152, 2009, doi: 10.1021/ma901794k.

[156] M. E. Schimpf and J. C. Giddings, “Characterization of thermal diffusion in polymer solutions by thermal field-flow fractionation: Dependence on polymer and solvent parameters,” *J Polym Sci B Polym Phys*, vol. 27, no. 6, pp. 1317–1332, May 1989, doi: 10.1002/polb.1989.090270610.

[157] J. E. Belgaied, M. Hoyos, and M. Martin, “Velocity profiles in thermal field-flow fractionation,” *J Chromatogr A*, vol. 678, no. 1, pp. 85–96, 1994, doi: 10.1016/0021-9673(94)87077-2.

[158] M. Martin, C. Van Batten, and M. Hoyos, “Determination of Thermodiffusion Parameters from Thermal Field-Flow Fractionation Retention Data,” pp. 250–284, 2002, doi: 10.1007/3-540-45791-7_13.

[159] S. Semenov and M. Schimpf, “Thermophoresis of dissolved molecules and polymers: Consideration of the temperature-induced macroscopic pressure gradient,” *Phys Rev E Stat Phys Plasmas Fluids Relat Interdiscip Topics*, vol. 69, no. 1, p. 8, 2004, doi: 10.1103/PhysRevE.69.011201.

[160] E. P. C. Mes, W. Th. Kok, and R. Tijssen, “Prediction of Polymer Thermal Diffusion Coefficients from Polymer-Solvent Interaction Parameters: Comparison with Thermal Field Flow Fractionation and Thermal Diffusion Forced Rayleigh Scattering Experiments,” *International Journal of Polymer Analysis and Characterization*, vol. 8, no. 2, pp. 133–153, Jan. 2003, doi: 10.1080/10236660304888.

[161] M. E. Schimpf and S. N. Semenov, “Mechanism of Polymer Thermophoresis in Nonaqueous Solvents,” *J Phys Chem B*, vol. 104, no. 42, pp. 9935–9942, Oct. 2000, doi: 10.1021/jp994334q.

[162] J. R. Runyon and S. K. R. Williams, “A theory-based approach to thermal field-flow fractionation of polyacrylates,” *J Chromatogr A*, vol. 1218, no. 39, pp. 7016–7022, Aug. 2011, doi: 10.1016/j.chroma.2011.08.007.

[163] M. E. Schimpf and S. N. Semenov, “Polymer thermophoresis in solvents and solvent mixtures,” *Philosophical Magazine*, vol. 83, no. 17–18, pp. 2185–2198, 2003, doi: 10.1080/0141861031000107926.

[164] J. Chan, J. J. Popov, S. Kolisnek-Kehl, and D. G. Leaist, “Soret Coefficients for Aqueous Polyethylene Glycol Solutions and Some Tests of the Segmental Model of Polymer Thermal Diffusion,” *J Solution Chem*, vol. 32, no. 3, pp. 197–214, 2003, doi: 10.1023/A:1022925216642.

[165] R. M. Sisson and J. C. Giddings, “Effects of Solvent Composition on Polymer Retention in Thermal Field-Flow Fractionation: Retention Enhancement in Binary Solvent Mixtures,” *Anal Chem*, vol. 66, no. 22, pp. 4043–4053, 1994, doi: 10.1021/ac00094a029.

[166] G. E. Kassalainen and S. K. R. Williams, “Lowering the molecular mass limit of thermal field-flow fractionation for polymer separations,” *J Chromatogr A*, vol. 988, no. 2, pp. 285–295, 2003, doi: 10.1016/S0021-9673(02)02061-7.

[167] P. M. Shiundu, S. M. Munguti, and S. K. R. Williams, “Practical implications of ionic strength effects on particle retention in thermal field-flow fractionation,” *J Chromatogr A*, vol. 984, no. 1, pp. 67–79, Jan. 2003, doi: 10.1016/S0021-9673(02)01769-7.

[168] M. Hartung, J. Rauch, and W. Köhler, “Thermal diffusion of dilute polymer solutions: The role of solvent viscosity,” *Journal of Chemical Physics*, vol. 125, no. 21, 2006, doi: 10.1063/1.2393230.

[169] G. Greyling and H. Pasch, “Tacticity Separation of Poly(methyl methacrylate) by Multidetector Thermal Field-Flow Fractionation,” *Anal Chem*, vol. 87, no. 5, pp. 3011–3018, Mar. 2015, doi: 10.1021/ac504651p.

[170] W. Hiller, W. van Aswegen, M. Hehn, and H. Pasch, “Online ThFFF-NMR: A novel tool for molar mass and chemical composition analysis of complex macromolecules,” *Macromolecules*, vol. 46, no. 7, pp. 2544–2552, 2013, doi: 10.1021/ma400350y.

[171] M. N. Myers, K. D. Caldwell, and J. Calvin Giddings, “A Study of Retention in Thermal Field-Flow Fractionation,” *Separation Science*, vol. 9, no. 1, pp. 47–70, 1974, doi: 10.1080/01496397408080043.

[172] L. Pasti, D. Melucci, C. Contado, F. Dondi, and I. Mingozzi, “Calibration in thermal field flow fractionation with polydisperse standards: Application to polyolefin characterization,” *J Sep Sci*, vol. 25, no. 10–11, pp. 691–702, Jul. 2002, doi: 10.1002/1615-9314(20020701)25:10/11<691::AID-JSSC691>3.0.CO;2-L.

[173] L. Pasti, F. Bedani, C. Contado, I. Mingozzi, and F. Dondi, “Programmed field decay thermal field flow fractionation of polymers: A calibration method,” *Anal Chem*, vol. 76, no. 22, pp. 6665–6680, 2004, doi: 10.1021/ac049399q.

[174] L. Pasti, E. A. Ventosa, I. Mingozzi, and F. Dondi, “Determination of calibration function in thermal field flow fractionation under thermal field programming,” *J Sep Sci*, vol. 29, no. 8, pp. 1088–1101, 2006, doi: 10.1002/jssc.200500429.

[175] P. S. Williams and J. C. Giddings, “Power Programmed Field-Flow Fractionation: A New Program Form for Improved Uniformity of Fractionating Power,” *Anal Chem*, vol. 59, no. 17, pp. 2038–2044, 1987, doi: 10.1021/ac00144a007.

[176] W. Cao, P. S. Williams, M. N. Myers, and J. C. Giddings, “Thermal field-flow fractionation universal calibration: Extension for consideration of variation of cold wall temperature,” *Anal Chem*, vol. 71, no. 8, pp. 1597–1609, 1999, doi: 10.1021/ac981094m.

[177] D.-W. Lee, S.-J. Jeon, and W.-C. Park, “A Study Effect of Mixed Solvents on the Retention of Polystyrenes Using Thermal Field-Flow Fractionation,” *Analytical Science and Technology*, vol. 6, no. 5. pp. 453–462, 1993.

[178] J. C. Giddings, L. R. K. Smith, and M. N. Myers, “Thermal Field-Flow Fractionation. Extension to Lower Molecular Weight Separations by Increasing the Liquid Temperature Range Using a Pressurized System,” *Anal Chem*, vol. 47, no. 14, pp. 2389–2394, 1975, doi: 10.1021/ac60364a036.

[179] C. Zhao, Z. Cao, J. Fraser, A. Oztekin, and X. Cheng, “Optimization of nanoparticle focusing by coupling thermophoresis and engineered vortex in a microfluidic channel,” *J Appl Phys*, vol. 121, no. 2, 2017, doi: 10.1063/1.4973272.

[180] D. Ross and L. E. Locascio, “Microfluidic temperature gradient focusing,” *Anal Chem*, vol. 74, no. 11, pp. 2556–2564, 2002, doi: 10.1021/ac025528w.

[181] C. B. Mast, S. Schink, U. Gerland, and D. Braun, “Escalation of polymerization in a thermal gradient,” *Proc Natl Acad Sci U S A*, vol. 110, no. 20, pp. 8030–8035, 2013, doi: 10.1073/pnas.1303222110.

[182] D. Vigolo, R. Rusconi, H. A. Stone, and R. Piazza, “Thermophoresis: Microfluidics characterization and separation,” *Soft Matter*, vol. 6, no. 15, pp. 3489–3493, 2010, doi: 10.1039/c002057e.

[183] P. F. Geelhoed, R. Lindken, and J. Westerweel, “Thermophoretic separation in microfluidics,” *Chemical Engineering Research and Design*, vol. 84, no. 5 A, pp. 370–373, 2006, doi: 10.1205/cherd05012.

[184] Y. Zhao, C. Zhao, J. He, Y. Zhou, and C. Yang, “Collective effects on thermophoresis of colloids: A microfluidic study within the framework of DLVO theory,” *Soft Matter*, vol. 9, no. 32, pp. 7726–7734, 2013, doi: 10.1039/c3sm27720h.

[185] T. Tsuji, K. Kozai, H. Ishino, and S. Kawano, “Direct observations of thermophoresis in microfluidic systems,” *Micro Nano Lett*, vol. 12, no. 8, pp. 520–525, 2017, doi: 10.1049/mnl.2017.0130.

[186] F. Basile, G. E. Kassalainen, and S. K. R. Williams, “Interface for direct and continuous sample-matrix deposition onto a MALDI probe for polymer analysis by thermal field flow fractionation and off-line MALDI-MS,” *Anal Chem*, vol. 77, no. 9, pp. 3008–3012, 2005, doi: 10.1021/ac048391d.

[187] W. van Aswegen, W. Hiller, M. Hehn, and H. Pasch, “Comprehensive triblock copolymer analysis by coupled thermal field-flow fractionation-NMR,” *Macromol Rapid Commun*, vol. 34, no. 13, pp. 1098–1103, 2013, doi: 10.1002/marc.201300286.

[188] T. F. Beskers, T. Hofe, and M. Wilhelm, “Development of a chemically sensitive online SEC detector based on FTIR spectroscopy,” *Polym Chem*, vol. 6, no. 1, pp. 128–142, 2015, doi: 10.1039/c4py01043d.

[189] N. W. Radebe, T. Beskers, G. Greyling, and H. Pasch, “Online coupling of thermal field-flow fractionation and Fourier transform infrared spectroscopy as a powerful tool for polymer characterization,” *J Chromatogr A*, vol. 1587, pp. 180–188, 2019, doi: 10.1016/j.chroma.2018.12.012.

[190] C. A. Ponyik, D. T. Wu, and S. K. R. Williams, “Separation and composition distribution determination of triblock copolymers by thermal field-flow fractionation,” *Anal Bioanal Chem*, vol. 405, no. 28, pp. 9033–9040, Nov. 2013, doi: 10.1007/s00216-013-7282-6.

[191] G. Greyling and H. Pasch, “Characterization of block copolymer self-assemblies by thermal field-flow fractionation,” *Polym Int*, vol. 66, no. 6, pp. 745–751, 2017, doi: https://doi.org/10.1002/pi.5350.

[192] S. J. Jeon and M. E. Schimpf, “Cross-Fractionation of Copolymers Using SEC and Thermal FFF for Determination of Molecular Weight and Composition,” vol. 1, no. 1, pp. 141–161, 1999.

[193] S. Park, D. Cho, K. Im, T. Chang, and J. W. Mays, “Utility of Interaction Chromatography for Probing Structural Purity of Model Branched Copolymers : 4-Miktoarm Star Copolymer,” pp. 5834–5838, 2003, doi: 10.1021/ma034603h.

[194] J. R. Runyon, “Thermal Field-Flow Fractionation of Polymers with High Molecular Weight and Complex Architecture,” Colorado School of Mines, Golden, 2009.

[195] J. F. Douglas, J. Roovers, and K. F. Freed, “Characterization of branching architecture through ‘universal’ ratios of polymer solution properties,” *Macromolecules*, vol. 23, no. 18, pp. 4168–4180, Sep. 1990, doi: 10.1021/ma00220a022.

[196] W. C. Smith, M. Geisler, A. Lederer, and S. K. R. Williams, “Thermal Field-Flow Fractionation for Characterization of Architecture in Hyperbranched Aromatic-Aliphatic Polyesters with Controlled Branching,” *Anal Chem*, vol. 91, no. 19, pp. 12344–12351, Oct. 2019, doi: 10.1021/acs.analchem.9b02664.

[197] M. T. Nguyen and R. Beckett, “Calibration of Thermal Field-Flow Fractionation Using Broad Molecular Weight Standards,” vol. 30, 1993.

[198] M. Geisler *et al.*, “Topology Analysis of Chain Walking Polymerized Polyethylene: An Alternative Approach for the Branching Characterization by Thermal FFF,” *Macromolecules*, vol. 52, no. 22, pp. 8662–8671, Nov. 2019, doi: 10.1021/acs.macromol.9b01410.

[199] C. A. Lohmann, W. G. Haseltine, J. R. Engle, and S. K. R. Williams, “A rapid separation method for gel content determination in pressure sensitive adhesive dispersions and acrylic-based latices for an industrial setting,” *Anal Chim Acta*, vol. 654, no. 1, pp. 92–96, 2009, doi: 10.1016/j.aca.2009.07.023.

[200] S. Lee and A. Molnár, “Determination of Molecular Weight and Gel Content of Natural Rubber Using Thermal Field-Flow Fractionation,” *Macromolecules*, vol. 28, no. 18, pp. 6354–6356, 1995, doi: 10.1021/ma00122a050.

CHAPTER 3

CHARACTERIZATION OF THE ARCHITECTURAL TRAITS OF MOLECULAR BRUSHES BY SORET COEFFICIENTS FROM THERMAL FIELD-FLOW FRACTIONATION

Michael Toney[1], Charles A. Ponyik[1], Joanna Burdyńska[2], James Oliver[1], William C. Smith[1], Krzysztof Matyjaszewski[2], S. Kim Ratanathanawongs Williams[1,3]

3.1 Abstract

The architecture of synthetic polymers has become increasingly complex and difficult to fully characterize, making it challenging to determine structure-function relationships. While nuclear magnetic resonance (NMR) has been a reliable tool to determine architecture, it relies on unique signatures that can be obscured by complex molecular environments and is not capable of providing information about distributions. Highly branched polymers with large molar masses (>1 MDa) often exhibit non-ideal chromatography behavior that further obfuscate characterization. Thermal field-flow fractionation (ThFFF) has shown promise as a novel characterization method which resolves some of these challenges. A series of poly(2-(2-bromoisobutyryloxy) ethyl methacrylate)-graft-poly (n-butyl acrylate) bottlebrushes with 100% grafting density and varied degrees of polymerization (DP) in backbone and sidechain were analyzed by ThFFF, NMR and SEC. Backbone DP ranged from 20-400 with sidechain DP from 20-120, which resulted in a range of molar masses from 10^5-10^7 Da. An additional series of bottlebrushes with 30% grafting density and a backbone DP of 100 were also analyzed. Molar masses determined by NMR and ThFFF agreed within 20% except for brushes whose molar mass exceeded 3 MDa. SEC molar mass results by calibration yielded values up to 600% lower than NMR and ThFFF. It was demonstrated that the Soret coefficient (S_T) exhibits a linear relationship with sidechain DP. A contraction ratio of the Soret coefficient (g'') was calculated by assuming a linear analog composed solely of the sidechain. A trend of increasing contraction with the number of chain ends was observed. A comparison of reported g'' values with those

[1]Department of Chemistry, Colorado School of Mines, 1500 Illinois St, Golden, Colorado 80401, United States

[2]Department of Chemistry, Carnegie Mellon University, 4400 Fifth Avenue, Pittsburgh, Pennsylvania 15213, Unites States

[3]Corresponding Author

from the current work suggests specific ranges of *g''* for different architectures. While the mechanism of architectural sensitivity is not fully understood, this work demonstrates the immediate usefulness of this method.

3.2 Introduction

Molecular weight, composition, architecture, and their respective distributions are examples of characteristics that dictate the properties of polymers and impact the performance of end products. While size exclusion chromatography is commonly used to determine molecular weight [1], the measurement of composition and architecture is considerably less developed. Strategies such as SEC with quintuple detectors [2], liquid interaction chromatography [3], and thermal field-flow fractionation (ThFFF) [4] rely on different principles and have been shown capable of separating and measuring the composition distributions of copolymers while stand-alone NMR can provide average values [5]. However, characterization methods for polymer architecture and their distributions remain sparse even though this trait is well exploited to reduce viscosity during processing [6,7], to self-assemble lithography templates, or to deliver drugs and image tumors [8,9]. NMR has been used for structural analysis because of its sensitivity to both the number and types of bonds present on a given atom [10]. It has provided branching information for synthetic polymers such as polyacrylates [11], polyethylenes [12], polystyrenes [13] and copolymers [14] as well as natural occurring macromolecules such as starch [15]. However, NMR yields an average value and on its own cannot provide details about the distribution of branching [16]. Other ensemble methods of acquiring architectural information at concentrations in the dilute regime include multi-angle light scattering (MALS) [17], dynamic light scattering (DLS) [18], and viscometry [19]. A common approach for the analysis of branching by these methods is to use a contraction factor which is the ratio of a property of a branched polymer to its linear analog [18]. For example, a branched polymer of the same molar mass as a linear analog occupies a smaller volume which results in a contraction of physical properties. The most used properties are viscosity and size and give rise to contraction factors g and g', respectively. There has also been a noted contraction in solubility parameters [20], second virial coefficients [18], and Soret coefficients [21–23]. The first two contraction factors are primarily qualitative and often do not yield quantitative information. The Soret contraction is a recently introduced approach that utilizes the ratio of thermal diffusion

coefficients of branched and linear polymers and will be discussed in detail in a later section as it is the focus of this present work.

The coupling of MALS, DLS, and viscometry to separation techniques enables detection and measurement of physicochemical properties of polymers as they elute from the column or channel. Hence, *distributions* in various traits can be obtained. Size exclusion chromatography with multiple detectors [24], temperature gradient interaction chromatography [25] and liquid chromatography at critical conditions [26] have been used for branching analyses. However, SEC requires a linear standard of the same molar mass (MM) for comparison, TGIC has high resolution but involves extensive method development, and LCCC is hindered by poor recovery and peak broadening with high MM (>10^5 Da) polymers [27]. Chromatographic methods are further complicated by the packing material in columns which increases the potential for undesirable interactions with the analytes and shear degradation of high molecular weight polymers [28,29]. These issues are alleviated in field-flow fractionation (FFF) because separation occurs in an open, ribbon-like channel [30]. Similar to chromatography, FFF relies on the differential migration of analytes in a column or channel. However, it differs in that separation is achieved in a single phase by leveraging a laminar flow profile coupled to a perpendicularly applied external "field". Furthermore, FFF's open channel design enables analyses that extends into ~10^8 Da polymers and sub-micrometer colloids [31].

The most common FFF systems used to study polymers are asymmetrical flow FFF (AF4) and thermal FFF (ThFFF) [31,32]. In AF4, the applied field is a crossflow which leads to a separation based solely on the diffusion coefficient (or hydrodynamic size) of the analytes in a carrier fluid. The correlation between measured AF4 retention times and D provides size distributions as well as insights into complexation, binding, and aggregation phenomena of challenging multi-component systems [33]. In ThFFF, the applied field is a temperature gradient that is typically achieved by heating one channel wall while cooling the opposite wall. Analytes usually migrate towards the cold wall in a phenomenon known as thermal diffusion, described by the thermal diffusion coefficient (D_T) [34,35]. The magnitude of D_T is dependent on factors such as the temperature gradient and polymer-solvent interactions [32,36]. Thermal diffusion is countered by the analyte's translational diffusion coefficient (D). When D_T is constant, such as the case for homopolymers with MM > 10^3 Da, separation is based on D with smaller polymers eluting first as they exhibit greater D and thus sample faster flow regimes of the parabolic flow

profile. The order of elution for homopolymers is thus low MM followed by increasingly high MM polymers. Thermal FFF has also been shown to separate analytes based on composition and as a tool for characterizing polymer composition distribution [32,36]. More recently, D_T has been leveraged to characterize microstructure [37] and architecture [21,38]. These ThFFF capabilities are a consequence of thermal diffusion, which lacks a theoretical description for dissolved polymers. Until recently, the selection of carrier liquids that impart sufficiently high D_Ts and consequently retention has primarily been achieved empirically. Recent advancements in a predictive model of thermal diffusion have decreased the reliance on a trial-and-error approach and streamlined the solvent selection process for ThFFF separations [39,40].

Analyte retention in ThFFF is described by Equation 3.1 where the retention factor (λ) is dependent on D, D_T, and the temperature difference between the hot and cold walls ΔT. The ratio of D_T to D is known as the Soret coefficient (S_T) [41].

$$\lambda = \frac{D}{D_T \Delta T} = \frac{1}{S_T \Delta T} \tag{3.1}$$

The retention time of an analyte (t_r) is related to the time for an unretained solute to elute from the channel (t^0), λ, and a correction factor (v) that accounts for perturbation of the parabolic flow profile due to the temperature gradient, as shown in Equation 3.2 [41].

$$\frac{t^0}{t_r} = 6\lambda \left[v + (1 - 6\lambda v) \left(\coth \frac{1}{2\lambda} \right) - 2\lambda \right] \tag{3.2}$$

By combining Equations 3.1 and 3.2, it is apparent that the retention time of a polymer is directly related to S_T. The ease of experimentally determining S_T forms the basis of recent developments in ThFFF analysis of polymer architecture [21,23,38]. The ratio of D_T/D, or S_T, for a branched and linear polymer may be leveraged as a contraction factor. The Soret contraction factor, g'', is described by Equation 3.3 and was successfully demonstrated to characterize hyperbranched polyesters [21], chain walking in polyethylenes [38], pom-pom and star polystyrenes [23], and miktoarm star polymers [23].

$$g'' = \frac{S_{T,branched}}{S_{T,linear}} \tag{3.3}$$

Estimation of $S_{T,linear}$ for the same MM as the branched polymer has been achieved using a calibration curve of S_T versus MM generated by ThFFF analysis of a linear polymer [23,42] or by an indirect method of approximation [38].

Polymer architectures include stars, pom-poms, combs, molecular brushes, dendrimers, and rings [43]. Molecular brushes, commonly referred to as bottlebrushes, are a promising class of materials which have diverse applications in solutions, at interfaces, and in thin films [44]. In this work, we explore the effectiveness of Soret contraction factors for the architectural analysis of a complex bottlebrush system with different chemistries in the backbone and sidechains. This presents an additional challenge in that both structural components must be considered in branching analysis as well as the density of grafted chains. A library of nine bottlebrushes consisting of three backbone lengths each with three sidechain lengths as well as two grafting densities are used to achieve our objectives. The effect of backbone and sidechain lengths and different grafting densities on S_T are investigated. The Soret contraction factors are determined for bottlebrushes and these values are compared to those for other polymer architectures. In addition to an architectural analysis, a comparison was made of molar masses determined by SEC calibration, NMR, and ThFFF-MALS-dRI as accurate values are needed for the determination of *g''*.

3.3 Materials and Methods

3.3.1 Materials

A library of nine ATRP polymerized bottlebrushes with poly(2-(2-bromoisobutyryloxy) ethyl methacrylate) (PBiBEM) backbones ranging from 20 to 400 monomer units and poly(n-butyl acrylate) (PnBA) sidechains ranging from 20 to 120 monomer units with near 100% and 30% nominal graft density were studied in this work. The 30% graft density samples also contain methyl methacrylate in the sidechain. The synthesis procedure and characterization by SEC and NMR are detailed elsewhere [45,46].

Bottlebrush polymer samples for ThFFF were prepared by dissolving neat polymer in methyl ethyl ketone (MEK) (Avantor Performance Chemicals, Center Valley, Pennsylvania) to yield concentrations ranging from 0.2 – 4.0 mg mL^{-1}. Sample solutions were allowed to sit for 72 hours prior to analysis.

3.3.2 Instrumentation

Fractionation was carried out in a TF2000 Polymer Fractionator (Postnova Analytics, Salt Lake City, Utah) outfitted with a 20 μL sample loop. The spacer was cut from 127 μm thick Kapton tape (Fralock, Valencia, California). HPLC grade MEK was pumped through the channel at flow rates ranging between 0.1-0.2 mL min^{-1}. The temperature difference between the hot and cold walls ranged from 30 to 95 °C with the cold wall temperature T_c varying between 25 and 30°C. The on-line detectors were comprised of a suite of instruments from Wyatt Technology Corporation (Santa Barbara, CA) that included a Dawn Heleos II multi-angle light scattering (MALS) instrument, dynamic light scattering (DLS), and an Optilab T-rEX differential refractometer. Data was collected and analyzed with ASTRA 7 software.

SEC and NMR equipment and conditions used to measure polymer MM are detailed in [45,46].

3.4 Theory and Calculations

3.4.1 Thermal Diffusion Model

As stated previously, polymer thermal diffusion is highly dependent on polymer-solvent interactions. The D_T of a random coil copolymer may be determined by a weighted average of each homopolymer's D_T [36] if a nonselective solvent is used as the carrier liquid. In this bottlebrush library, PnBA comprised more than 86% of the mass of a bottlebrush. In addition, the densely grafted brushes are expected to limit the diffusion of solvent to the backbone of the brush [47] – further limiting its contribution to the overall thermal diffusion behavior. This serves as the justification for choosing PnBA as a linear analog in the calculation of $S_{T,linear}$.

A model (Eq. 4) which assigns the chemical potential for thermal diffusion to the temperature dependence of the Flory-Huggins interaction parameter (X) was shown to accurately predict D_T for polystyrene in several organic solvents [48]. This model is also dependent upon the segmental diffusion coefficient, D_{seg}, and the solvent volume fraction, ϕ_1, which approaches unity in a dilute system.

$$D_T = \phi_1^2 \frac{D_{seg}}{T} \frac{\partial[T^2(\partial\chi/\partial T)]}{\partial T} \tag{3.4}$$

Recent work used Hansen solubility theory to approximate X (instead of Hildebrand solubility parameters) which increased both the accuracy of D_T predictions and Equation 3.4's scope to more polymer and solvent chemistries [39]. This recent work accurately predicted D_T for

polyacrylates in general and identified MEK as the solvent that yielded the largest D_T for PnBA (1.02×10^{-7} $cm^2\ s^{-1}$), which expedited the carrier liquid selection in this current study.

3.4.2 Estimating D of a Linear Polymer

The translational diffusion coefficient of a linear polymer can be related to its hydrodynamic radius (R_H) by the Stokes-Einstein relationship expressed in Equation 3.5. Here, k_B is the Boltzmann constant, T is temperature, and η is the temperature corrected solvent viscosity. For an idealized random coil in a thermodynamically good solvent, the ratio of the root mean square radius (R_{RMS}) to R_H is equal to 1.5 [49].

$$D = \frac{k_B T}{6\pi\eta R_H} \tag{3.5}$$

Given these relationships, it is possible to estimate D by first approximating R_{RMS} using the freely rotating chain theory of polymers in dilute solutions, Eq. 6 [50]. This model is dependent on the number of segments (N) and the length of a segment (l) which has been approximated to be two times the radius of the monomer [39]. The number of segments is equal to the mass of the polymer, as measured by MALS, divided by the mass of a monomer unit.

$$R_{RMS}^2 = \frac{Nl^2}{6} \tag{3.6}$$

3.4.3 Measuring D for Branched Polymers

Experimental diffusion coefficients of the branched polymers were measured via online dynamic light scattering. Reported values for D, D_T, S_T, and g'' were determined at the apex of the MALS signal.

3.4.4 Calculating S_T for Branched and Linear Polymers

Numerical values for bottlebrush S_T are calculated from measured ThFFF retention times using Equations 3.1 and 3.2. To determine $S_{T,linear}$ at an equivalent molar mass, it was assumed the calculated D_T (1.02×10^{-7} $cm^2 s^{-1}$) was constant at all molar masses [39]. D for a linear polymer was approximated using Equations 3.5 and 3.6 in conjunction with online molar mass data of the branched polymer.

3.5 Results and Discussion

3.5.1 Comparison of Molar Masses Determined by SEC, NMR, and ThFFF-MALS-dRI

Architectural analysis of polymers through *g"* relies on accurate molar mass to estimate S_T of an equivalent linear analog. To this end, ThFFF-MALS-dRI was used as an additional method to determine the number average and weight average molar mass (M_n and M_w, respectively) for each polymer. The molar masses for bottlebrushes with different backbone and sidechain degree of polymerization (DP) are compared to values previously determined by NMR and SEC [45,46] and are summarized in Table 3.1. The nominal M_ns listed for NMR were derived from the percent conversion of monomers (monitored by NMR) and a known backbone length [45,51]. The SEC values were determined using linear calibration standards [45,51]and are substantially lower than the other two techniques. This underestimation is caused by the different relationships between size and MM for linear and branched polymers [1].

Table 3.1. Summary of bottlebrush characterization results by NMR, SEC, and ThFFF-MALS-dRI.

Nominal BB (DP)	Nominal SC[4] (DP)	Grafting Density (%)	NMR[5] M_n (kDa)	SEC			ThFFF-MALS[6]		
				M_n (kDa)	M_w (kDa)	$Đ$	M_n (kDa)	M_w (kDa)	$Đ$
20	22	95	90	45	56	1.25	102	137	1.34
20	55	98	222	67	81	1.21	227	267	1.18
20	112	99	449	156	186	1.19	522	768	1.47
100	20	95	412	-	-	-	344	350	1.02
100	60	98	910	129	168	1.3	1,166	1,188	1.02
100	120	99	2,404	344	396	1.15	2,422	2,916	1.20
400	24	95	1,646	335	395	1.18	2,067	2,515	1.22
400	40	98	3,240	416	495	1.19	7,562	8,990	1.19
400	120	99	9,617	1,450	1,987	1.37	11,190	13,500	1.21
400	14	30	464	156	190	1.22	459	643	1.40
400	49	30	-	-	-	-	1,068	1,109	1.04
400	95	30	-	-	-	-	1,660	1,700	1.02

The agreement between M_ns from NMR and ThFFF-MALS-dRI range between 1% and 25% with the 400g40 sample being an exception. While we currently have no explanation for the substantial deviation for 400g40, there are several possible reasons for the apparent bias towards larger molar mass from ThFFF-MALS. Since the sidechain is comprised of PnBA it is possible that these chains are branched and not linear due to the chain transfer mechanism discussed previously [52]. Sidechain DP was recalculated based upon ThFFF-MALS-dRI molar mass and the assumption that every sidechain is of equal length and the backbone is monodisperse (see Figure 3.6. Rg *is* unavailable for some polymers in the series (where Rg < 10 nm), a plot of gRh (or the contraction in Rh) is used in comparison to g" *results* seen in Figures 3.5 and 3.7.).

[4] Assumes every backbone monomer has a side chain of equal length
[5] Based on percent conversion of monomers as monitored by NMR
[6] dn/dc of 0.0778 ml/g and 0.0889 ml/g were experimentally determined for 100% and 30% grafting density samples, respectively.

There is no clear trend when comparing dispersity ($Đ$) between SEC and ThFFF-MALS-dRI measurements. For both methods, there is also no consistent increase in $Đ$ as the length of the sidechains increases. This is an unexpected result as ATRP was used to grow sidechains and $Đ$ should increase with increasing sidechain length (monomer conversion) [53].

These results illustrate the pitfalls of using SEC with linear polymer calibration standards to determine MMs of branched polymers. The MMs determined by monitoring monomer conversion using NMR and by ThFFF-MALS-dRI mostly agree to within < 25%. The MMs determined by ThFFF-MALS-dRI have % relative standard deviations below 6% and are the values used in the calculation of D and S_T for linear polymer analogues as described in sections 3.2 and 3.4, respectively.

3.5.2 Impact of Backbone and Sidechain DP on Thermal and Translational Diffusion Coefficients

Table 3.2 summarizes the experimentally determined S_T, D and D_T values for the bottlebrush polymers. Within each series of backbone degree of polymerization (DP), S_T is observed to increase with increasing sidechain DP. This is attributed to a decrease in D that accompanies the increase in size as more sidechains are added. Similar S_T and D trends are also observed for bottlebrushes with the same side chain DP but increasing backbone DP. However, the D_T values are significantly lower than those predicted for linear copolymers (1.01 – 1.07 x 10^{-7} $cm^2\,s^{-1}\,K^{-1}$) of the same composition [36]. Additionally, it was expected that an increase in persistence length (because of branching) would lead to an increase in D_T [54]. While the overall decrease in D_T is unexpected, the larger D_T for bottlebrushes with 30% grafting density could be explained by greater solvent accessibility to the backbone. The backbone of the 30% grafting density brush is a random copolymer of PBIBEM and PMA. The experimental D_T of linear PBIBEM and PMA homopolymers (1.7 and 1.8 $cm^2\,K^{-1}\,s^{-1}$, respectively) is greater than that of 'linear' PBnA standards (1.01 $cm^2\,K^{-1}\,s^{-1}$). It is expected that the backbone of a densely grafted brush will behave more like a nondraining coil, which will limit polymer-solvent interaction and thus reduce its contribution to the overall D_T of the polymer [47].

Table 3.2. Measured S_T, D_T, and D values for bottlebrush library.

Nominal Backbone (DP)	**Nominal Sidechain (DP)**	**Grafting Density (%)**	***S_T*[7] *(±0.5%)* (K^{-1})**	***D*[8] *(±5%)* (10^{-7} cm^2s^{-1})**	***D_T*[9] *(±5%)* (10^{-7} $cm^2s^{-1}K^{-1}$)**
20	22	95	0.08	9.82	0.79
20	55	98	0.10	6.48	0.67
20	112	99	0.16	4.33	0.68
100	20	95	0.12	6.38	0.79
100	60	98	0.21	3.99	0.84
100	120	99	0.32	2.77	0.87
400	24	95	0.25	2.67	0.66
400	40	98	0.43	1.57	0.68
400	120	99	0.62	0.98	0.61
400	14	30	0.18	5.40	0.97
400	49	30	0.26	3.48	0.91
400	95	30	0.35	2.71	0.95

For polymers of the same composition, separation in ThFFF is attributed to differences in *D*. Based on previous studies, retention should decrease with an increase in branching (as the contraction from branching leads to a decrease in R_h for the same molar mass polymer and thus an increase in *D*) [55]. Since *D* can be directly related to the number of monomers in a polymer, or molar mass, the relationship between retention can also be associated with changes in molar mass. In this study, it was expected that *D*, and thus retention time, will change with respect to the lengths of the bottlebrushes' sidechains and backbones. A ratio of the R_{RMS} to the hydrodynamic radius R_H provides information on the polymer conformation in solution with literature values ranging from 1.05 to 2 [56–58]. Experimental values ranged from 1.05-1.2, which is similar to literature data for bottlebrushes of similar molar mass but of various chemistries [59] and is presented Table S1. Due to the limitations of MALS, it was not possible

[7] S_T calculated from MALS peak maximum retention time
[8] *D* measured by online DLS
[9] D_T calculated from experimental S_T and *D*

to determine R_{RMS} for the smallest brushes in the library due to their size relative to the laser wavelength. In the 400-backbone series, with 100% grafting density, a decrease in the R_{RMS}/R_H ratio suggests that the polymer is adopting a more spherical shape as the sidechains increase in length, which agrees with previous work [56].

D will change with molar mass as well as branching and the effect that sidechain and backbone DP have on hydrodynamic radius is not well known. The effect of sidechain DP on retention is reflected by the overlaid fractograms of the 100% graft density 100-backbone series (denoted as 100g20, 100g60, and 100g120) shown in Figure 3.1. The differences in retention level R_L are primarily an effect of molar mass and the elution order is as expected. All three peaks exhibit shoulders that become more prominent as the sidechain DP increases. This may be due to an increase in sidechain dispersity which is unexpected from the polymerization mechanism employed. Figure 3.1 also shows the fractograms of 100% (100g60) and 30% graft density (400g49) bottlebrush polymers (both with a M_w near 1,100 kDa). The observed higher R_L for the 30% grafting density brush is as expected based on its higher D_T value (Table 3.2).

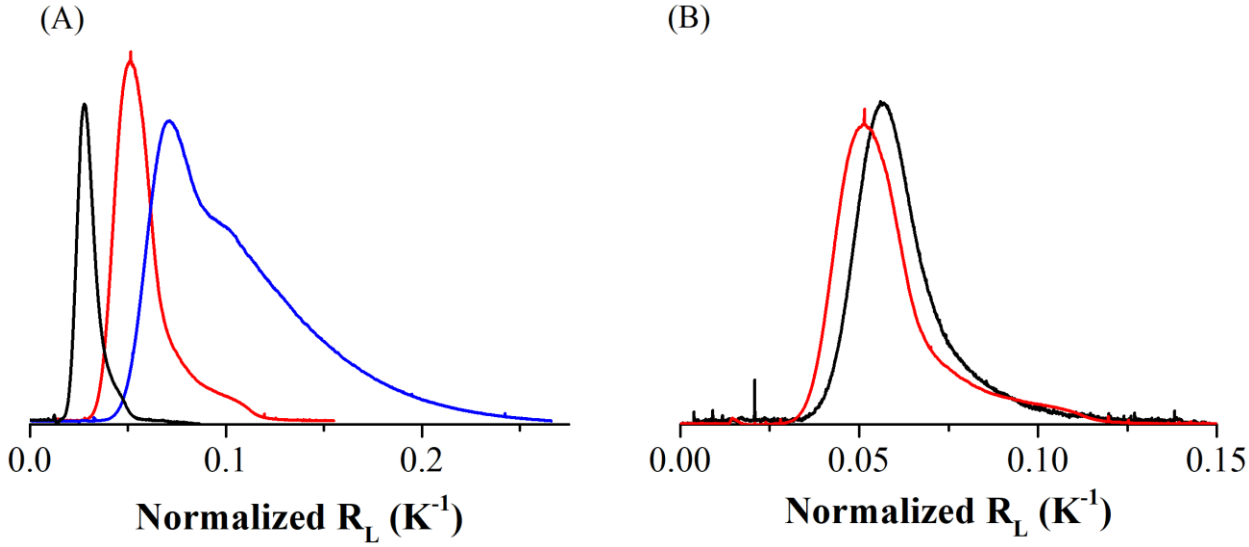

Figure 3.1. Effect of polymer architecture on retention level R_L (normalized to account for varied flowrates and MALS detector intensity). A) fractograms of 100g22 (black), 100g60 (red), and 100g120 (blue) and B) fractograms of 400g49 (black) and 100g60 (red). The channel flow rate was 0.2 mL min^{-1} except for 100g22 which was 0.1 mL min^{-1}.

3.5.3 Impact of Backbone and Sidechain DP on S_T

The S_T values listed in Table 3.2 are plotted as a function of backbone and sidechain DP in Figure 3.2. The observed proportional relationships between S_T and DP are as expected. When the backbone DP increases (constant sidechain DP), the polymer radius increases, *D* decreases, t_r

increases, and S_T increases. Fig. 2A also includes results for brushes with a PBiBEM-PMA backbone and 30% PnBA grafting density. The S_Ts for these brushes are higher than for the 100% graft density series and are consistent with higher retention times and D_T values (Table 3.2).

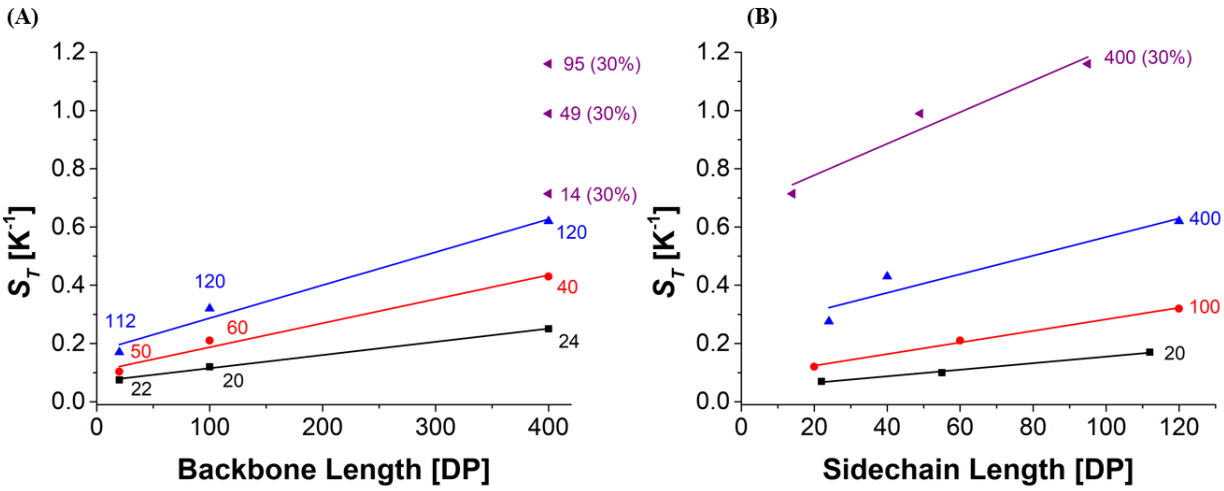

Figure 3.2 Change in Soret coefficient with respect to A) backbone length (DP) and B) sidechain length (DP). Labels indicate the DP of the sidechain (A) and backbone (B).

Interestingly, the slope of the plot increases as the backbone DP increases. This is unexpected if one only considers relative changes in size (or D) and hints at a more complex explanation possibly involving polymer conformation. The R_{RMS}/R_H for the 400 DP backbone increases with decreasing sidechain DP suggesting an increasingly extended conformation. Unfortunately, shape factors could not be measured for the complete 20 and 100 backbone series due to the lower size limit for MALS. Figure 3.2B shows that similar trends are observed when the sidechain length is varied.

In addition, the slope for the 30% graft density series is larger than the 100% graft density of the same backbone DP. This suggests that S_T has better selectivity for sidechain length with larger polymer backbones and lower grafting density. These correlations between backbone DP, sidechain DP, and S_T allows the sidechain length to be estimated from S_T if backbone length is known. To the authors' knowledge, no prior work offering this level of detailed information has been previously available from a single experiment except by small-angle neutron scattering [60].

3.5.4 Estimation of Linear S_T

A drawback in the characterization of branching though contraction factors is the requirement for linear analogues (linear polymers of the same molar mass and composition). A benefit of ThFFF is the ability to estimate S_T of the linear analogue from a known composition. For this system no linear analog was available, despite a highly controlled polymerization processes, due to branching present as the result of intramolecular chain transfer [52,61]. As each bottlebrush is comprised primarily of PnBA, and the PBiBEM backbone is shielded by the sidechains, the composition was treated as 100% *n*-butyl acrylate to simplify these calculations. D_T of PnBA was estimated using the most recent methods outlined in literature [39,48].

Theoretical *D* values were calculated from measured M_w of the polymers and literature data relating the molar mass of PnBA to *D*. $S_{T,lin}$ was then calculated from the ratio of D_T and *D* values at a given molar mass; the results are tabulated in Table 3.2. Predicted $S_{T,lin}$ of an equivalent linear analog may then be compared to observed S_T for a polymer with nonlinear architecture. This analysis yielded *g"* values that range from 0.266 – 0.422, decreasing with molar mass. The level of contraction for a polymer may indicate the architecture of the polymer. These values are similar to g_{Rh} (contraction in R_h) for this system as well as typical contraction factors for other branched systems [13,18,21,38,62]. A comparison of *g"* calculated through various alternate methods and other contraction factors is made in Figures 3.6 and 3.7.

3.5.5 Architectural Analysis of Bottlebrushes Via the Soret Contraction Factor

A plot of $S_{T,bottlebrush}$ with respect to $S_{T,lin}$ provides some qualitative insight into architecture. Figure 3.3 is similar to previous work in that any non-linear polymer should fall below the line y = x [23]. One interesting feature of this plot is the trend in contraction for bottlebrush polymers appears to be linear, including brushes with lower grafting density.

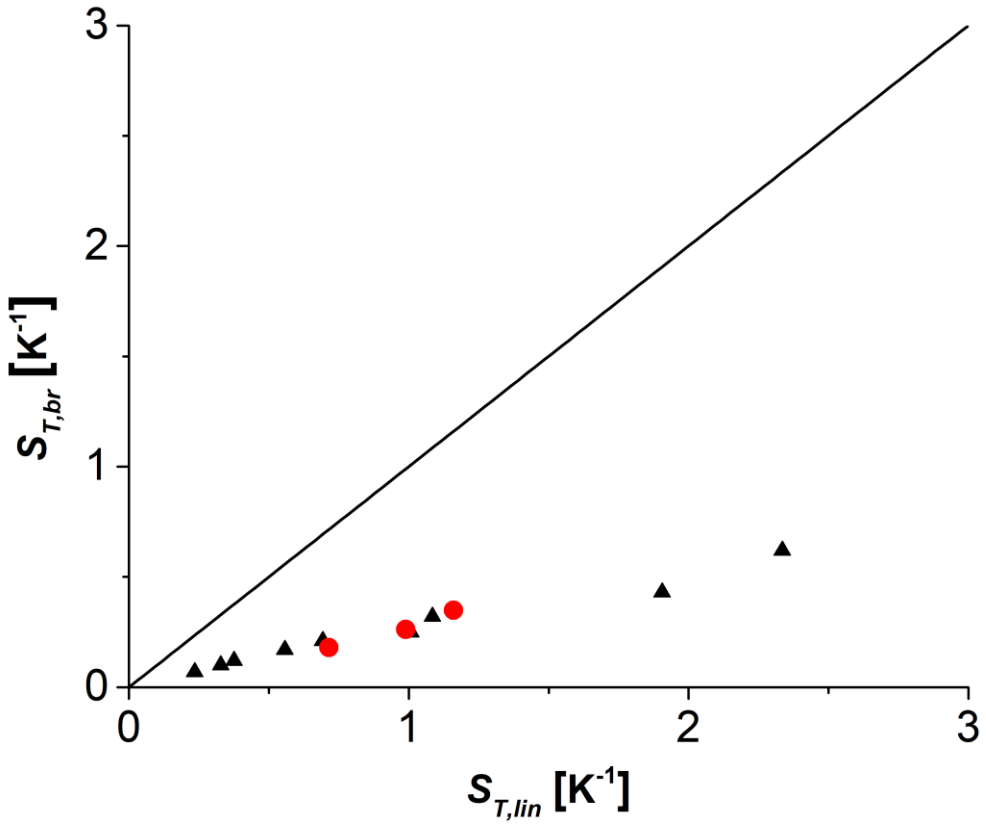

Figure 3.3. Plot of $S_{T,br}$ vs. $S_{T,lin}$ for bottlebrushes with 100% (▲) and 30% (●) grafting density, where $S_{T,lin}$ is approximated at an equivalent molar mass to $S_{T,br}$. Branched polymers are expected to fall below the solid line (y = x), as their physiochemical properties are contracted relative to that of a linear analog.

Despite the general usefulness of this plot, it shows little sensitivity to grafting density. A similar lack of sensitivity was observed when comparing the contraction of the hydrodynamic radii (Figure 3.6). An alternative is to plot log (g'') as a function of molar mass as seen in Figure 3.4. A negative slope is observed for the 100% graft density brushes where a positive slope is observed for 30% graft density. Currently we have no explanation for this behavior, however, sensitivity to graft density is greatly improved.

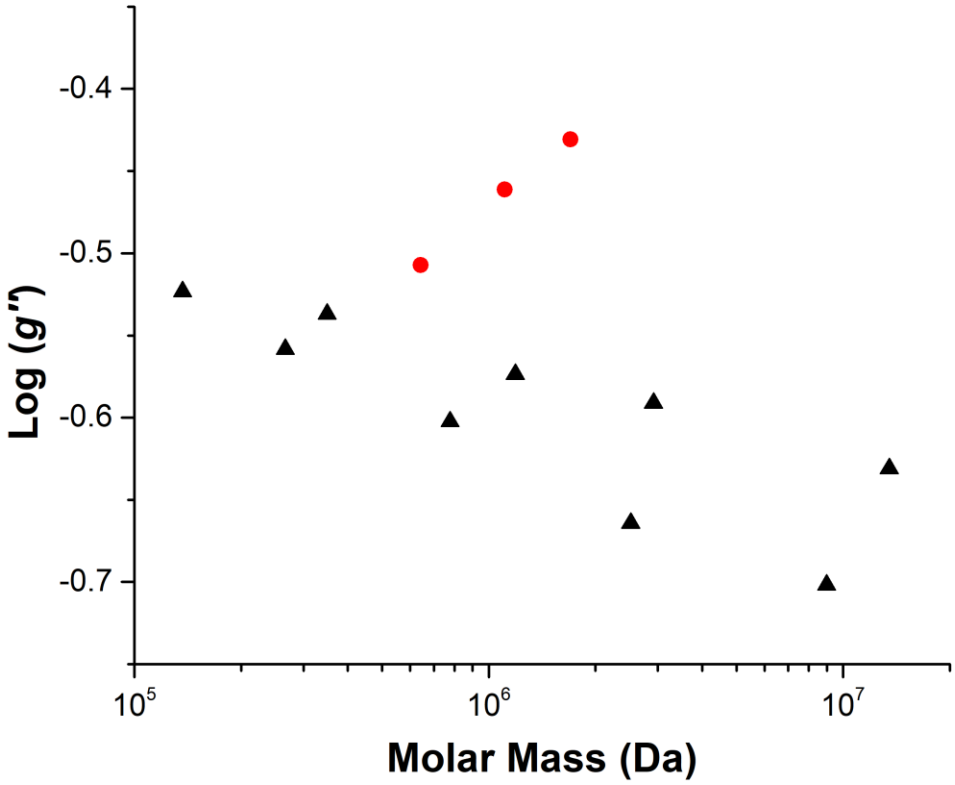

Figure 3.4. Plot of log (*g"*) versus molar mass for bottlebrushes with 100% (▲) and 30% (●) grafting density.

Initial development of the Soret contraction factor showed that a plot of log (*g"*) with respect to the number of chain ends was effective in the characterization of a series of stars and pom-poms [23]. When the data set from this work is plotted as such it becomes easy to discern between bottlebrushes of varied grafting density and two types of architectures, making Figure 3.5 especially useful. Recent *g"* analysis of a branched polyester system whose number of chain ends can be inferred from degree of branching and molar mass was compared to the bottlebrush results. This results in what appears to be distinct regions of polymer architectures, where bottlebrushes may be distinguished from a randomly branched pseudo dendritic polymer. For bottlebrushes this is convenient due to the nature of the synthetic process and ease of determining number of chain ends. In other systems, especially natural polymers, this may be more difficult to determine. This work introduces the ability to differentiate between grafting density and architecture of a polymer without the need for linear standards of same chemistry and molar mass.

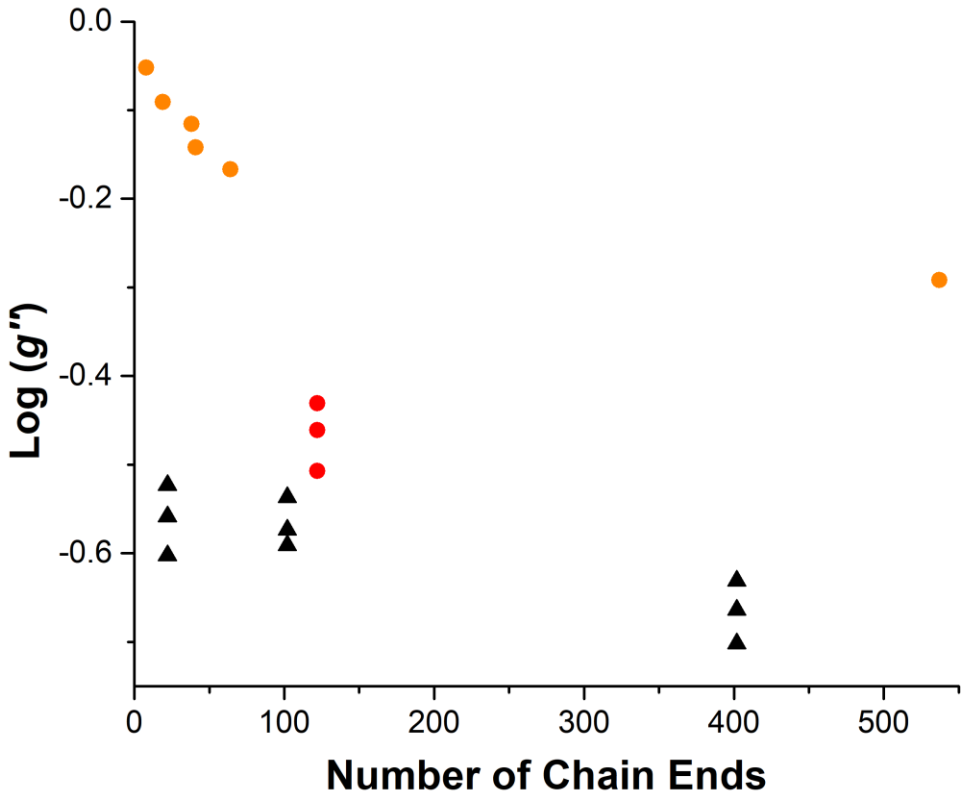

Figure 3.5. Plot of log (*g"*) with respect to the number of chain ends for branched polyesters (●), bottlebrushes of 30% (●), and 100% (▲) grafting density. Data for hyperbranched polyesters is from literature [21].

3.6 Conclusions

This study conveys the usefulness of the Soret coefficient and ThFFF in the determination of architectural traits in polymers. The simplicity of measuring S_T and M_w of a polymer to obtain dimensional traits combined with advancements in accuracy over both NMR and SEC must not be understated. Additionally, it appears that disparate architectures (hyperbranched and bottlebrush) correspond to distinct domains in a plot of log *g"* and number of chains. Furthermore, other methods which evaluate contraction of viscosity or other properties require linear standards of the same chemistry to accurately assess polymer architecture. These are not always available and make ThFFF particularly desirable to this end.

This work clearly illustrates that the Soret coefficient is sensitive to the architectural traits of polymers and is correlated to the magnitudes of polymer dimensions in a solution, regardless of its nominal architecture. This is particularly useful for the development of synthetic materials, as polymers of similar theoretical and measured S_T values may provide comparable performance in the development of artificial materials.

3.7 Acknowledgments

This work was supported by the National Science Foundation [CHE- 1808805].

3.8 Supporting Information

Table 3.3. Bottlebrush root-mean-square (R_{rms}) and hydrodynamic radii (R_h) determined by online MALS and QELS.

Backbone (DP)	**Sidechain (DP)**	**PnBA content (%)**	**ThFFF-MALS**				
			R_{rms}	**RSD (%)**	***R_h***	**RSD (%)**	**R_g/R_h**
20	22	95	<10	-	5.6	4.6	-
20	55	98	<10	-	8.8	0.9	-
20	112	99	13.7	3.0	12.7	3.5	1.08
100	20	95	<10	-	8.6	2.1	-
100	60	98	14.1	2.2	12.6	3.0	1.12
100	120	99	23.8	2.2	19.9	4.1	1.20
400	24	95	24.8	2.0	20.7	2.0	1.20
400	40	98	41.1	1.5	35.3	5.0	1.16
400	120	99	59.6	0.4	52.6	3.6	1.13
400	14	30	10.8	5.2	9.4	3.5	1.15
400	49	30	16.6	4.5	15.8	1.0	1.05
400	95	30	19.9	8.5	18.7	1.3	1.06

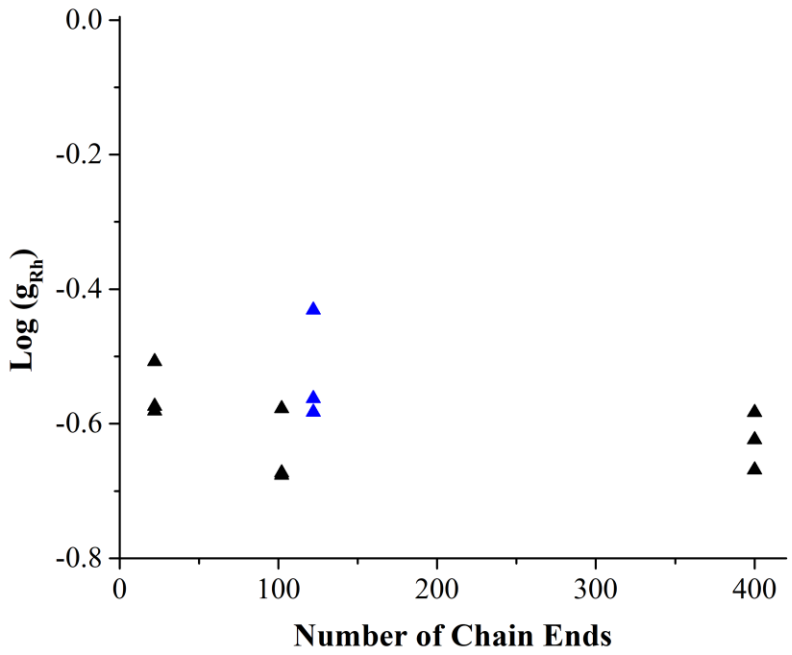

Figure 3.6. R_g is unavailable for some polymers in the series (where R_g < 10 nm), a plot of g_{Rh} (or the contraction in R_h) is used in comparison to *g''* results seen in Figures 3.5 and 3.7.

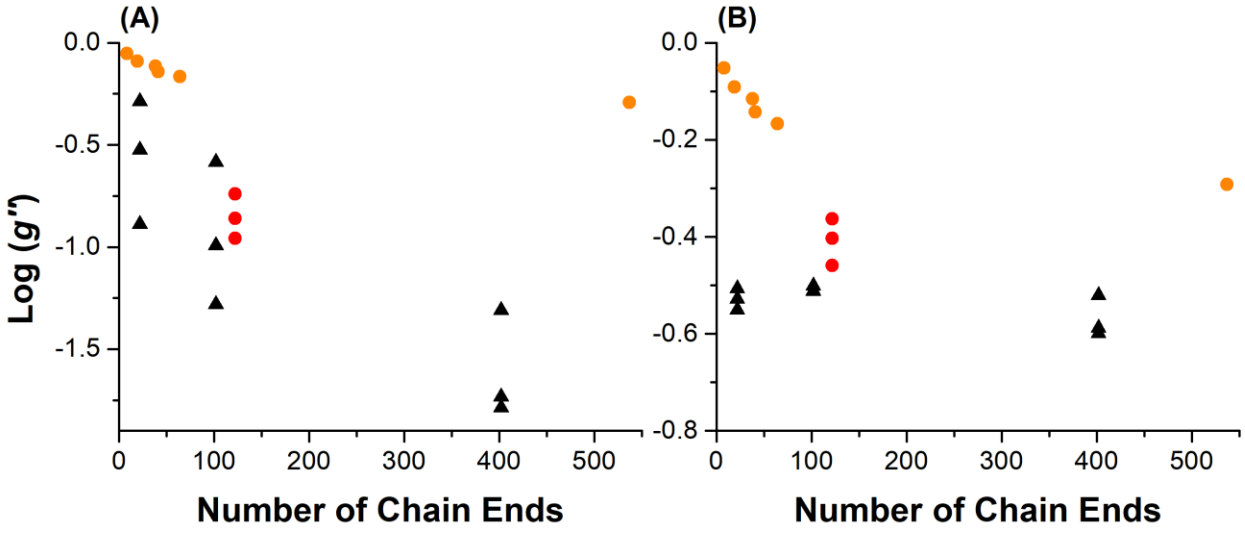

Figure 3.7 A plot of log (*g''*) with respect to the number of chain-ends for branched polyesters (●), bottlebrushes of 30% (●), and 100% (▲) grafting density. Poly(methyl methacrylate) (PMMA), like PnBA but with readily available linear standards, was chosen as an alternative linear analog. $S_{T,lin}$ in **(A)** was estimated as outlined in *Theory and Calculations*. $S_{T,lin}$ in **(B)** was estimated via an experimentally determined calibration curve of S_T with respect to the molar mass (from 100-300 kDa). The degree of contraction for higher molar mass brushes was considerably increased using PMMA instead of PnBA in the theoretical approach. The experimentally determined calibration curve yielded results more similar to Figure 3.5.

3.9 References

[1] S. Podzimek, Molar mass distribution by size exclusion chromatography: Comparison of multi-angle light scattering and universal calibration, J Appl Polym Sci. 136 (2019) 47561. https://doi.org/10.1002/app.47561.

[2] S.M. Rowland, A.M. Striegel, Characterization of copolymers and blends by quintuple-detector size-exclusion chromatography, Anal Chem. 84 (2012) 4812–4820. https://doi.org/10.1021/ac3003775.

[3] T. Chang, Polymer characterization by interaction chromatography, J Polym Sci B Polym Phys. 43 (2005) 1591–1607. https://doi.org/10.1002/polb.20440.

[4] M. Toney, L. Baiamonte, W.C. Smith, S. Kim Ratanathanawongs Williams, Field-flow fractionation techniques for polymer characterization, Elsevier Inc., 2021. https://doi.org/10.1016/b978-0-12-819768-4.00004-x.

[5] W. Hiller, W. van Aswegen, M. Hehn, H. Pasch, Online ThFFF-NMR: A novel tool for molar mass and chemical composition analysis of complex macromolecules, Macromolecules. 46 (2013) 2544–2552. https://doi.org/10.1021/ma400350y.

[6] P. Kratochvil, M. Netopilik, On the contraction factors of long-chain branched macromolecules, Eur Polym J. 51 (2014) 177–181. https://doi.org/10.1016/j.eurpolymj.2013.11.010.

[7] M. Haerth, J. Kaschta, D.W. Schubert, Shear and Elongational Flow Properties of Long-Chain Branched Poly(ethylene terephthalates) and Correlations to Their Molecular Structure, Macromolecules. 47 (2014) 4471–4478. https://doi.org/10.1021/ma5002657.

[8] N.T. Hieu Ha, G.M. Moran, Branching features of a polymer, Journal of Macromolecular Science, Part B: Physics. 51 (2012) 1942–1975. https://doi.org/10.1080/00222348.2012.663698.

[9] L.R. Hutchings, Complex Branched Polymers for Structure-Property Correlation Studies: The Case for Temperature Gradient Interaction Chromatography Analysis, Macromolecules. 45 (2012) 5621–5639. https://doi.org/10.1021/ma3005422.

[10] A.R. Maniego, A.T. Sutton, M. Gaborieau, P. Castignolles, Assessment of the Branching Quantification in Poly(acrylic acid): Is It as Easy as It Seems?, Macromolecules. 50 (2017) 9032–9041. https://doi.org/10.1021/acs.macromol.7b01411.

[11] S.Y. Yu-Su, F.C. Sun, S.S. Sheiko, D. Konkolewicz, H. Lee, K. Matyjaszewski, Molecular Imaging and Analysis of Branching Topology in Polyacrylates by Atomic Force Microscopy, Macromolecules. 44 (2011) 5928–5936. https://doi.org/10.1021/ma200821a.

[12] K. Klimke, M. Parkinson, C. Piel, W. Kaminsky, H.W. Spiess, M. Wilhelm, Optimisation and Application of Polyolefin Branch Quantification by Melt-State13C NMR Spectroscopy, Macromol Chem Phys. 207 (2006) 382–395. https://doi.org/10.1002/macp.200500422.

[13] M. Schappacher, A. Deffieux, New polymer chain architecture: Synthesis and characterization of star polymers with comb polystyrene branches, Macromolecules. 33 (2000) 7371–7377. https://doi.org/10.1021/ma0001436.

[14] C. Zhang, J. Li, J. zhang, L. Zhang, H. Li, Synthesis, and characterization of hyperbranched polystyrene copolymers by atom transfer radical self-condensing vinyl copolymerization, Polym Adv Technol. 21 (2009) 710–719. https://doi.org/10.1002/pat.1491.

[15] M.J. Tizzotti, M.C. Sweedman, D. Tang, C. Schaefer, R.G. Gilbert, New (1)h NMR procedure for the characterization of native and modified food-grade starches., J Agric Food Chem. 59 (2011) 6913–9. https://doi.org/10.1021/jf201209z.

[16] P. Castignolles, R. Graf, M. Parkinson, M. Wilhelm, M. Gaborieau, Detection and quantification of branching in polyacrylates by size-exclusion chromatography (SEC) and melt-state 13C NMR spectroscopy, Polymer (Guildf). 50 (2009) 2373–2383. https://doi.org/10.1016/j.polymer.2009.03.021.

[17] T. Otte, H. Pasch, T. Macko, R. Brüll, F.J. Stadler, J. Kaschta, F. Becker, M. Buback, Characterization of branched ultrahigh molar mass polymers by asymmetrical flow field-flow fractionation and size exclusion chromatography, J Chromatogr A. 1218 (2011) 4257–4267. https://doi.org/10.1016/j.chroma.2010.12.072.

[18] J.F. Douglas, J. Roovers, K.F. Freed, Characterization of branching architecture through "universal" ratios of polymer solution properties, Macromolecules. 23 (1990) 4168–4180. https://doi.org/10.1021/ma00220a022.

[19] M. Gaborieau, J. Nicolas, M. Save, B. Charleux, J.P. Vairon, R.G. Gilbert, P. Castignolles, Separation of complex branched polymers by size-exclusion chromatography probed with multiple detection, J Chromatogr A. 1190 (2008) 215–223. https://doi.org/10.1016/j.chroma.2008.03.031.

[20] P.D. Butler, C. Hawker, Effective Interaction Parameter between Branched and Linear Polystyrene, (2001) 2549–2561. https://doi.org/10.1002/polb.0000.

[21] W.C. Smith, M. Geisler, A. Lederer, S.K.R. Williams, Thermal Field-Flow Fractionation for Characterization of Architecture in Hyperbranched Aromatic-Aliphatic Polyesters with Controlled Branching, Anal Chem. 91 (2019) 12344–12351. https://doi.org/10.1021/acs.analchem.9b02664.

[22] M. Geisler, W.C. Smith, L. Plüschke, R. Mundil, J. Merna, S.K.R. Williams, A. Lederer, SI - Topology Analysis of Chain Walking Polymerized Polyethylene: An Alternative Approach for the Branching Characterization by Thermal FFF, Macromolecules. 52 (2019) 8662–8671. https://doi.org/10.1021/acs.macromol.9b01410.

[23] J.R. Runyon, S.K.R. Williams, Thermal Field-Flow Fractionation of Polymers with High Molecular Weight and Complex Architecture, Colorado School of Mines, 2009.

[24] S. Podzimek, T. Vlcek, C. Johann, Characterization of branched polymers by size exclusion chromatography coupled with multiangle light scattering detector. I. Size

exclusion chromatography elution behavior of branched polymers, J Appl Polym Sci. 81 (2001) 1588–1594. https://doi.org/10.1002/app.1589.

[25] H. Lee, J. Yang, T. Chang, Branching analysis of star-shaped polybutadienes by temperature gradient interaction chromatography-triple detection, Polymer (Guildf). 112 (2017) 71–75. https://doi.org/10.1016/j.polymer.2017.01.070.

[26] W. Hiller, P. Sinha, M. Hehn, H. Pasch, T. Hofe, Separation analysis of polyisoprenes regarding microstructure by online LCCC-NMR and SEC-NMR, Macromolecules. 44 (2011) 1311–1318. https://doi.org/10.1021/ma102750s.

[27] M.I. Malik, H. Pasch, Basic principles of size exclusion and liquid interaction chromatography of polymers, Elsevier Inc., 2021. https://doi.org/10.1016/b978-0-12-819768-4.00007-5.

[28] H. Pasch, A.C. Makan, H. Chirowodza, N. Ngaza, W. Hiller, Analysis of complex polymers by multidetector field-flow fractionation Field-Flow Fractionation, Anal Bioanal Chem. 406 (2014) 1585–1596. https://doi.org/10.1007/s00216-013-7308-0.

[29] R.A. Cave, S.A. Seabrook, M.J. Gidley, R.G. Gilbert, Characterization of starch by size-exclusion chromatography: The limitations imposed by shear scission, Biomacromolecules. 10 (2009) 2245–2253. https://doi.org/10.1021/bm900426n.

[30] M.I. Malik, H. Pasch, Field-flow fractionation: New and exciting perspectives in polymer analysis, Prog Polym Sci. 63 (2016) 42–85. https://doi.org/10.1016/j.progpolymsci.2016.03.004.

[31] C.L. Plavchak, W.C. Smith, C.R.M. Bria, S.K.R. Williams, New Advances and Applications in Field-Flow Fractionation, Annual Review of Analytical Chemistry. 14 (2021) 257–279. https://doi.org/10.1146/annurev-anchem-091520-052742.

[32] M. Toney, L. Baiamonte, W.C. Smith, S. Kim Ratanathanwongs Williams, S. Kim Ratanathanawongs Williams, S.K.R. Williams, Field-flow fractionation techniques for polymer characterization, in: Molecular Characterization of Polymers, Elsevier, 2021: pp. 129–171. https://doi.org/10.1016/B978-0-12-819768-4.00004-X.

[33] F.A. Messaud, R.D. Sanderson, J.R. Runyon, T. Otte, H. Pasch, S.K.R. Williams, An overview on field-flow fractionation techniques and their applications in the separation and characterization of polymers, Progress in Polymer Science (Oxford). 34 (2009) 351–368. https://doi.org/10.1016/j.progpolymsci.2008.11.001.

[34] C.A. Rue, M.E. Schimpf, Thermal Diffusion in Liquid Mixtures and Its Effect on Polymer Retention in Thermal Field-Flow Fractionation, Anal Chem. 66 (1994) 4054–4062. https://doi.org/10.1021/ac00094a030.

[35] M.E. Schimpf, J.C. Giddings, Characterization of thermal diffusion in polymer solutions by thermal field-flow fractionation: Dependence on polymer and solvent parameters, J Polym Sci B Polym Phys. 27 (1989) 1317–1332. https://doi.org/10.1002/polb.1989.090270610.

[36] C.A. Ponyik, D.T. Wu, S.K.R. Williams, Separation, and composition distribution determination of triblock copolymers by thermal field-flow fractionation, Anal Bioanal Chem. 405 (2013) 9033–9040. https://doi.org/10.1007/s00216-013-7282-6.

[37] G. Greyling, H. Pasch, Tacticity Separation of Poly(methyl methacrylate) by Multidetector Thermal Field-Flow Fractionation, Anal Chem. 87 (2015) 3011–3018. https://doi.org/10.1021/ac504651p.

[38] M. Geisler, W.C. Smith, L. Plüschke, R. Mundil, J. Merna, S.K.R. Williams, A. Lederer, Topology Analysis of Chain Walking Polymerized Polyethylene: An Alternative Approach for the Branching Characterization by Thermal FFF, Macromolecules. 52 (2019) 8662–8671. https://doi.org/10.1021/acs.macromol.9b01410.

[39] M. Geisler, L. Plüschke, J. Merna, A. Lederer, The Role of Solubility in Thermal Field-Flow Fractionation: A Revisited Theoretical Approach for Tuning the Separation of Chain Walking Polymerized Polyethylene, Anal Chem. 92 (2020) 14822–14829. https://doi.org/10.1021/acs.analchem.0c03686.

[40] J.R. Runyon, S.K.R. Williams, A theory-based approach to thermal field-flow fractionation of polyacrylates, J Chromatogr A. 1218 (2011) 7016–7022. https://doi.org/10.1016/j.chroma.2011.08.007.

[41] M.E. Schimpf, K. Caldwell, J.C. Giddings, Field-Flow Fractionation Handbook, John Wiley & Sons, 2000.

[42] W.C. Smith, M. Geisler, A. Lederer, S.K.R. Williams, Thermal Field-Flow Fractionation for Characterization of Architecture in Hyperbranched Aromatic-Aliphatic Polyesters with Controlled Branching, Anal Chem. 91 (2019) 12344–12351. https://doi.org/10.1021/acs.analchem.9b02664.

[43] L.Y. Qiu, Y.H. Bae, Polymer architecture and drug delivery, Pharm Res. 23 (2006) 1–30. https://doi.org/10.1007/s11095-005-9046-2.

[44] T. Pelras, C.S. Mahon, M. Müllner, Synthesis and Applications of Compartmentalised Molecular Polymer Brushes, Angewandte Chemie - International Edition. 57 (2018) 6982–6994. https://doi.org/10.1002/anie.201711878.

[45] K. Mukumoto, Y. Li, A. Nese, S.S. Sheiko, K. Matyjaszewski, Synthesis and characterization of molecular bottlebrushes prepared by iron-based ATRP, Macromolecules. 45 (2012) 9243–9249. https://doi.org/10.1021/ma3020867.

[46] A. Nese, Y. Li, S.S. Sheiko, K. Matyjaszewski, Synthesis of molecular bottlebrushes by atom transfer radical polymerization with ppm amounts of cu catalyst, ACS Macro Lett. 1 (2012) 991–994. https://doi.org/10.1021/mz3002484.

[47] K.I. Morozov, W. Köhler, Thermophoresis of polymers: Nondraining vs draining coil, Langmuir. 30 (2014) 6571–6576. https://doi.org/10.1021/la501695n.

[48] E.P.C. Mes, W.Th. Kok, R. Tijssen, Prediction of Polymer Thermal Diffusion Coefficients from Polymer-Solvent Interaction Parameters: Comparison with Thermal Field Flow Fractionation and Thermal Diffusion Forced Rayleigh Scattering Experiments,

International Journal of Polymer Analysis and Characterization. 8 (2003) 133–153. https://doi.org/10.1080/10236660304888.

[49] K. Haydukivska, V. Blavatska, J. Paturej, Universal size ratios of Gaussian polymers with complex architecture: radius of gyration vs hydrodynamic radius, Sci Rep. 10 (2020) 1–11. https://doi.org/10.1038/s41598-020-70649-z.

[50] M. Fixman, Radius of gyration of polymer chains, J Chem Phys. 36 (1962) 306–310. https://doi.org/10.1063/1.1732501.

[51] B.S. Sumerlin, D. Neugebauer, K. Matyjaszewski, Initiation efficiency in the synthesis of molecular brushes by grafting from via atom transfer radical polymerization, Macromolecules. 38 (2005) 702–708. https://doi.org/10.1021/ma048351b.

[52] N.M. Ahmad, B. Charleux, C. Farcet, C.J. Ferguson, S.G. Gaynor, B.S. Hawkett, F. Heatley, B. Klumperman, D. Konkolewicz, P.A. Lovell, K. Matyjaszewski, R. Venkatesh, Chain transfer to polymer and branching in controlled radical polymerizations of n-butyl acrylate, Macromol Rapid Commun. 30 (2009) 2002–2021. https://doi.org/10.1002/marc.200900450.

[53] E. Mastan, S. Zhu, A Molecular Weight Distribution Polydispersity Equation for the ATRP System: Quantifying the Effect of Radical Termination, Macromolecules. 48 (2015) 6440–6449. https://doi.org/10.1021/acs.macromol.5b01525.

[54] D. Stadelmaier, W. Köhler, From small molecules to high polymers: Investigation of the crossover of thermal diffusion in dilute polystyrene solutions, Macromolecules. 41 (2008) 6205–6209. https://doi.org/10.1021/ma800891p.

[55] M. Gaborieau, P. Castignolles, Size-exclusion chromatography (SEC) of branched polymers and polysaccharides, Anal Bioanal Chem. 399 (2011) 1413–1423. https://doi.org/10.1007/s00216-010-4221-7.

[56] A. Chremos, J.F. Douglas, A comparative study of thermodynamic, conformational, and structural properties of bottlebrush with star and ring polymer melts, Journal of Chemical Physics. 149 (2018). https://doi.org/10.1063/1.5034794.

[57] M. Gerle, K. Fischer, S. Roos, A.H.E. Müller, M. Schmidt, S.S. Sheiko, S. Prokhorova, M. Möller, Main Chain Conformation and Anomalous Elution Behavior of Cylindrical Brushes As Revealed by GPC/MALLS, Light Scattering, and SFM ‡ , Macromolecules. 32 (2002) 2629–2637. https://doi.org/10.1021/ma9816463.

[58] M. Wintermantel, M. Gerle, K. Fischer, M. Schmidt, I. Wataoka, H. Urakawa, K. Kajiwara, Y. Tsukahara, Molecular Bottlebrushes † , Macromolecules. 29 (2002) 978–983. https://doi.org/10.1021/ma950227s.

[59] S.L.L. Pesek, X. Li, B. Hammouda, K. Hong, R. Verduzco, Small-angle neutron scattering analysis of bottlebrush polymers prepared via grafting-through polymerization, Macromolecules. 46 (2013) 6998–7005. https://doi.org/10.1021/ma401246b.

[60] S. Rathgeber, T. Pakula, A. Wilk, K. Matyjaszewski, H. il Lee, K.L.L. Beers, Bottle-brush macromolecules in solution: Comparison between results obtained from scattering

experiments and computer simulations, Polymer (Guildf). 47 (2006) 7318–7327. https://doi.org/10.1016/j.polymer.2006.06.010.

[61] S.Y. Yu-Su, F.C. Sun, S.S. Sheiko, D. Konkolewicz, H. Lee, K. Matyjaszewski, Molecular Imaging and Analysis of Branching Topology in Polyacrylates by Atomic Force Microscopy, Macromolecules. 44 (2011) 5928–5936. https://doi.org/10.1021/ma200821a.

[62] W.R. Krigbaum, Q.A. Trementozzi, Use of the second virial coefficient to estimate chain branching, Journal of Polymer Science. 28 (1958) 295–307. https://doi.org/10.1002/pol.1958.1202811705.

CHAPTER 4

SAMPLE PREPARATION AND ARCHITECTURAL ANALYSIS OF AN INDUSTIRAL POLYMER FORMULATION VIA THERMAL FIELD-FLOW FRACTIONATION

Michael Toney[1], Yongfu Li[2], Ryan Baumgartner[3], Margo McIvor[2], David Meunier[2], Wei Gao[4], Edwin Mes[5], S. Kim Ratanathanawongs Williams[1,6]

4.1 Abstract

Polysiloxanes are a class of highly tunable semi-inorganic polymers which are widely used in industrial formulations. Low molar mass polysiloxanes are typically liquids at room temperature and are useful lubricants and diluents. Crosslinking of these polymers can result in an increased solution viscosity or the formation of semi-solids. Size exclusion chromatography of these materials is challenged by non-ideal elution due to their branching and high molar mass. Thermal field-flow fractionation (ThFFF) is a useful method for the analysis of polymers with high molar mass due to its open channel design and greater resolution (than SEC with a single column) for polymers whose mass is >~10^4 Da) [1]. Two formulations of a crosslinked polysiloxane were analyzed by ThFFF with online light scattering to determine the Soret contraction factor (*g''*). These polymers were synthesized by a platinum catalyzed reaction between a poly(methylhydrosiloxane)-polydimethylsiloxane copolymer (PHMS-PDMS) and a vinyl terminated polydimethylsiloxane (PDMS-Vi). Due to the high viscosity of the product, the reaction was carried out in a solution of at least 90% diluent. This presented challenges for ThFFF due to the low concentration of analyte and presence of insoluble gel material. Precipitation of the product from the diluent followed by ultracentrifugation and filtration resulted in fractograms with reproducible peak shape and molar mass results with less than 6% RSD. A comparison of the two formulations by *g''* analysis showed the expected result that an increase in the ratio of backbone (PHMS-PDMS) to crosslinker (PDMS-Vi) resulted in an

[1]Department of Chemistry, Colorado School of Mines, 1500 Illinois St, Golden, Colorado 80401, United States
[2]Dow Chemical Company, Analytical Science, Midland, MI 48674
[3]Dow Chemical Company, Dow Performance Silicone, Midland, MI 48674
[4]Dow Chemical Company, Analytical Science, Collegeville, PA19426
[5]Dow Chemical Company, Analytical Science, Terneuzen, 4542 NM, Netherlands
[6]Corresponding Author

increase in overall crosslinking. These results were validated by GC-MS of the depolymerized materials.

4.2 Introduction

4.2.1 Crosslinked Polysiloxanes

Polysiloxanes are a class of inorganic or semi-inorganic polymers which are a widely used alternative to oil-based polymers due to their chemical and thermal stability, low coefficient of friction, low glass-transition temperature, and the natural abundance of silica - the principal precursor material. These physicochemical properties have been modified by altering the composition and structure of the Si-O backbone [2]–[4]. This is achieved by various combinations of mono-, di-, tri-, or tetravalent units with the respective symbols and general formulas: M = $R_3SiO_{1/2}$, D = $R_2SiO_{2/2}$, T = $R_1SiO_{1/2}$, and Q = $SiO_{4/2}$ [5]. Typical R groups are methyl, alkyl, phenyl, hydrogen, and trifluoro propyl. A linear polysiloxane may consist of two end groups (M) and some number of repeat difunctional units (D) along the backbone. These are generally fluids at room temperature and are frequently used as lubricants. Non-linear architectures may be achieved by incorporating pendant groups and/or chain-ends capable of crosslinking. A wide range of physical properties may be accessed by altering the density of crosslinked sites in a network. An increase in crosslinking is directly correlated to an increase in moduli and hardness which vary from a soft gel to stiff rubber [3], [6]. This, in combination with strong chemical stability, allows for a diverse set of applications such as medical devices to nonstick coatings, hydrophobic surfaces, castings, cosmetics, and others.

4.2.2 Current Sample Preparation and Characterization Methods

Formulation of crosslinked polysiloxane can result in multiple heterogeneities: molar mass, degree of crosslinking, size, and composition. Additionally, reaction conditions may require a diluent (often a low molar mass polysiloxane, <10 kDa) due to the formation of a semi-solid which could slow or halt reaction progress. The broad heterogeneous nature of these mixtures presents numerous analytical challenges. Often, these systems include soluble and insoluble (gel) crosslinked polymer which are of high molar mass (>10^6 Da). Although size exclusion chromatography (SEC) has been optimized for broad polydispersity [7], branched or crosslinked polymers with high molar mass often elute non-ideally [7]–[9]. This non-ideal elution has been attributed to multiple factors, such as slalom chromatography, chain scissions,

and anchoring to pores of the SEC column [7]. The mechanisms of these non-ideal interactions are not completely understood but some of the non-ideal interactions may be explained by a decrease in the thermodynamic quality of the solvent, due to branching, which increases the interaction between the polymer and stationary phase [7].

This hinders the analysis of crosslinking through conformation or Mark-Houwink plots. Additionally, injection of gel material will clog a column, requiring its removal prior to analysis. Removal of gels is typically achieved by filtration and is known to result in loss of low molar mass material. This is likely due to membrane fouling which can lead to error in reported mass percent of gel content, as it is often reported as percent of mass lost after filtration. One other method of gel removal is sedimentation, a classic experiment for determination of molar mass distributions of polymers [10]. Macromolecules differentially sediment according to their physical properties like mass, size, density, and shape. Sedimentation is accelerated by utilizing equipment like ultracentrifugation devices. The Lamm equation is used to model the change in concentration over time with parameters like the diffusion coefficient, sedimentation coefficient, rotator angular velocity, and radial position [10], [11]. In the case of gel containing polymer formulations, separation has an added layer of complexity due to the heterogeneity of the system and presence of swollen networks. Separations by this method benefit from the lack of stationary phase but involved time consuming method development and limited detection schemes. Microgels are known to sediment more than 20 times the rate of linear and branched polymers and they may be quickly separated by ultracentrifugation [12].

As previously mentioned, analysis of soluble polymers by SEC is challenged by high molar mass in combination with the non-linear architecture. Field-flow fractionation (FFF) is an alternative technique with greater resolution than single column SEC for polymers whose mass is greater than 10^4 Da [13]. Similar to chromatography, separation is achieved by the differential elution of analytes in a column or channel, except that FFF is characterized by its open channel design and parabolic flow profile. Analytes are retained by the application of an external field perpendicular to the flow path, driving them towards an accumulation wall. In the case of thermal field-flow fractionation (ThFFF), the channel is comprised of two copper blocks separated by a thin polyimide spacer [13]. The field is a temperature gradient generated by heating the top block while cooling the bottom block. In the presence of a temperature gradient,

analytes generally migrate towards the cold block in a process known as thermophoresis. This flux is characterized by the thermal diffusion coefficient (D_T) and results in the concentrating of the analyte near the channel surface. Brownian motion, characterized by the translational diffusion coefficient (D), opposes this motion and their ratio is known as the Soret coefficient (S_T) [14]. Upon injection into the ThFFF channel, the analyte undergoes a relaxation process where equilibrium between the two fluxes is achieved, and an equilibrium cloud height is established. Under equilibrium conditions, retention can be equated to physiochemical properties related to the retaining field. In ThFFF, the parabolic flow is distorted by a temperature induced viscosity gradient and can be described by Equation 4.1 [14].

$$R = 6\lambda\left(\upsilon + (1 - 6\lambda\upsilon)\left[coth\frac{1}{2\lambda} - 2\lambda\right]\right), where\ \lambda = \frac{1}{S_T\Delta T} = \frac{D}{D_T\Delta T} \quad (4.1)$$

The precise relationship between retention time and S_T allows ThFFF to simultaneously separate and characterize a sample [15]–[18]. This has been leveraged to determine branching in polymers using a contraction factor based on S_T [19]–[21]. The open channel design combined with the ability to characterize branching allows for the total characterization of gel containing materials without a pre-analysis filtration step. However, this analysis depends on the accurate molar mass determination of the analyte at a given retention time. There are few publications on the analysis of gel containing polymer solutions for FFF [22], [23] and ThFFF [24]. In addition, the only reported D_T values in literature were for linear PDMS measured by thermal diffusion forced Rayleigh scattering (TDFRS) [25].

4.2.3 Objective of This Work

In this work, vinyl terminated polydimethylsiloxane (PDMS) was reacted with a copolymer of PDMS and poly(methylhydrosiloxane) (PHMS), ~5% statistical random addition of PHMS. Variation of the mole ratio of Si-H groups to vinyl chain ends yielded two differently crosslinked samples denoted as PDMSx1 and PDMSx2, where -x1 and -x2 refer to SiH:Vi of low and high, respectively. This reaction was conducted in a 200 cSt silicone oil diluent to prevent the rapid solidification of the mixture. This formulation, intended for commercial uses, is a polymer mixture with heterogeneities in size/mass (10^2-10^9 Da) and architecture. A polymer formulation containing multiple architectures, both insoluble gels and soluble microgels, as well as a diluent has never been studied by ThFFF. This sample set presented novel challenges in the

reproducibility and accuracy of molar mass determination via online detection (multi-angle light scattering and different refractometry). It is the goal of this study to assess the impact of sample preparation on the molar mass determination of PDMSx1 and PDMSx2, as well as their branching (or crosslinking) by *g"* analysis. Given the novelty of this application, the results were orthogonally validated by depolymerizing the samples and then analyzing the fragments by GC-MS.

4.3 Materials and Methods

4.3.1 Synthesis of Crosslinked Polysiloxane

Crosslinked polysiloxane was synthesized according to a patent [26] with various SiH:Vi ratios.

4.3.2 Removal of the Diluent Via Precipitation

The product formulations contained < 10% by weight crosslinked polysiloxane. Remaining mass was a 200 cSt polydimethylsiloxane diluent which contributed to the overloading behavior (see Figure 4.5**)** of the formulation. To remove the diluent, the formulation was first dissolved in toluene (10 mg/mL of crosslinked polysiloxane). HPLC grade methanol (Sigma Aldrich) was added dropwise, with constant stirring, in a ratio of 5:1. The 'solids' were collected via filtration, dried, and massed to determine the percent recovery, which was >99% for PDMSx1 and PDMSx2. All further sample preparation was performed using the recovered precipitate.

4.3.3 Removal of Insoluble Gels and Soluble Microgels (> 1 µm)

Insoluble gel materials were removed via three separate methods: filtration, ultracentrifugation, and ultracentrifugation followed by filtration. All filtration was performed with a 1.0 µm PTFE syringe filter (Whatman Puradisc, 13mm) and at a concentration of five $mgmL^{-1}$.

Ultracentrifugation was performed on a Beckman XL-70 centrifuge with a model SW 32ti rotor. All experiments were conducted at 250,000 G and concentration of 10 $mgmL^{-1}$. Two separate schemes involving ultracentrifugation were used to remove insoluble gels. The first was a 2-hour centrifugation followed by decanting the solution into a vial and collecting the gel into a separate vial. The solution was then filtered using a 1.0 µm PTFE syringe filter to remove large

soluble microgels and the gel was dried and massed. The second scheme was centrifugation for varied times (3, 6, and12 hours) and fraction collection via volumetric layers. A 6 mL volume of solution was separated into 3 – 2mL fractions by careful pipetting. Layer one refers to the first, or top, layer. Layers 2 and 3 are subsequent fractions. The remainder of the insoluble gel was collected, dried in an oven at 40 ^{o}C overnight, and massed.

4.3.4 Summary of Sample Preparation Steps

Three sample preparation schemes were devised to eliminate insoluble gel and soluble microgels whose size is greater than 1.0 µm. First, the polymer formulation is dissolved in toluene to form a stock solution. Methanol precipitation was then used to separate the diluent from the semi-solid product of the crosslinking reaction. These 'solids' were then dissolved again in toluene and processed by (1) filtration, (2) ultracentrifugation, and (3) ultracentrifugation followed by filtration (Figure 4.1).

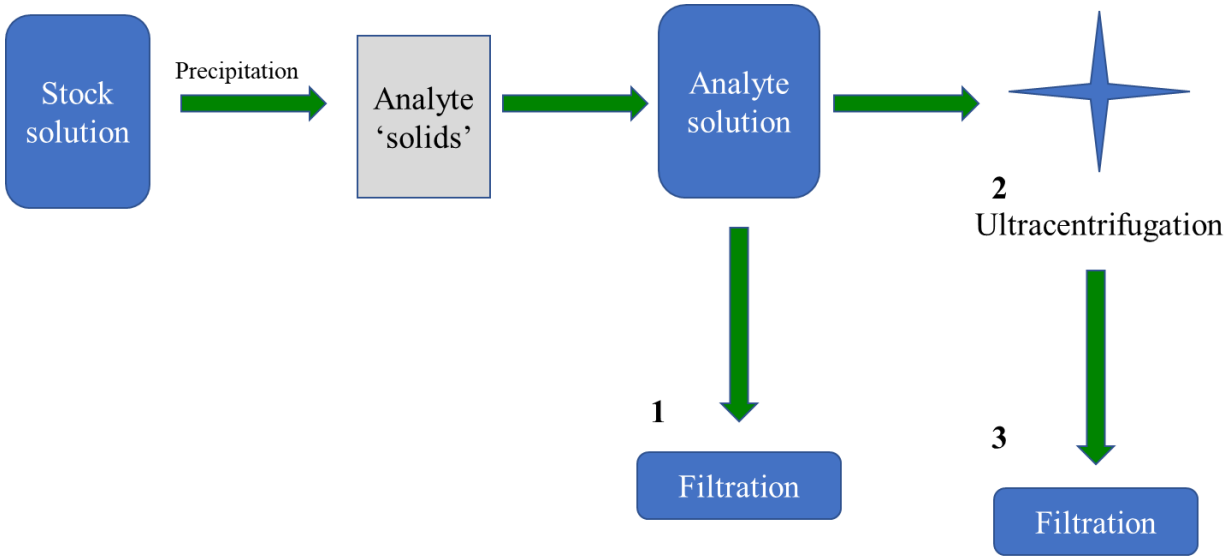

Figure 4.1. Sample preparation schemes for gel containing polymer formulation.

4.3.5 Thermal Field-Flow Fractionation (ThFFF) with Online Detection

Fractionation was conducted in a TF2000 Polymer Fractionator (Postnova Analytics, Salt Lake City, Utah) outfitted with a 20 µL sample loop and a stop-flow switching valve. The spacer was cut from 127 µm thick Kapton tape (Fralock, Valencia, California). HPLC grade toluene (Sigma Aldrich) was pumped through the channel at a flow rate of 0.2 mLmin^{-1}. The temperature difference between the hot and cold walls ranged from 80 to 95 °C with the cold wall temperature T_c varying between 25 and 30°C. A stop-flow time of 90 sec was incorporated for

reported data unless indicated otherwise. The on-line detectors were comprised of two instruments from Wyatt Technology Corporation (Santa Barbara, CA), a Dawn Heleos II multi-angle light scattering (MALS) instrument and an Optilab T-rEX differential refractometer (dRI). Data was collected and analyzed with ASTRA 7 software using a Berry second order fit for all MALS data.

4.3.6 Solvent Selection

Since there is no first principles theory which can be used to calculate the thermal diffusion coefficient of a polymer in a given solvent, choice of carrier fluid is often determined by a trial-and-error approach. Despite this, there is a predictive model of thermal diffusion which has shown promise for estimating D_T of organic soluble polymers [18], [27]. The model is based on the estimated temperature dependence of the Flory-Huggins interaction parameter and was calculated for PDMS using available Hansen solubility parameters (HSP) [28]. Two distinct experimental literature values for HSP of PDMS [28] were used to calculate two separate thermal diffusion coefficients using the updated methods outlined in the work by Geisler *et al.* and the results are summarized in Table 4.1. Toluene was chosen as the solvent for analysis due to its experimental D_T and its common use in the analysis of PDMS [29].

Table 4.1. Calculated D_T values for linear PDMS in various organic solvents as determined by methods outline in literature[18], [26].

Polymer	HSP Parameters [27]	Solvent	Experimental D_T x10^{-8} $cm^2s^{-1}K^{-1}$	Estimated D_T x10^{-8} $cm^2s^{-1}K^{-1}$	Percent Difference %
PDMS	HSP: 17, 2, 4	Ethylbenzene	2.28	0.018	-99
		Toluene	2.39	0.294	-88
		Cyclooctane	-1.22	1.07	-188
		Ethyl Acetate	2.57	1.64	-36
PDMS	HSP: 14, 1, 1	Ethylbenzene	2.28	0.593	-74
		Toluene	2.39	1.49	-38
		Cyclooctane	-1.22	2.40	-297
		Ethyl Acetate	2.57	4.39	71

4.3.7 Calculation of g”

The Soret contraction factor (*g”*) is the ratio of S_T for a branched polymer ($S_{T,br}$) to a linear S_T for a linear analogue ($S_{T,lin}$) of equivalent molar mass. $S_{T,br}$ is determined from the experimental retention time and Equation 4.1. Due to the hyperbolic cotangent, it is not possible

to analytically solve for λ and thus S_T. To approximate this value for a given retention ratio, solver methods were employed which can determine S_T to some arbitrary accuracy. Error in experimental determination of S_T is typically less than ±0.5% [14], thus error in solver was arbitrarily limited to less than 0.001%. S_T for the linear analog, vinyl terminated PDMS, and the crosslinked PDMS product was determined experimentally using Equation 4.1 with the Excel solver tool.

To approximate $S_{T,lin}$ at an arbitrary molar mass, a calibration curve relating S_T of the linear analog to molar mass was generated by the ThFFF-MALS-dRI analysis of vinyl terminated PDMS (DOWSIL SCV 128 Polymer). Triplicate analysis of the linear analog demonstrated low error in the determination of this relationship with an R^2 greater than 0.998 and an average RSD of approximately 1% (Figure 4.7). The molar mass range of the calibration curve spanned from 130 kDa to 1300 kDa.

4.3.8 Depolymerization and GC-MS of Crosslinked Polysiloxanes

The silicon-oxygen bond in the backbone of the polysiloxane chain was cleaved by a base catalyzed reaction in the presence of excess tetraethyl orthosilicate (TEOS, DOWSIL™ 200 Fluid 2 cSt). Approximately 100 mg of precipitated polysiloxane product with 0.1 g of n-octane as an internal standard, and 0.1 g of potassium hydroxide (Sigma Aldrich) was dissolved in 4 g of TEOS. The reaction vessel was purged with nitrogen, sealed, and heated at 120 °C for 1 hour. The base was neutralized by purging with CO_2 gas which resulted in the formation of a precipitate. After centrifuging the sample at 5000 RCF for 10 minutes, the samples were filtered and loaded in GC vials.

4.3.9 GC-MS of Depolymerization Products

Gas chromatography mass spectrometry analysis was carried out with an Agilent Technologies 7890B GC system paired with a 7693 Autosampler and 5977B MSD. A 30 m Rxi®-5sil MS column with Integra-Guard (Restek #13623-127) was used. The inlet temperature was held at 270 °C. The oven ramp began at 50 °C, held for 6 minutes, then increased to 200 °C at a rate of 8 °/minute. With no hold time, the oven was ramped to 300 °C at 30 °/minute and held for 5 minutes. The carrier gas was helium (constant, 1.5 $mLmin^{-1}$) and a split ratio of 150:1 to was used to demonstrate conditions without overloading, followed by a ratio of 20:1 to observe low concentration species. Spectra were analyzed with Agilent

MassHunter software and the peaks were plotted and integrated in Origin 9. This method was used to validate the depolymerization procedure by the analysis of five cSt PDMS and a series of silane standards with some of the expected depolymerization products: trimethyl ethoxy silane, vinyl dimethyl ethoxy silane, dimethyl diethoxy silane, vinyl methyl diethoxy silane, methyl triethoxy silane, and vinyl triethoxy silane – all acquired from Dow Chemical.

4.4 Results

The overloading behavior of this formulation resulted in irreproducible peak shape and unstable baselines which prevented the accurate determination of molar mass. Even after removal of the diluent, overloading persisted (Figure 4.6). Since architectural analysis by the Soret coefficient is dependent on accurate molar mass results, an investigation into the impact of sample preparation was necessary. Preparation by filtration, ultracentrifugation, and ultracentrifugation followed by filtration resulted in varied molar mass results and determination of insoluble gel content. An analysis of the impact of these methods on molar mass as well as the architectural traits as determined by g'' can be found in the following sections.

4.4.1 Gravimetric Determination of Insoluble Gel Content

The mass recovery was calculated for each sample preparation process and the mass lost was determined to be the amount of insoluble gel content removed, summary in Table 4.2. Method 3, ultracentrifugation followed by filtration, removed the least amount of gel content for both formulations. Ultracentrifugation alone resulted in a greater mass loss for PDMSx1 but not for PDMSx2.

4.4.2 ThFFF-MALS-dRI Fractograms of Ultracentrifugation Layer Fractions

Ultracentrifugation times of 3, 6, and 12 hours were study. An ultracentrifugation run time of 12 hours yielded a layer one fraction whose molar mass was similar to the linear starting materials. A comparison of layer 1 fractions for each run time can be seen in Figure 4.8, the remainder of the ultracentrifugation data presented herein is for a 12-hour run time. Figure 4.2 is an overlayed fractogram of PDMSx1 prepared by ultracentrifugation. From layer 1 to 3 there is an increase in concentration, molar mass, and size due to the nature of the ultracentrifugation separation mechanism.

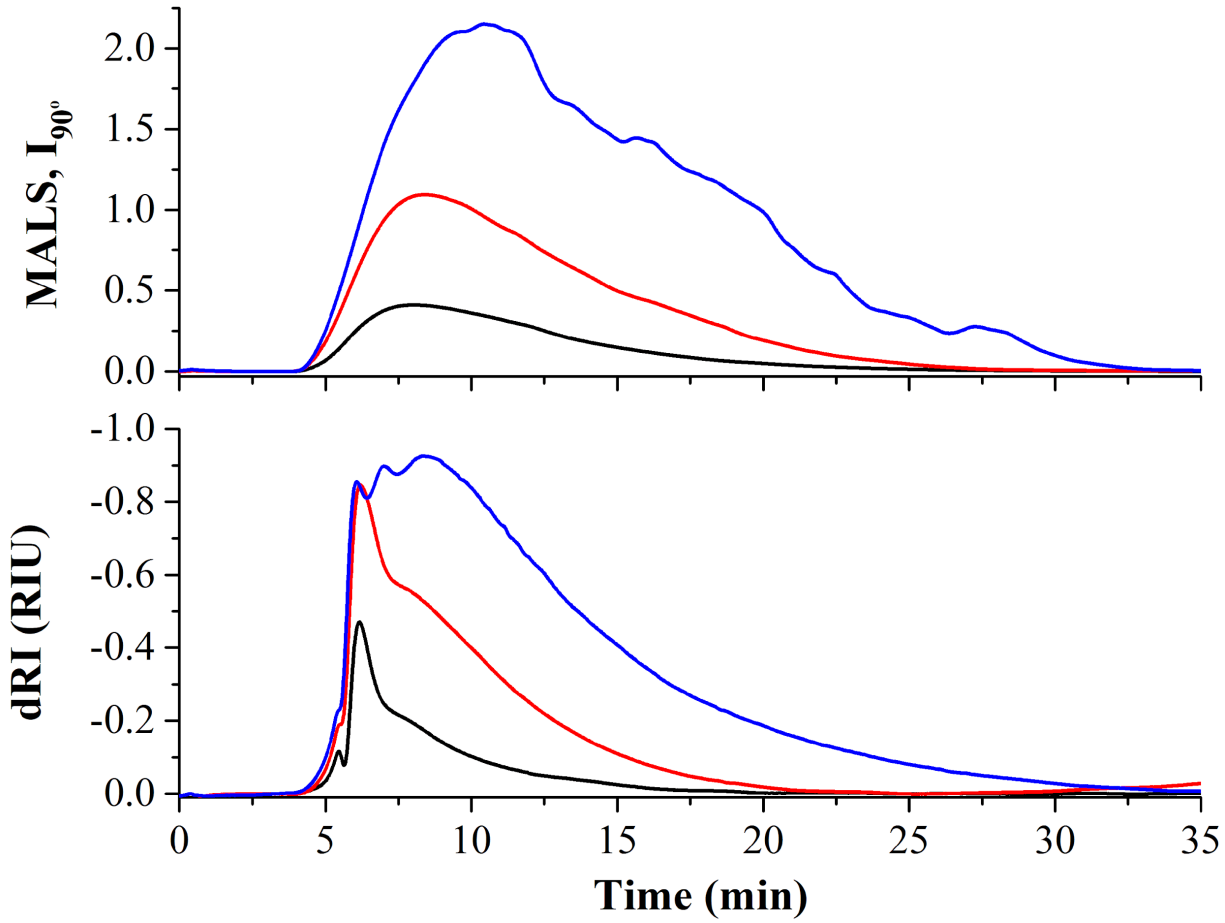

Figure 4.2. MALS (upper) and dRI (lower) fractograms of PDMSx1 fractionated by ultracentrifugation into three volumetric layers. Layer one is in black, layer two in red, and layer three in blue.

4.4.3 Light Scattering Results from Filtered Samples

Filtration was used in schemes one and three, where in scheme three the sample was first processed by ultracentrifugation for two hours and then filtered. Fractograms and light scattering results for these preparation methods are shown in Figure 4.3.

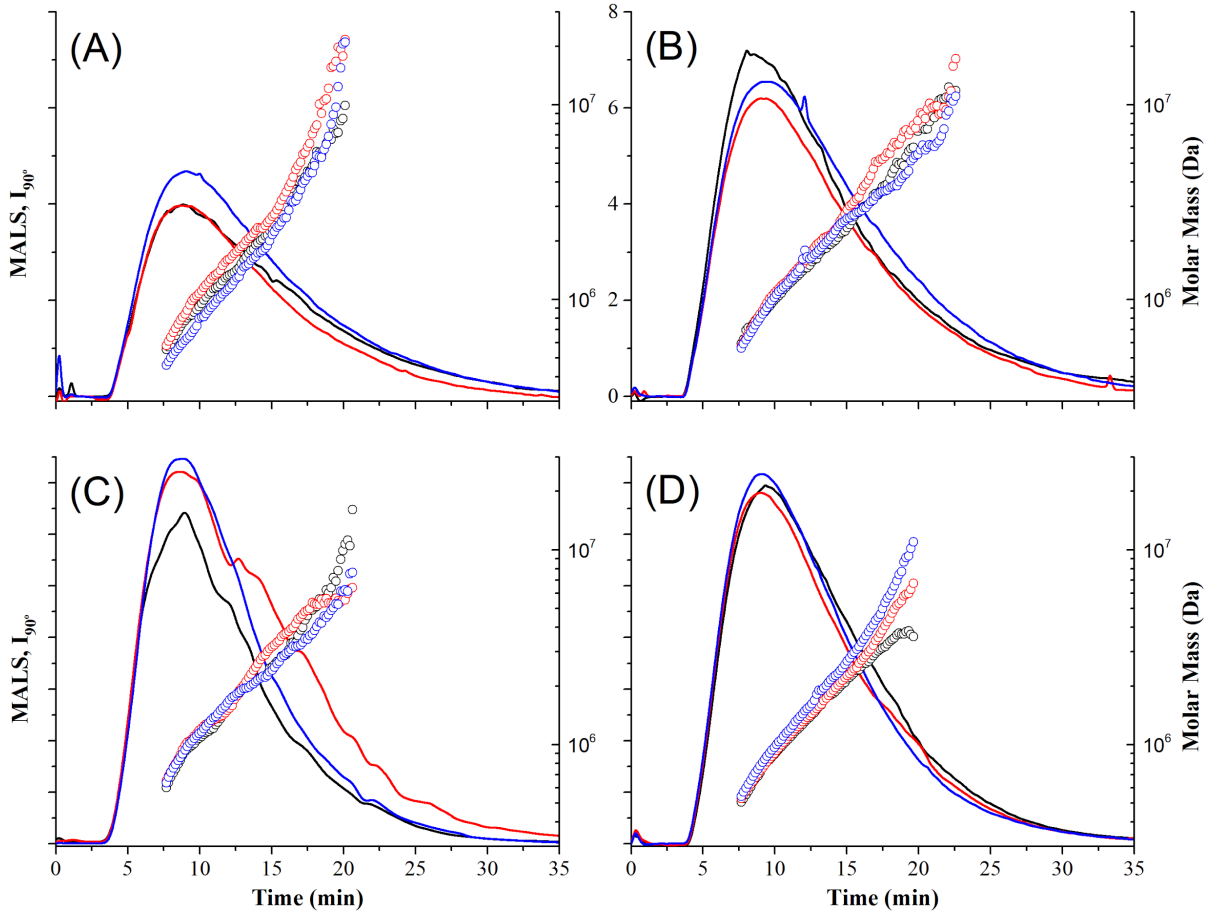

Figure 4.3. Fractograms with molar mass and root mean square radii results for filtered PDMSx1 (A), filtered PDMSx2 (C), ultracentrifuged and filtered PDMSx1 (B), and ultracentrifuged and filtered PDMSx2 (D).

4.4.4 Summary of ThFFF-MALS-dRI Results for Each Sample Preparation Method

A summary of the molar mass, root mean square (RMS) radii, and percent insoluble gel content can be found in Table 4.2. The molar mass of PDMSx1 and PDMSx2 were not significantly different when prepared by filtration alone. Ultracentrifugation followed by filtration yields molar mass results which are significantly different. In general, percent insoluble gel content and polydispersity is greater for PDMSx2 regardless of sample preparation method. Ultracentrifugation fraction layers generally increased in molar mass, RMS, and polydispersity. In comparison to filtration methods, layers 2 and 3 exhibited significantly larger molar masses for both formulations.

Table 4.2. Molar mass and gel content results for PDMSx1 and PDMSx2.

Process	Sample	Mw (kDa)	Mn (kDa)	Đ	Insoluble Gel (%)
Unfiltered	PDMSx1	-	-	-	-
	PDMSx2	31470 ± 2614	2005 ± 347	16.1 ± 4.1	-
Filtered (1.0 µm)	PDMSx1	1578 ± 163	1186 ± 76	1.3 ± 0.1	12
	PDMSx2	1407 ± 198	982 ± 137	1.4 ± 0.2	58
Ultracentrifuged and filtered	PDMSx1	1308 ± 68	975 ± 24	1.3 ± 0.1	8
	PDMSx2	1658 ± 85	1124 ± 21	1.5 ± 0.1	28
Ultracentrifugation Layer 1	PDMSx1	738 ± 46	608 ± 13	1.2 ± 0.1	36
	PDMSx2	1214 ± 203	821 ± 80	1.5 ± 0.4	44
Ultracentrifugation Layer 2	PDMSx1	3325 ± 110	1809 ± 29	1.8 ± 0.1	-
	PDMSx2	2158 ± 86	1273 ± 28	1.7 ± 0.1	-
Ultracentrifugation Layer 3	PDMSx1	13341 ± 1702	3543 ± 544	3.8 ± 0.8	-
	PDMSx2	4224 ± 697	1427 ± 59	3.0 ± 0.5	-

4.4.5 Thermal Diffusion Coefficient of Linear and Crosslinked PDMS

The thermal diffusion coefficients of vinyl terminated linear PDMS and PDMSx2 were determined using Equation 4.1 and the diffusion coefficient determined from batch experiments. D_T values determined from stop-flow and experiments without stop-flow are reported in Table 4.3. The value for PDMS-Vi with a 90 s stop-flow is similar to a literature value of 2.38 x10^{-8} $cm^2s^{-1}K^{-1}$ for linear PDMS in toluene, as determined by TDFRS [30].

Table 4.3. Thermal diffusion coefficients for linear PDMS and PDMSx2.

Sample	Stop-flow (s)	$D_{T,exp}$ (x 10^8) $cm^2s^{-1}K^{-1}$
PDMS-Vi	0	3.77 ± 0.11
PDMS-Vi	90	2.50 ± 0.03
PDMSx2	0	1.56 ± 0.01
PDMSx2	90	1.20 ± 0.01

4.4.6 Soret Contraction Factor (g")

The log of the Soret contraction factor (*g"*) for PDMSx1 and PDMSx2 was calculated across the range of reported molar masses and processed into a histogram, Table 4.4. An increase in contraction (decrease in log *g"*) is observed across the chromatogram, which coincides with an increase in mass corresponding to the crosslinking of chains. The histogram for PDMSx1 and PDMSx2 clearly shows a difference in contraction, or crosslinking, between the two formulations where PDMSx1 shows a maximum log g" of -0.5 while PDMSx2 stretches to -1.0.

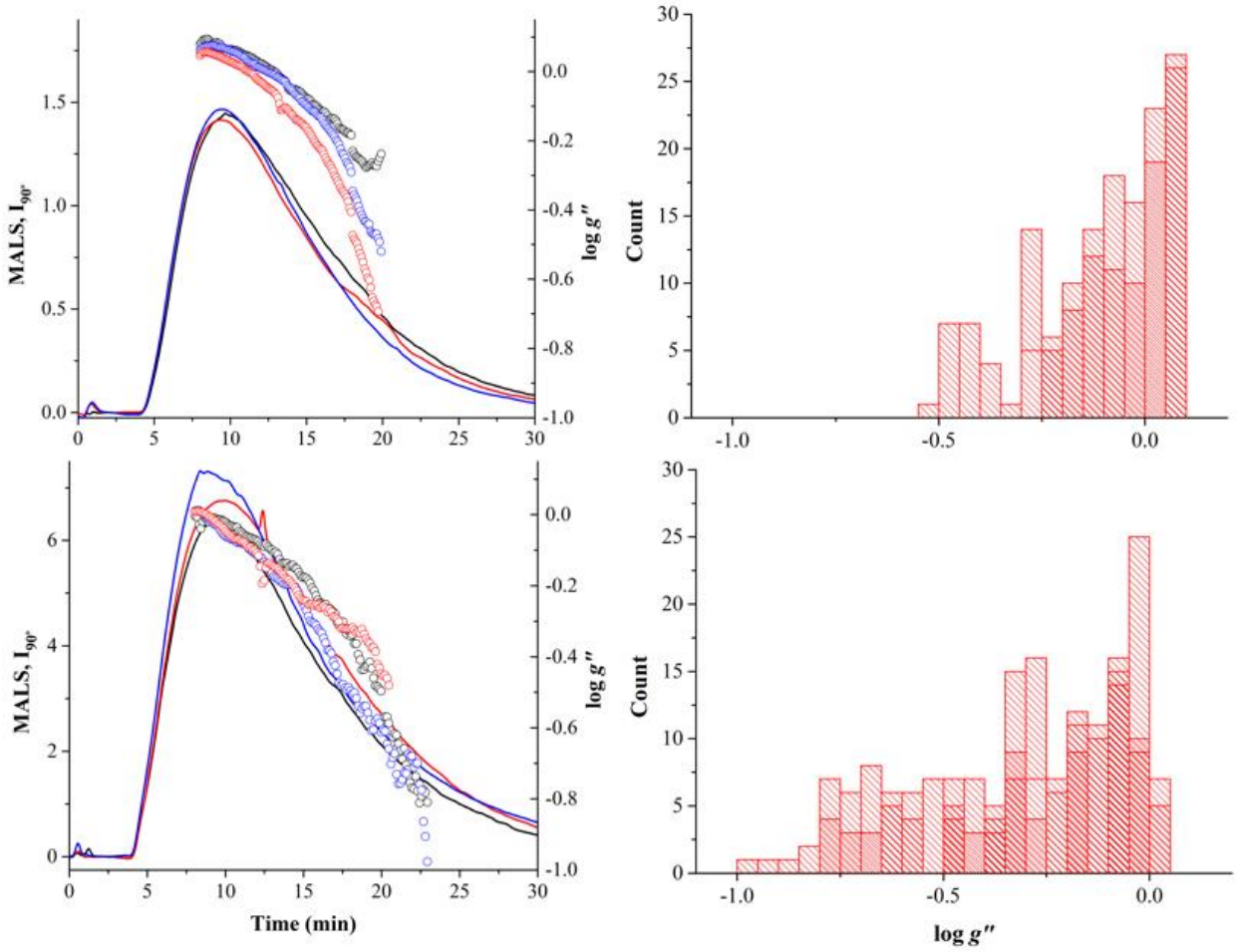

Figure 4.4. Plots of triplicate chromatograms with the MALS intensity at 90° and log g" for PDMSx1 (top) and PDMSx2 (bottom) with their corresponding histograms on the right.

4.4.7 Semi-Quantitative Gas Chromatography (GC-MS)

In order to orthogonally validate *g''* results, relative degree of branching in PDMSx1 and PDMSx2 may be assessed by depolymerizing the sample and comparing the relative amount of ethylene linkage fragments via GC-MS. The peak associated with the ethylene linkage was observed at 16.85 minutes and its area was normalized to the internal standard, n-octane. Principle mass fragments at 103.0, 133.0, 191.1, and 249.1 m/z were characteristic for the ethylene linkage and the peak was not present in the depolymerization products of linear PDMS. The area of the n-octane peak, ethylene linkage peak, and subsequent normalized area for PDMSx1 and PDMSx2 is reported in Table 4.4.

Table 4.4. Peak area of relevant GC-MS peaks and the normalized area of the ethylene linkage.

Sample	Peak area of n-octane	Peak area of ethylene linkage	Ethylene linkage normal peak area ($x10^2$)	RSD %
PDMSx1	8.98E+06	1.08E+05	1.20	6
PDMSx2	7.86E+06	1.21E+05	1.54	4

4.5 Discussion

In ThFFF method development, it is important to determine the overloading concentration of an analyte so that separation occurs under ideal conditions. Injection of the formulation, at typical concentrations for polymers (~2.0 $mgmL^{-1}$), resulted in light scattering with jagged features and poor reproducibility. This is due to the presence of the diluent, which is the majority component by mass (>94%). Precipitation resulted in a semi-solid material, which again exhibited overloading behavior at concentrations which were too low (<0.25 $mgmL^{-1}$) for accurate molar mass determination. While the light scattering traces showed poor reproducibility with jagged features, molar mass and root mean square radii as measured by online MALS-dRI exhibited good triplicate standard deviation (<8.5%) for a crosslinked polymer.

Insoluble gel particles are known to clog SEC columns, thus are typically removed by filtration prior to injection. While it is possible to analyze these materials in FFF without additional sample preparation, it was observed that tubing smaller than 0.01” in diameter clogged after several injections. This resulted in unstable system pressure and dRI baseline. Removal of the gel material from the sample by syringe filtration is known to result in the unintended loss of lower molar mass components. To study the impact of sample preparation on molar mass results (a key component in *g”* analysis), three different schemes were devised to remove insoluble gels prior to ThFFF analysis: filtration, ultracentrifugation, and ultracentrifugation followed by filtration.

4.5.1 Removal of Insoluble Gel Content

A standard practice in liquid chromatography is to filter samples prior to injection. This is often achieved by use of a syringe filter whose pore size permits the analyte to pass through the filter. In FFF, the crossover point for normal mode and steric mode separations is typically around one µm, thus a syringe filter with this pore size was selected. Qualitatively, it was observed that PDMSx2 more quickly clogged the pores of the filter than PDMSx1. An expected

result since an increase in crosslinking was expected for a larger SiH:Vi ratio. However, due to the high standard deviation in molar mass results the two samples did not have distinguishable differences in molar mass or Đ. In contrast, the percentage gel content between to the two samples is different by greater than a factor of four. Syringe filtration yielded the largest difference in gel content between PDMSx1 and PDMSx2. Gel content by ultracentrifugation alone yielded more similar values. Ultracentrifugation pushes all analytes, which are not buoyant relevant to the solvent, to the bottom of the vessel. This mechanism of separation may have trapped non-gel material in the 'solid' layer – resulting in similar determined gel content for extended centrifugation times.

4.5.2 Comparison of Molar Mass Results for PDMSx1 and PDMSx2

In the solvent selection process, it is ideal to choose a solvent which yields good retention ($R < 0.6$) at low field strength. This is reflected in the thermal diffusion coefficient, where a value greater than 1.0×10^{-7} $cm^2 s^{-1} K^{-1}$ will result in the retention of polymer with mass on the order of 10^4 Da under typical operating conditions. No such solvent condition was available for PDMS and thus polymers whose mass was less than 300 kDa were unretained in the void peak. Given that the Mw of the crosslinker, vinyl terminated PDMS, was 650 kDa, the low retention was considered to have a small impact on analysis of the crosslinked species whose mass is expected to be greater than the retention threshold. However, all reported values for Đ will be systematically lower than the true value since low molar mass species will elute in the void peak and will not be analyzed by MALS.

PDMSx2 was analyzed prior to removal of gel content resulting in molar masses greater than 30,000 kDa. Due to the impact of clogged tubing in the ThFFF-MALS-dRI system, PDMSx1 was not measured without additional sample preparation. Samples prepared by ultracentrifugation followed by filtration and filtration alone showed a greater molar mass for PDMSx2. However, by filtration alone M_w, M_n, and Đ were not significantly different. This may be a result of the decreased precision in molar mass for samples prepared by filtration. PDMSx2 was expected to have a greater amount of crosslinking and thus molar mass. It is also reasonable to expect an increase in dispersity due to the creation of networks with relatively large mass.

The molar mass results of sample prepared by ultracentrifugation alone did not follow the expected profile. In layer one, PDMSx1 exhibited a molar mass similar to the crosslinker,

indicating a signification portion of material with a low degree of crosslinking. PDMSx2 exhibited a significantly larger molar mass in layer one. The opposite was observed in layers 2 and 3, where PDMSx1 showed a greater molar mass than PDMSx2. This may reflect a change in the molar mass distribution of the material as a result of an increase in insoluble gel material which is removed by sample preparation.

4.5.3 Linear Calibration of S_T

Determination of *g''* is facilitated by a calibration curve relating molar mass to S_T. The crosslinking process by nature increases the average molar mass of the system significantly as observed by the molar mass results of the minimally processed sample. Given the broad molar mass range of the analyte, it is prohibitive to find a linear analog which spans the full range of analyzed masses. In this system, the crosslinker was used as a linear analog due to its similarity in chemistry to the crosslinked system and molar mass range (10^4-10^6 Da).

It has been recently reported in literature [19], [31] and my own work in Chapter 3, that polymer architecture may influence its thermal diffusion coefficient. Generally, branching results in a contraction in size-based properties such as *D*. This contraction then causes a coelution of species with increasingly disparate mass to size relationships. Likewise, the decrease in D_T of the branched relative to the linear exacerbates this effect resulting in an even greater contraction in *g''* and coelution of linear and crosslinked species. This was an unavoidable effect as toluene was the only suitable solvent for this analysis.

4.5.4 Soret Contraction Factor Analysis

The Soret contraction factor is a mass-based property and thus molar mass data representative of the sample and capable of distinguishing between other samples is crucial for accurate analysis. Due to this, all samples analyzed by the *g''* were prepared by ultracentrifugation followed by filtration. Both the range and average of *g''* were greater for PDMSx2 indicating an increase in overall crosslinking. This matches the expectation and shows the expected relationship between the SiH:Vi ratio, molar mass, and contraction (or branching). In combination with the percent of gel content in the sample, branching of industrial formulation can be fully characterized by ThFFF-MALS-dRI.

4.5.5 Validation of g" by GC-MS

The Soret contraction factor has now been utilized to study bottlebrushes, short and long chain branching in polyethylene, stars, pom-poms, and hyperbranched polyesters. Each of these studies have relied upon model systems which preclude the need for an orthogonal method to validate *g"* results. Analysis of depolymerized PDMSx1 and PDMSx2 yielded a relative amount of tri-functional chain sites (or branch points). Since this is a bulk average of the material, it is directly comparable to the number average *g"*. As the number of branch points as determined by GC-MS increases the log *g"* for the sample decreases, showing a general agreement between the two methods.

4.6 Conclusion

An industrial formulation which spans seven orders of magnitude in molar mass posed unique challenges to branching analysis via ThFFF. In contrast to AF4, the solid accumulation wall resulted in the retention of the diluent which contributed significantly to the overloading behavior of the sample. In addition, insoluble gel material clogged tubing and destabilized dRI baselines. This resulted in the need for additional sample preparation, an atypical step in ThFFF analysis. Removal of insoluble gels by syringe filtration resulted in molar masses which were insignificantly different for the two formulations. Ultracentrifugation followed by filtration yielded molar masses which were significantly different. A comparison of *g"* for the two formulations showed the expected result that an increase in the SiH:Vi ratio during synthesis increased the overall degree of crosslinking. These results were validated by depolymerization of the crosslinked materials followed by GC-MS to semi-quantify the number of tri-functional sites (branch points) in each formulation.

4.7 Supplemental Information

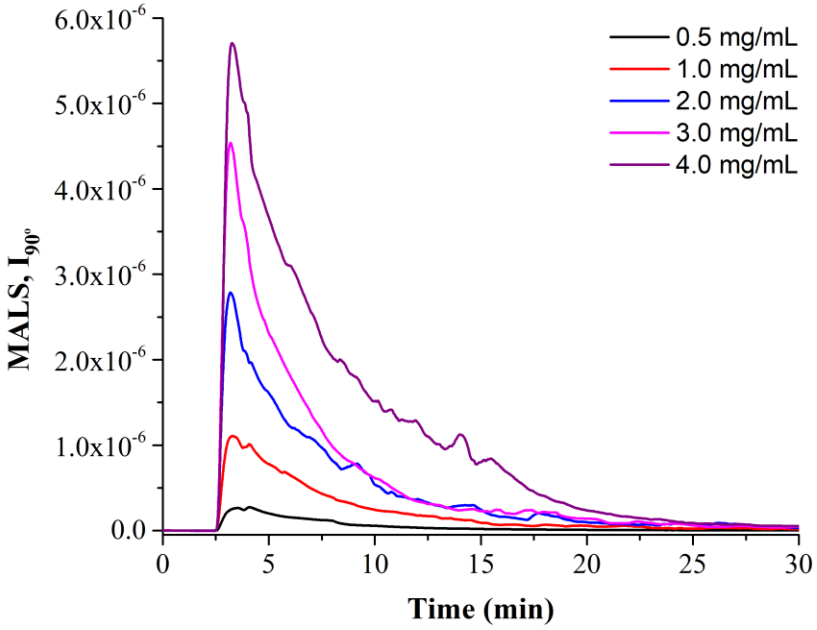

Figure 4.5. Overloading behavior of PMDSx2 as a function of concentration before removal of the diluent.

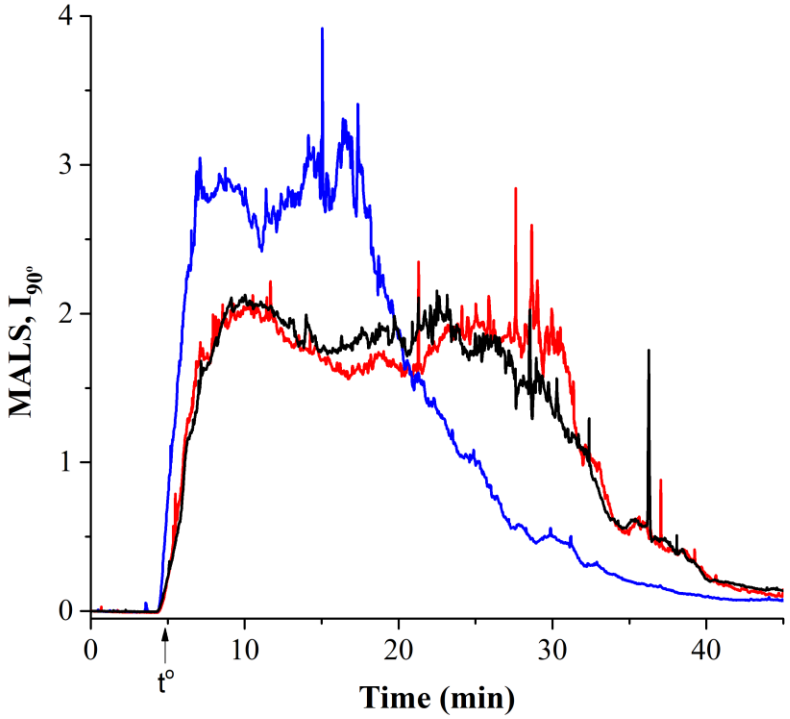

Figure 4.6. A fractogram, where the Y-axis is the MALS intensity at 90°, of replicate injections of PDMSx2 at a concentration of 2 mgmL^{-1}. These samples were injected after the diluent was removed and with no further preparation.

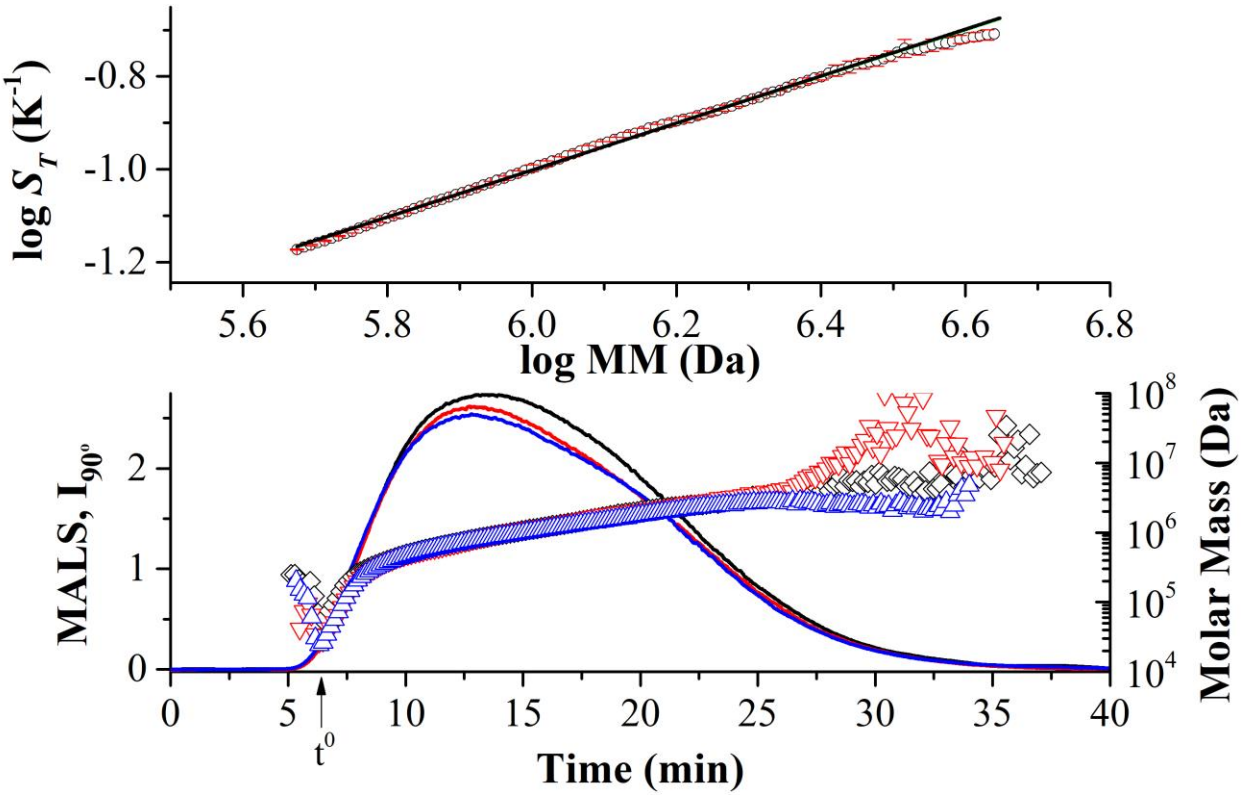

Figure 4.7. The bottom plot is a fractogram of triplicate injections of the linear analog, vinyl terminated PDMS, with molar mass (MM) plotted in a log scale. Using Equation 4.1, this data was processed into a log-log plot (top) relating molar mass to S_T.

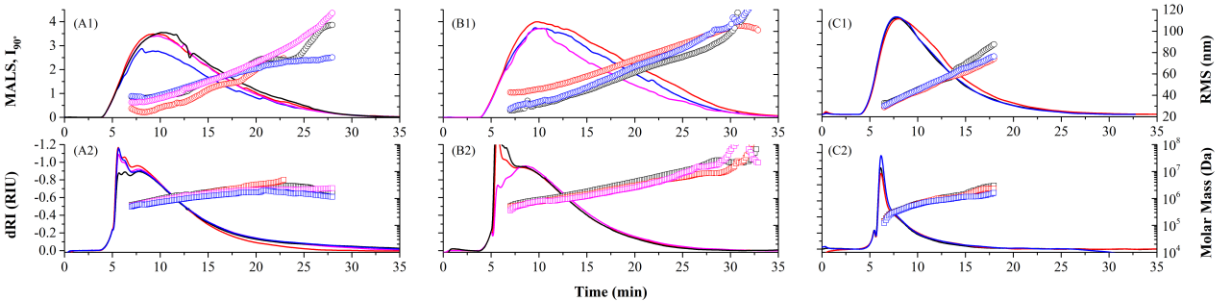

Figure 4.8. Triplicate fractograms of PDMSx2 layer one fractions from ultracentrifugation carried out for different times: (A) 3 hours, (B) 6 hours, and (C) 12 hours. Results displaying RMS (A1-C1) are accompanied by the MALS trace and results displaying molar mass (A2-C2) are accompanied by the dRI trace.

4.8 References

[1] S. Podzimek and C. Johann, "Asymmetric Flow Field-Flow Fractionation: Current Status, Possibilities, Analytical Limitations and Future Trends," *Chromatographia*, vol. 84, no. 6, pp. 531–534, Jun. 2021, doi: 10.1007/s10337-021-04035-w.

[2] F. Abbasi, H. Mirzadeh, and A. A. Katbab, “Modification of polysiloxane polymers for biomedical applications: A review,” *Polym Int*, vol. 50, no. 12, pp. 1279–1287, 2001, doi: 10.1002/pi.783.

[3] J. J. Chruściel and E. Leśniak, “Modification of epoxy resins with functional silanes, polysiloxanes, silsesquioxanes, silica and silicates,” *Prog Polym Sci*, vol. 14, pp. 67–121, 2015, doi: 10.1016/j.progpolymsci.2014.08.001.

[4] E. A. Grushevenko, I. L. Borisov, and A. v. Volkov, “High-Selectivity Polysiloxane Membranes for Gases and Liquids Separation (A Review),” *Petroleum Chemistry*, vol. 61, no. 9, pp. 959–976, 2021, doi: 10.1134/S0965544121090103.

[5] “J of Applied Polymer Sci - 2014 - Mu - Synthesis and effects of MDT silicone resin on PMPS-based ablative composites.pdf.”

[6] I. B. Meshkov, A. A. Kalinina, V. v. Kazakova, and A. I. Demchenko, “Densely Cross-Linked Polysiloxane Nanogels,” *INEOS OPEN*, vol. 3, Nov. 2020, doi: 10.32931/io2022r.

[7] S. Podzimek, “Comparative Study of SEC and AF4 in the Characterization of Organic Soluble Synthetic Polymers,” *Chromatographia*, vol. 85, no. 12, pp. 1097–1105, Dec. 2022, doi: 10.1007/s10337-022-04217-0.

[8] A. C. Makan, T. Otte, and H. Pasch, “Analysis of High Molar Mass Branched Polybutadienes by SEC-MALLS and AF4-MALLS,” *Macromolecules*, vol. 45, no. 12, pp. 5247–5259, Jun. 2012, doi: 10.1021/ma3007812.

[9] S. Podzimek and T. Vlcek, “Characterization of branched polymers by SEC coupled with a multiangle light scattering detector. II. Data processing and interpretation,” *J Appl Polym Sci*, vol. 82, no. 2, pp. 454–460, Oct. 2001, doi: 10.1002/app.1871.

[10] K. L. Planken and H. Cölfen, “Analytical ultracentrifugation of colloids,” *Nanoscale*, vol. 2, no. 10. pp. 1849–1869, Oct. 2010. doi: 10.1039/c0nr00215a.

[11] I. Perevyazko, A. S. Gubarev, and G. M. Pavlov, “Analytical ultracentrifugation and combined molecular hydrodynamic approaches for polymer characterization,” in *Molecular Characterization of Polymers*, Elsevier, 2021, pp. 223–259. doi: 10.1016/b978-0-12-819768-4.00003-8.

[12] V. E. Shashoua and R. G. Beaman, “Microgel: An idealized polymer molecule,” *Journal of Polymer Science*, vol. 33, no. 126, pp. 101–117, Dec. 1958, doi: 10.1002/pol.1958.1203312611.

[13] M. Toney, L. Baiamonte, W. C. Smith, S. Kim Ratanathanwongs Williams, S. Kim Ratanathanawongs Williams, and S. K. R. Williams, “Field-flow fractionation techniques for polymer characterization,” in *Molecular Characterization of Polymers*, Elsevier, 2021, pp. 129–171. doi: 10.1016/B978-0-12-819768-4.00004-X.

[14] M. E. Schimpf, K. Caldwell, and J. C. Giddings, *Field-Flow Fractionation Handbook*. John Wiley & Sons, 2000.

[15] G. Greyling and H. Pasch, *Thermal Field-Flow Fractionation of Polymers*. Cham: Springer International Publishing, 2019. doi: 10.1007/978-3-030-10650-8.

[16] G. Greyling and H. Pasch, “Fractionation of poly(methacrylic acid) and poly(vinyl pyridine) in aqueous and organic mobile phases by multidetector thermal field-flow fractionation,” *J Chromatogr A*, vol. 1512, pp. 115–123, 2017, doi: 10.1016/j.chroma.2017.07.016.

[17] C. A. Ponyik, D. T. Wu, and S. K. R. Williams, “Separation and composition distribution determination of triblock copolymers by thermal field-flow fractionation,” *Anal Bioanal Chem*, vol. 405, no. 28, pp. 9033–9040, Nov. 2013, doi: 10.1007/s00216-013-7282-6.

[18] M. Geisler, L. Plüschke, J. Merna, and A. Lederer, “The Role of Solubility in Thermal Field-Flow Fractionation: A Revisited Theoretical Approach for Tuning the Separation of Chain Walking Polymerized Polyethylene,” *Anal Chem*, vol. 92, no. 21, pp. 14822–14829, Nov. 2020, doi: 10.1021/acs.analchem.0c03686.

[19] M. Geisler *et al.*, “Topology Analysis of Chain Walking Polymerized Polyethylene: An Alternative Approach for the Branching Characterization by Thermal FFF,” *Macromolecules*, vol. 52, no. 22, pp. 8662–8671, Nov. 2019, doi: 10.1021/acs.macromol.9b01410.

[20] W. C. Smith, M. Geisler, A. Lederer, and S. K. R. Williams, “Thermal Field-Flow Fractionation for Characterization of Architecture in Hyperbranched Aromatic-Aliphatic Polyesters with Controlled Branching,” *Anal Chem*, vol. 91, no. 19, pp. 12344–12351, Oct. 2019, doi: 10.1021/acs.analchem.9b02664.

[21] J. Ray. Runyon and S. K. R. K. R. Williams, “Thermal Field-Flow Fractionation of Polymers with High Molecular Weight and Complex Architecture,” Colorado School of Mines, Golden, 2009.

[22] C. Fuentes, J. Castillo, J. Vila, and L. Nilsson, “Application of asymmetric flow field-flow fractionation (AF4) and multiangle light scattering (MALS) for the evaluation of changes in the product molar mass during PVP-b-PAMPS synthesis,” *Anal Bioanal Chem*, vol. 410, no. 16, pp. 3757–3767, Jun. 2018, doi: 10.1007/s00216-018-1039-1.

[23] S. Dubascoux *et al.*, “Comparative study of the mesostructure of natural and synthetic polyisoprene by size exclusion chromatography-multi-angle light scattering and asymmetrical flow field flow fractionation-multi-angle light scattering,” *J Chromatogr A*, vol. 1224, pp. 27–34, Feb. 2012, doi: 10.1016/j.chroma.2011.12.010.

[24] D. Lee and S. K. R. Williams, “Thermal field-flow fractionation and multiangle light scattering of polyvinyl acetate with broad polydispersity and ultrahigh molecular weight microgel components,” *J Chromatogr A*, vol. 1217, no. 10, pp. 1667–1673, 2010, doi: 10.1016/j.chroma.2010.01.035.

[25] J. Rauch and W. Köhler, “On the molar mass dependence of the thermal diffusion coefficient of polymer solutions,” *Macromolecules*, vol. 38, no. 9, pp. 3571–3573, 2005, doi: 10.1021/ma050231w.

[26] P. J. Fryfogle, D. A. Kadlec, K. T. Nguyen, and R. C. Thomas, “Pituitous silicone fluid,” 08-Jan-2017.

[27] E. P. C. Mes, W. Th. Kok, and R. Tijssen, “Prediction of Polymer Thermal Diffusion Coefficients from Polymer-Solvent Interaction Parameters: Comparison with Thermal Field Flow Fractionation and Thermal Diffusion Forced Rayleigh Scattering Experiments,” *International Journal of Polymer Analysis and Characterization*, vol. 8, no. 2, pp. 133–153, Jan. 2003, doi: 10.1080/10236660304888.

[28] C. M. Hansen, “Hansen Solubility Parameters: A User’s Handbook,” *Hansen Solubility Parameters: A Users Handbook, Second Edition*, pp. 113–123, Jan. 2007, doi: 10.1201/9781420006834/HANSEN-SOLUBILITY-PARAMETERS-CHARLES-HANSEN.

[29] W. Chassé, M. Lang, J. U. Sommer, and K. Saalwächter, “Cross-link density estimation of PDMS networks with precise consideration of networks defects,” *Macromolecules*, vol. 45, no. 2, pp. 899–912, 2012, doi: 10.1021/ma202030z.

[30] D. Stadelmaier and W. Köhler, “Thermal diffusion of dilute polymer solutions: The role of chain flexibility and the effective segment size,” *Macromolecules*, vol. 42, no. 22, pp. 9147–9152, 2009, doi: 10.1021/ma901794k.

[31] G. Greyling and H. Pasch, “Tacticity Separation of Poly(methyl methacrylate) by Multidetector Thermal Field-Flow Fractionation,” *Anal Chem*, vol. 87, no. 5, pp. 3011–3018, Mar. 2015, doi: 10.1021/ac504651p.

CHAPTER 5
THE ROLE OF CHAIN DYNAMICS IN THERMAL DIFFUSION

5.1 Abstract

Thermophoresis of polymers in solution is a poorly understood phenomenon and thus method development for separation techniques like thermal field-flow fractionation are done by a trial-and-error approach. Novel insights into the relationship between thermal diffusion and the physiochemical properties of a polymer could lead to improvements in predictive models or the development of a first principles theory. This communication reports an experimentally observed relationship between the thermal diffusion coefficient (D_T) and glass transition temperature (T_g) in polymers across a series of organic solvents. The correlation between these properties is further extended by the locally correlated lattice model of polymers which relates the segmental entropy of a polymer to T_g, and thus D_T. While the leading predictive model of thermal diffusion accurately predicts D_T for many polymer-solvent systems, error is still sometimes large (up to 200%). This model relies primarily on enthalpic forces and may be further improved by the consideration of entropic forces.

5.2 Introduction

Thermophoresis is a transport phenomenon which occurs in the presence of a temperature gradient. First described by Ludwig, and later in detail by Soret, this process was known to result in the differential separation of diffusing species in liquid or gas phase. In this description of thermophoresis, the concentrating force of thermal diffusion is opposed by dispersive Fickian diffusion and the ratio of these two fluxes known as the Soret coefficient. The sign of S_T indicates the directionality of the overall flux where a positive S_T is assigned for species which migrate to the cold wall and a negative for those which migrate to the hot wall. Generally, it has been observed that macromolecules tend to have a positive S_T, although there may be size and environmental dependencies on the sign [1], [2]. A first principles theory of thermal diffusion in the gas phase has been developed by Chapman [3]. Despite this success, no such theory has been developed for thermophoresis in solution [4]–[8]. While the mechanism of thermophoresis macromolecules is not well understood, it has been leveraged to purify silicon wafers and characterize a variety of nanoscale materials [9]–[12]. This transport process is characterized by

the thermal diffusion coefficient (D_T) and when it is multiplied by the temperature gradient returns the overall flux in the units of cm^2s^{-1}. Typical values for D_T of polymers and colloids are on the order of those observed in Brownian motion for particles of their respective size, 10^{-9} to 10^{-7} $cm^2K^{-1}s^{-1}$ [13], [14]. Colloidal and polymer thermal diffusion have shown different dependencies on physiochemical properties and thus have often been treated differently in the development of predictive models [4], [5], [7], [14]–[18]. For the purposes of this communication, only polymer thermal diffusion will be considered with an emphasis on organic solvent polymers as they have the largest available data set [8], [13].

5.2.1 Polymer Thermal Diffusion

Thermal diffusion coefficients are typically measured by thermal field-flow fractionation (ThFFF) or thermal diffusion forced Rayleigh scattering (TDFRS). ThFFF is a separation technique where the retention time of an analyte is directly related to S_T and thus D_T can be calculated if D is measured or known. TDFRS is typically a two-laser technique where the concentration gradient induced by thermal diffusion is optically observed. Literature values for D_T of polymers in solution determined by these two methods typically agree, however, TDFRS is better suited for the analysis of small molecules which cannot be sufficiently retained in ThFFF due to instrumental limitations. It is through TDFRS measurements that the molar mass dependence of D_T was observed. This dependence was shown to plateau around one kDa [1], [19], [20] and all polymers with mass greater than 10 kDa have shown a D_T which is not mass dependent [8]. In addition to a mass dependency, thermal diffusion of polymers is known to vary significantly with choice of solvent [8]. The D_T of polystyrene ranges from an apparent zero due to lack of retention in ThFFF to 1.7 $cm^2K^{-1}s^{-1}$ depending on which solvent or mixture of solvents are utilized. Due to the wide variance in D_T, and thus retention in ThFFF, solvent selection is a trial-and-error process.

5.2.2 Impact of Composition and Architecture

Polymers can be characterized by many physiochemical properties: size, molecular mass, linear or nonlinear chain structure, tacticity, chain rigidity, glass transition temperature, and more. Without an insightful theory of polymer thermophoresis, the dependence of D_T on each of these properties has been investigated utilizing model systems. It has been shown that D_T of a copolymer, in nonselective solvent, can be approximated if the D_T and mole ratio of each

component is known [21]–[24]. In reverse, this can be used to rapidly assess compositional drift [25]. In 1986 Giddings reported that D_T has no dependence on architecture for polystyrene in ethylbenzene [26]. Only recently was it shown that a separation based on the tacticity of a series of stereoregular atactic, syndiotactic, and isotactic poly(methyl methacrylate) was demonstrated to have a strong solvent dependence [27]. Similarly, work with a series of hyperbranched polyesters showed a correlation between degree of branching and D_T when dissolved in tetrahydrofuran but not in cyclohexane [28]. However, this dependency could have been impacted by compositional differences as branching was controlled by silyl protecting group. Despite this, it is now well established that D_T can be dependent on architecture as evidenced in the bottlebrush polymers described in Chapter 3, crosslinked polydimethylsiloxanes in Chapter 4, and work with differently branched polyethylenes [29].

5.2.3 Predictive Models of Thermal Diffusion

There have been numerous models developed to predict the thermal diffusion coefficients of polymers [4]–[7], [17]. An early model by Khazanovich predicted that D_T is dependent on the stiffness of a chain [7]. It was expected that greater chain stiffness, as approximated by the freely jointed chain model, will lead to a greater D_T relative to a less stiff chain. Kohler echoed this due to the observed molar mass plateau of D_T [1]. As a polymer chain grows, the effective segment size continues to grow until it reaches a maximum. A model published by Mes assigned the source of chemical potential for thermal diffusion to the temperature dependence of the Flory-Huggins interaction parameter as calculated from temperature dependence of the Hildebrand solubility parameter [4]. Since entropic effects are not temperature dependent, they were ignored in the derivation. The resulting formula, Equation 5.1, was used to accurate predict D_T of polystyrene of organic solvents [4].

$$D_T = \phi_1^2 \frac{D_{seg}}{T} \frac{\partial[T^2(\partial\chi/\partial T)]}{\partial T} \tag{5.1}$$

Where φ_1 is the solvent volume fraction, D_{seg} is the diffusion coefficient of a segment, and X refers to the enthalpic portion of the Flory-Huggins interaction parameter. While these parameters are accessible for well-studied polymers, modifications to the approximation of φ_1, D_{seg}, and X were made to allow for the calculation of D_T for a wider scope of materials [13], [30]. Calculation of D_{seg} incorporated the Kuhn segment which led to an accurate predicted difference

in D_T for stereoregular PMMA. In addition, X was approximated from Hansen solubility parameters (HSP) which are more widely available than Hildebrand parameters. However, approximating the temperature dependence of HSP is non-trivial and dependent on the availability of accurate physical constants for a specific polymer (i.e., the volumetric thermal expansion coefficient). Despite this, an overall increase in the accuracy of predictions and was observed for polystyrene, poly methacrylate, poly methyl methacrylate, poly butyl acrylate, and polyisoprene in various solvents [13]. However, my own calculations for D_T of PDMS (Chapter 4) indicate an inherent flaw in the use of HSPs. PDMS has two sets of reported HSPs which resulted in D_Ts which spanned an of magnitude for the same solvent. Additionally, D_T calculations for polyvinylpyrrolidone led to highly inaccurate predictions (error greater than 200%). This model, while successful, has shown limitations for specific polymer-solvent systems where the contributors to thermal diffusion may not be fully captured or not accurately represented.

5.2.4 The Locally Correlated Lattice Model

In an assessment of reported D_T for polymers in various solvents, it was observed that there is a correlation between the glass transition temperature (T_g) of a polymer and D_T. This led to an investigation into the fundamental forces which govern polymer T_g. Recently a first principles model was developed which accurately predicts the glass transition temperature (T_g) of over 50 polymers [31], [32]. Similar to D_T, T_g is known to be mass dependent until a molar mass plateau has been reached. In addition, there have been numerous models which attempt to fully describe the phenomenon but fail to explain observations, such as the relationship between free volume and T_g. Through the locally correlated lattice model and historical pressure-volume-temperature data, it was shown that there is a strong correlation between the entropy per segment of a polymer and experimental T_g. This communication demonstrates and explores the observed correlation between T_g, D_T, and the calculated entropy per segment derived from the locally correlated lattice model.

5.3 Results and Discussion

A plot of experimental D_Ts for polyvinylpyrrolidone (PVP) [13], polydimethylsiloxane (PDMS) [19], poly tetrahydrofuran (PTHF) [33], polyisoprene (PI) [13], poly n-butyl acrylate (PnBA) [13], poly methacrylate (PMA) [13], poly(methyl methacrylate) (PMMA) [13],

polystyrene (PS) [13], poly (α-methyl styrene) (PaMS) [13], poly(2-(2-bromoisobutyryloxy) ethyl methacrylate) (PBiBEM), 1-2 polybutadiene (PBD 1-2) , 1-4 polybutadiene (PBD 1-4), isotactic PMMA (PMMA-I) [13], atactic PMMA (PMMA-A) [13], and syndiotactic PMMA (PMMA-S) [13] in their respective solvents, in order of increasing relative polarity, can be seen in Figure 5.1. To the author's knowledge, this plot demonstrates the full scope of organic soluble linear homopolymers with reported D_T values to date. From this plot there appears to be no obvious trend relating the thermal diffusion coefficient to solvent polarity, as would be expected given the strong polymer-solvent dependence which is unique with each set of chemistries. However, a plot of the experimental D_T with experimental T_g reveals an overall trend, in each solvent series there is a positive correlation, Figure 5.2.

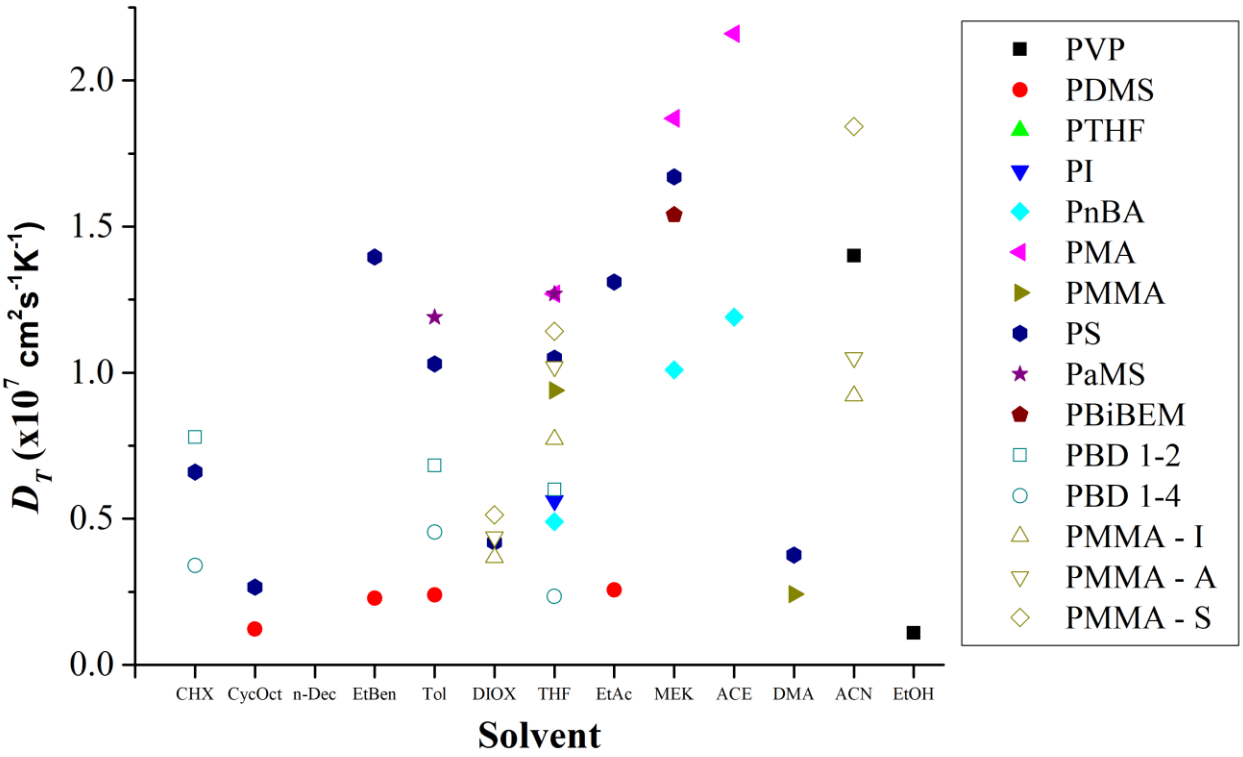

Figure 5.1. Experimental D_T of polymers dissolved in organic solvents where the x-axis is arranged in order of increasing relative polarity.

Generally, it appears that if a polymer has a high T_g there may be a solvent combination which will yield a large D_T. This is supported by the fact that branching typically results in a decrease in T_g. This trend has also been observed for D_T in the bottlebrushes, hyperbranched polyesters [28], [34], chain walking polyethylene [29], and crosslinked PDMS. The apparent

correlation between these physiochemical properties indicates that there may be an underlying physical connection between thermophoresis and the glass transition.

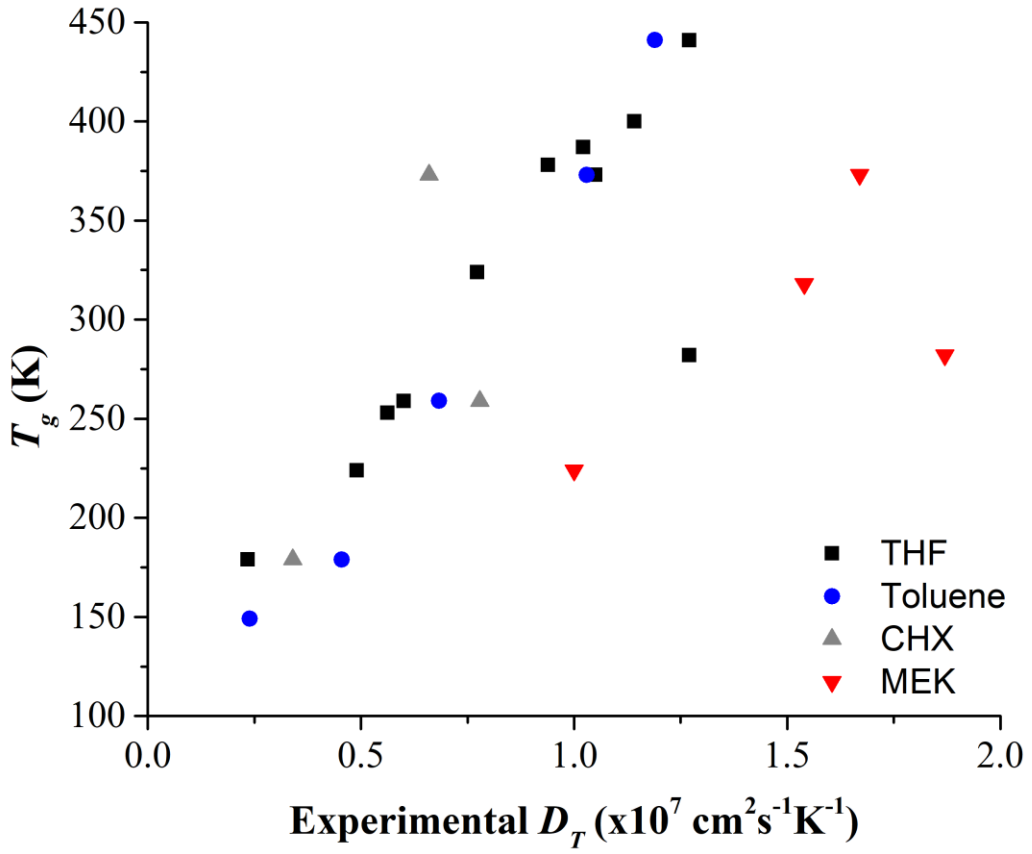

Figure 5.2. Observed relationship between D_T and T_g for polymers dissolved in tetrahydrofuran, toluene, cyclohexane, and methyl ethyl ketone.

A locally correlated lattice model was used to derive the entropy per segment of a series of polymers from literature pressure-volume-temperature data. This model showed a strong correlation between segmental entropy and T_g. It should be noted that while this appears to be a positive correlation, the entropy per segment is determined at the glass transition temperature of the respective polymer. Given that entropy is a temperature dependent property, the relationship is actually inverse – polymers with lower entropy have a larger T_g. These are polymers which typically have fewer degrees of freedom and larger Kuhn segments, or greater chain stiffness. This aligns with trends in D_T previously reported in literature [13], [19]. The plot in Figure 5.3 shows the correlation between segmental entropy and D_T with a notable outlier for PMA in MEK. Given the phenomenologically strong polymer-solvent dependence of D_T, and success of

the predictive model based on enthalpic interactions, it is reasonable that entropy would contribute less to the overall D_T and thus outliers would be expected. Further investigation into the connection between T_g and D_T is warranted and may lead to an improvement to the current predictive model.

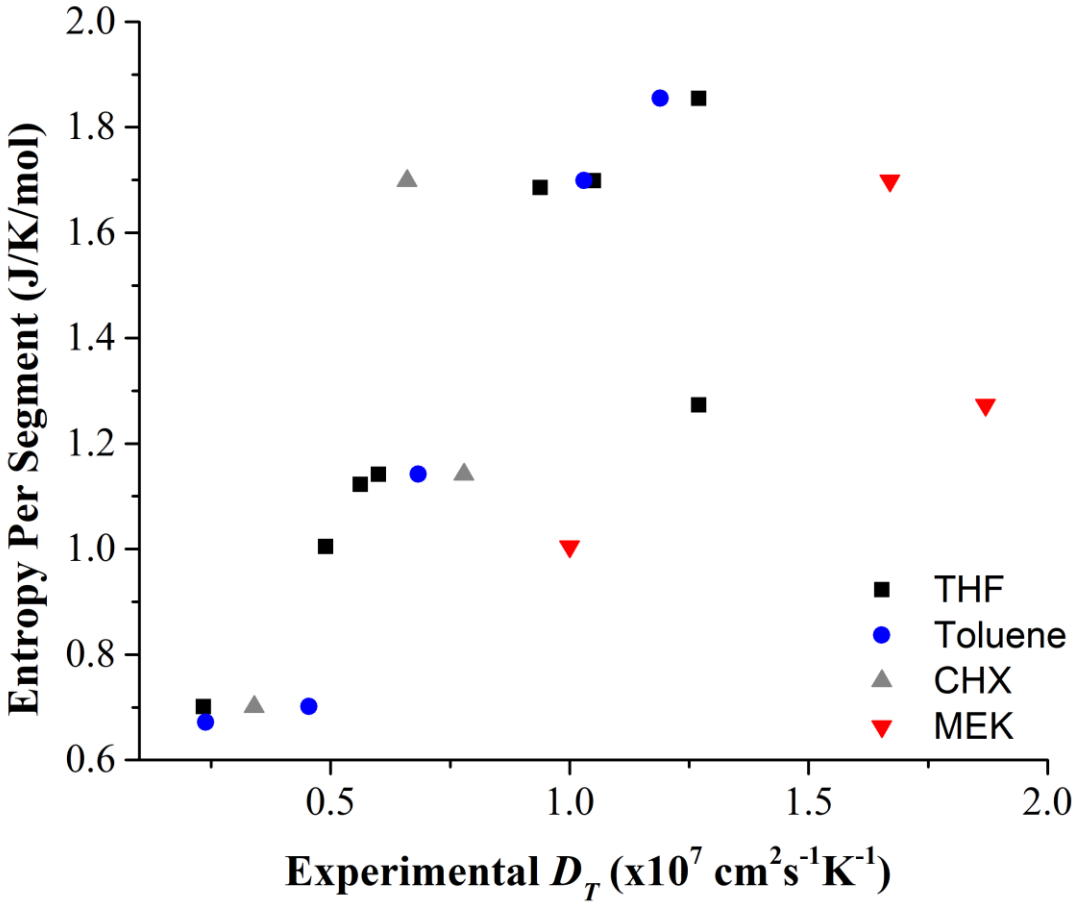

Figure 5.3. Observed relationship between D_T and entropy per segment, as calculated by the locally correlated lattice model [31], for polymers in tetrahydrofuran, toluene, cyclohexane, and methyl ethyl ketone.

5.4 Conclusions

The dominant in predictive models of polymer thermal diffusion leads to erroneous predictions for PVP, a relatively polar polymer, and PDMS, which has multiple HSP spheres. Improvement to predictive models and development of a first principles theory is driven by discovery of novel relationships. The correlation between D_T and T_g indicates there may be an underlying physical connection. Segmental entropy is known to be a strong predictor of T_g and thus correlated with D_T. Entropic forces are ignored in the leading predictive model of thermal

diffusion. Further investigation into the relationship between these properties could yield insight into modeling thermophoresis of polymers.

5.5 Experimental

All polymer D_Ts were collected from references [13], [19], [33] and original data reported in this thesis. Polymer T_g and segmental entropy were collected from reference [31]. Calculation of D_T was performed following the method outline in references [4] and [13].

5.6 References

[1] D. Stadelmaier and W. Köhler, "From small molecules to high polymers: Investigation of the crossover of thermal diffusion in dilute polystyrene solutions," *Macromolecules*, vol. 41, no. 16, pp. 6205–6209, 2008, doi: 10.1021/ma800891p.

[2] R. Kita, S. Wiegand, and J. Luettmer-Strathmann, "Sign change of the Soret coefficient of poly(ethylene oxide) in water/ethanol mixtures observed by thermal diffusion forced Rayleigh scattering," *Journal of Chemical Physics*, vol. 121, no. 8, pp. 3874–3885, Aug. 2004, doi: 10.1063/1.1771631.

[3] G. E. Uhlenbeck, "The Mathematical Theory of Non-uniform Gases. By S. Chapman and T. G. Cowling.," *J Phys Chem*, vol. 45, no. 5, pp. 876–877, May 1941, doi: 10.1021/j150410a017.

[4] E. P. C. Mes, W. Th. Kok, and R. Tijssen, "Prediction of Polymer Thermal Diffusion Coefficients from Polymer-Solvent Interaction Parameters: Comparison with Thermal Field Flow Fractionation and Thermal Diffusion Forced Rayleigh Scattering Experiments," *International Journal of Polymer Analysis and Characterization*, vol. 8, no. 2, pp. 133–153, Jan. 2003, doi: 10.1080/10236660304888.

[5] S. Semenov and M. Schimpf, "Thermophoresis of dissolved molecules and polymers: Consideration of the temperature-induced macroscopic pressure gradient," *Phys Rev E Stat Phys Plasmas Fluids Relat Interdiscip Topics*, vol. 69, no. 1, p. 8, 2004, doi: 10.1103/PhysRevE.69.011201.

[6] S. N. Semenov and M. E. Schimpf, "Molecular thermodiffusion (thermophoresis) in liquid mixtures," *Phys Rev E Stat Nonlin Soft Matter Phys*, vol. 72, no. 4, pp. 1–9, 2005, doi: 10.1103/PhysRevE.72.041202.

[7] M. Bender, "Reassessment of Khazanovich's Theory of Thermal Diffusion of Polymers in Solution," *Macromolecules*, vol. 28, no. 4, pp. 1309–1311, 1995, doi: 10.1021/ma00108a071.

[8] M. E. Schimpf, K. Caldwell, and J. C. Giddings, *Field-Flow Fractionation Handbook*. John Wiley & Sons, 2000.

[9] S. K. R. Williams, J. R. Runyon, and A. A. Ashames, "Field-flow fractionation: Addressing the nano challenge," *Anal Chem*, vol. 83, no. 3, pp. 634–642, 2011, doi: 10.1021/ac101759z.

[10] M. Toney, L. Baiamonte, W. C. Smith, S. Kim Ratanathanwongs Williams, S. Kim Ratanathanawongs Williams, and S. K. R. Williams, “Field-flow fractionation techniques for polymer characterization,” in *Molecular Characterization of Polymers*, Elsevier, 2021, pp. 129–171. doi: 10.1016/B978-0-12-819768-4.00004-X.

[11] S. Wiegand, H. Ning, and H. Kriegs, “Thermal diffusion forced Rayleigh scattering Setup optimized for aqueous mixtures,” *Journal of Physical Chemistry B*, vol. 111, no. 51, pp. 14169–14174, 2007, doi: 10.1021/jp076913y.

[12] W. Koehler and P. Rossmanith, “Aspects of Thermal Diffusion Forced Rayleigh Scattering: Heterodyne Detection, Active Phase Tracking, and Experimental Constraints,” *J Phys Chem*, vol. 99, no. 16, pp. 5838–5847, 2005, doi: 10.1021/j100016a018.

[13] M. Geisler, L. Plüschke, J. Merna, and A. Lederer, “The Role of Solubility in Thermal Field-Flow Fractionation: A Revisited Theoretical Approach for Tuning the Separation of Chain Walking Polymerized Polyethylene,” *Anal Chem*, vol. 92, no. 21, pp. 14822–14829, Nov. 2020, doi: 10.1021/acs.analchem.0c03686.

[14] R. Piazza, “Thermophoresis: Moving particles with thermal gradients,” *Soft Matter*, vol. 4, no. 9, pp. 1740–1744, 2008, doi: 10.1039/b805888c.

[15] R. Piazza and A. Guarino, “Soret Effect in Interacting Micellar Solutions,” *Phys Rev Lett*, vol. 88, no. 20, p. 4, 2002, doi: 10.1103/PhysRevLett.88.208302.

[16] R. Piazza and A. Parola, “Thermophoresis in colloidal suspensions,” *Journal of Physics Condensed Matter*, vol. 20, no. 15, 2008, doi: 10.1088/0953-8984/20/15/153102.

[17] M. E. Schimpf and S. N. Semenov, “Polymer thermophoresis in solvents and solvent mixtures,” *Philosophical Magazine*, vol. 83, no. 17–18, pp. 2185–2198, 2003, doi: 10.1080/0141861031000107926.

[18] M. E. Schimpf and S. N. Semenov, “Latex particle thermophoresis in polar solvents,” *Journal of Physical Chemistry B*, vol. 105, no. 12, pp. 2285–2290, 2001.

[19] D. Stadelmaier and W. Köhler, “Thermal diffusion of dilute polymer solutions: The role of chain flexibility and the effective segment size,” *Macromolecules*, vol. 42, no. 22, pp. 9147–9152, 2009, doi: 10.1021/ma901794k.

[20] J. Rauch and W. Köhler, “On the molar mass dependence of the thermal diffusion coefficient of polymer solutions,” *Macromolecules*, vol. 38, no. 9, pp. 3571–3573, 2005, doi: 10.1021/ma050231w.

[21] W. Van Aswegen, W. Hiller, M. Hehn, and H. Pasch, “Comprehensive triblock copolymer analysis by coupled thermal field-flow fractionation-NMR,” *Macromol Rapid Commun*, vol. 34, no. 13, pp. 1098–1103, 2013, doi: 10.1002/marc.201300286.

[22] M. E. Schimpf, L. M. Wheeler, and P. F. Romeo, “Copolymer Retention in Thermal Field-Flow Fractionation,” 1993, pp. 63–76. doi: 10.1021/bk-1993-0521.ch005.

[23] C. A. Ponyik, D. T. Wu, and S. K. R. Williams, “Separation and composition distribution determination of triblock copolymers by thermal field-flow fractionation,” *Anal Bioanal Chem*, vol. 405, no. 28, pp. 9033–9040, Nov. 2013, doi: 10.1007/s00216-013-7282-6.

[24] J. R. Runyon and S. K. R. Williams, “Composition and molecular weight analysis of styrene-acrylic copolymers using thermal field-flow fractionation,” *J Chromatogr A*, vol. 1218, no. 38, pp. 6774–6779, 2011, doi: 10.1016/j.chroma.2011.07.076.

[25] E. P. C. Mes, R. Tijssen, and W. T. Kok, “Rapid detection of compositional drift of polydisperse copolymers using thermal field-flow fractionation and multi-angle light scattering,” *Chromatographia*, vol. 50, no. 1–2, pp. 45–51, 1999, doi: 10.1007/BF02493616.

[26] J. J. Gunderson and J. C. Giddings, “Chemical composition and molecular-size factors in polymer analysis by thermal field-flow fractionation and size exclusion chromatography,” *Macromolecules*, vol. 19, no. 10, pp. 2618–2621, Oct. 1986, doi: 10.1021/ma00164a027.

[27] G. Greyling and H. Pasch, “Tacticity Separation of Poly(methyl methacrylate) by Multidetector Thermal Field-Flow Fractionation,” *Anal Chem*, vol. 87, no. 5, pp. 3011–3018, Mar. 2015, doi: 10.1021/ac504651p.

[28] W. C. Smith, M. Geisler, A. Lederer, and S. K. R. Williams, “Thermal Field-Flow Fractionation for Characterization of Architecture in Hyperbranched Aromatic-Aliphatic Polyesters with Controlled Branching,” *Anal Chem*, vol. 91, no. 19, pp. 12344–12351, Oct. 2019, doi: 10.1021/acs.analchem.9b02664.

[29] M. Geisler *et al.*, “Topology Analysis of Chain Walking Polymerized Polyethylene: An Alternative Approach for the Branching Characterization by Thermal FFF,” *Macromolecules*, vol. 52, no. 22, pp. 8662–8671, Nov. 2019, doi: 10.1021/acs.macromol.9b01410.

[30] J. R. Runyon and S. K. R. Williams, “A theory-based approach to thermal field-flow fractionation of polyacrylates,” *J Chromatogr A*, vol. 1218, no. 39, pp. 7016–7022, Aug. 2011, doi: 10.1016/j.chroma.2011.08.007.

[31] R. P. White and J. E. G. Lipson, “A Simple New Way to Account for Free Volume in Glassy Dynamics: Model-Free Estimation of the Close-Packed Volume from PVT Data,” *Journal of Physical Chemistry B*, vol. 125, no. 16, pp. 4221–4231, 2021, doi: 10.1021/acs.jpcb.1c01620.

[32] R. P. White and J. E. G. Lipson, “How Free Volume Does Influence the Dynamics of Glass Forming Liquids,” *ACS Macro Lett*, vol. 6, no. 5, pp. 529–534, 2017, doi: 10.1021/acsmacrolett.7b00179.

[33] A. C. van Asten, W. T. Kok, R. Tijssen, and H. Poppe, “Thermal field flow fractionation of polytetrahydrofuran,” *J Chromatogr A*, vol. 676, no. 2, pp. 361–373, 1994, doi: 10.1016/0021-9673(94)80437-0.

[34] A. Khalyavina, L. Häußler, and A. Lederer, “Effect of the degree of branching on the glass transition temperature of polyesters,” *Polymer (Guildf)*, vol. 53, no. 5, pp. 1049–1053, 2012, doi: 10.1016/j.polymer.2012.01.020.

CHAPTER 6
SUMMARY AND OUTLOOK

This dissertation describes several advancements in ThFFF methodology for the analysis of complex polymers. ThFFF is uniquely suited to study complex polymer materials that are at the forefront of innovation and industrial relevance. At the same time, these complex materials have provided new avenues for research into the fundamental processes that dictate thermal diffusion. The advancements presented in this dissertation not only contribute to the scientific understanding of complex polymers but also highlight the importance of innovation and perseverance in research. With this in mind, it is worthwhile to offer some practical advice for future users, which is not readily available in the literature. Components of an analytical instrument (and the overall system), like all things, degrade with time, which impacts their performance. Proper maintenance and cleaning can extend the life of the equipment and should be prioritized. However, some wear cannot be avoided. For instance, ThFFF channels regularly undergo thermal expansion and contraction which can eventually warp the channel. A review of the aqueous ThFFF literature will reveal that there are few works in this space – this may be due in part to the susceptibility of the channel surface to corrosion. The impact of ThFFF channel surface corrosion and surface composition has not been well studied. While FFF benefits from a lack of packing material, the quality of the surface of the accumulation wall can strongly impact performance. It is good practice for researchers to identify key performance indicators (KPIs) relevant to their systems and track them through a logbook. For instance, peak broadening is known to occur with an increase in surface roughness of an FFF channel and can be tracked by monitoring the full-width at half max of a MALS normalization standard. In addition to KPIs, recording as much information about the experiment as possible can be crucial to understanding the results. For many years, the temperature of the cold wall was not reported in ThFFF literature, only for the community to later learn that this value has an impact on retention time and thus should be reported.

6.1 Summary

Thermal FFF with online detectors has been shown to be capable of characterizing distributions in molar mass, chemical composition, and architecture, as evidenced in Chapter 2. The work presented here has expanded this capability to novel architectures and chemical compositions not previously studied. In Chapter 3, both the D_T of a novel polymer (PBiBEM)

and the *g''* values for a library of bottlebrush polymers were reported. It was also shown that architecture does indeed impact D_T, a property of branched polymers that is only recently discovered and still poorly understood. In addition, contraction factors are historically limited by the requirement of a linear analog for comparison. This was circumvented for *g''* by using an accurate predictive model of thermal diffusion and polymer chain theory. The results indicated that if the number of chain ends is known, it may be possible to assess the type of architectures present in a sample system. Building off this work, Chapter 4 demonstrated that *g''* analysis can be applied to an industrial product to discriminate between formulations. Crosslinked polysiloxanes formulated in a diluent presented challenges for ThFFF-MALS-dRI analysis which are not regularly encountered. Sample preparation methods were developed for accurate molar mass determination and to achieve the ideal elution behavior, a condition required for the valid use of the retention equation. Measured D_T values for the branched polymers in Chapters 3 and 4 indicated that thermal diffusion may be affected by architecture. Inspired by this and literature, it was hypothesized that polymer chain dynamics may play a significant role in polymer thermal diffusion. Chapter 5 highlights an observed relationship between the glass transition temperature and D_T. An investigation into glass transition temperature revealed that chain dynamics, specifically segmental entropy, strongly correlate with a polymer's T_g. The leading predictive model of thermal diffusion is calculated by using the enthalpic Flory-Huggins interaction parameter, ignoring entropic contributions. This work proposes that the link between segmental entropy and polymer thermal diffusion may be used to expand upon the current model or develop a novel one which incorporates contributions from segmental motion.

6.2 Outlook

Field-flow fractionation has seen significant growth in the number of publications over the past decade. This is in large part due to the introduction of on-line multi-detectors that provide a wealth of information about the separated components that are eluting. First, MALS-dRI showed that size exclusion chromatography (SEC) of high molar mass polymers did not follow the expected trend of a monotonic decrease in size (or molar mass) with retention volume. This phenomenon has been attributed to sheer degradation of the polymer or pinning of the polymer on the column packing material. These issues and anomalies are not observed in FFF, and it is now well accepted that FFF is the technique of choice for (ultra)high molar mass polymers. Furthermore, online detectors such as MALS-dRI represent an orthogonal method (to

FFF theory and calibration) for determining polymer characteristics as well as reducing the learning curve for new FFF users. Asymmetrical flow FFF (AF4) has been readily adopted by environmental, pharmaceutical, and materials researchers. This has culminated in the recent development of an ASTM method for the analysis of liposomal drug formulations by AF4 [1]. ThFFF has capabilities (e.g., composition, architecture) that exceed AF4's diffusion-based separation. However, ThFFF has seen significantly less adoption due to a poor understanding of thermal diffusion, not only of polymers but also particles. To date, there is no first principles theoretical description of polymer or particle thermal diffusion. The dominant model of polymer thermal diffusion has only been shown to be accurate for polymers in non-polar organic solvents and is limited by the accessibility of polymer-solvent interaction data. A theoretical description of thermal diffusion could significantly elevate the technique and allow for greater adoption of the methodology. Additionally, many applications which have boosted the prominence of AF4 are for aqueous based materials. Aqueous ThFFF literature is sparse because the commercially available channel has a surface that is a nickel-chrome plating which corrodes under most aqueous conditions. Advancements in instrument design would allow for a continuation in research to better understand thermal diffusion in aqueous environments. For instance, it is known that some buffers may change the sign of D_T and/or change its magnitude for colloidal polystyrene [2]. Recent work has also shown that the addition of salts or surfactants may alter the selectivity for particles with various levels of acid content on their surface. A greater fundamental understanding of thermal diffusion for polymers in both aqueous and organic solvent systems would greatly propel the field forward.

6.3 References

[1] Vincent Hackley, "New Test Method for Analysis of Liposomal Drug Formulations using Multidetector Asymmetrical-Flow Field-Flow Fractionation (AF4)," *ASTM.org*, May 02, 2019.

[2] K. A. Eslahian, A. Majee, M. Maskos, and A. Würger, "Specific salt effects on thermophoresis of charged colloids," *Soft Matter*, vol. 10, no. 12, pp. 1931–1936, Mar. 2014, doi: 10.1039/c3sm52779d.

APPENDIX A

COPYRIGHT PERMISSIONS

Chapter: Chapter 4 Field-flow fractionation techniques for polymer characterization
Book: Molecular Characterization of Polymers
Author:
Michael Toney,Luca Balamonte,William C. Smith,S. Kim Ratanathanwongs Williams
Publisher: Elsevier
Date: Jan 1, 2021

Order Completed

Thank you for your order.

This Agreement between Michael Toney ("You") and Elsevier ("Elsevier") consists of your order details and the terms and conditions provided by Elsevier and Copyright Clearance Center.

License number	Reference confirmation email for license number
License date	Mar, 03 2023

Licensed Content

Licensed Content Publisher	Elsevier
Licensed Content Publication	Elsevier Books
Licensed Content Title	Molecular Characterization of Polymers
Licensed Content Author	Michael Toney,Luca Balamonte,William C. Smith,S. Kim Ratanathanwongs Williams
Licensed Content Date	2021
Licensed Content Pages	43

Order Details

Type of Use	reuse in a thesis/dissertation
Portion	full chapter
Circulation	1
Format	both print and electronic
Are you the author of this Elsevier chapter?	Yes
How many pages did you author in this Elsevier book?	43
Will you be translating?	No

About Your Work

Title	Applications of Thermal Field-Flow Fractionation for Branched Polymers
Institution name	Colorado School of Mines
Expected presentation date	Apr 2023

Additional Data

Michael Toney (STUDENT)

From: Kim Williams
Sent: Tuesday, April 11, 2023 10:21 AM
To: Michael Toney (STUDENT)
Subject: Re: Book chapter

Hi Michael,

You have my permission to use this book chapter in your thesis.
Kim

From: Michael Toney (STUDENT) <mtoney@mines.edu>
Sent: Tuesday, April 11, 2023 8:34 AM
To: Kim Williams <krwillia@mines.edu>
Subject: Book chapter

Hi Kim,

I would like your permission to reprint the Elsevier book chapter we co-authored (https://doi.org/10.1016/C2019-0-00391-3) in a copyrighted thesis. A response to this email will satisfy Mines' thesis requirements.

-Michael

Michael Toney (STUDENT)

From: Smith, William <William.Smith@fda.hhs.gov>
Sent: Tuesday, April 11, 2023 7:51 AM
To: Michael Toney (STUDENT)
Subject: RE: [EXTERNAL] Request for permission to use book chapter

Hey Michael!

I provide my explicit permission for your use of the aforementioned book chapter in your thesis.

Good luck man! You got this 😊

-Billy

From: Michael Toney (STUDENT) <mtoney@mines.edu>
Sent: Monday, April 10, 2023 8:41 PM
To: Smith, William <William.Smith@fda.hhs.gov>
Subject: [EXTERNAL] Request for permission to use book chapter

Hey Billy,

My defense is nigh and I would like your permission to reprint the Elsevier book chapter we co-authored (https://doi.org/10.1016/C2019-0-00391-3) in a copyrighted thesis. A response to this email will satisfy Mines' thesis requirements. 😊

Best,
Michael

Michael Toney (STUDENT)

From: Luca Baiamonte <luca.baiamonte@gmail.com>
Sent: Tuesday, April 11, 2023 10:04 AM
To: Michael Toney (STUDENT)
Subject: [EXTERNAL] Re: Book chapter request

Hi Michael,

Sure, it'd be my pleasure.
Good luck for the defense and what will come later!

Best
Luca

Il Mar 11 Apr 2023, 17:57 Michael Toney (STUDENT) <mtoney@mines.edu> ha scritto:

> Hi Luca,
>
> My defense is nigh and I would like your permission to reprint the Elsevier book chapter we co-authored (https://doi.org/10.1016/C2019-0-00391-3) in a copyrighted thesis. A response to this email will satisfy Mines' thesis requirements. 😊
>
> Best,
> Michael